Topology optimization of acoustic metamaterials

2014

LIRONG LU

KYOTO UNIVERSITY

TOPOLOGY OPTIMIZATION OF ACOUSTIC METAMATERIALS

BY

LIRONG LU

A DISSERTATION SUBMITTED IN PARTIAL FULFILLMENT

OF THE REQUIREMENTS FOR THE DEGREE OF DOCTOR OF ENGINEERING

IN THE

GRAGUATE SCHOOL OF ENGINEERING

DEPARTMENT OF MECHANICAL ENGINEERING AND SCIENCE

MAY 2014

Abstract

The past decade has seen an explosion of interest in structural composite materials that display novel properties in the acoustic realm. A primary objective of research in this area is development of acoustic metamaterials, and phononic crystals that can be regarded as the predecessor or counterpart of acoustic metamaterials. Phononic crystals are fabricated as periodic distributions of inclusions (scatterers) embedded in a matrix and are designed to control the dispersion of waves through Bragg scattering; the dimensions and periodicities of these inclusions are comparable to the wavelength. On the other hand, acoustic metamaterials interact with incoming waves due to local resonance. They are also often fabricated as a periodic array of unit cells, but their novel properties are independent of the periodicity. The size of acoustic metamaterial unit cells is at least an order of magnitude smaller than the wavelength, enabling more practical treatment of the design problems dealing with the low frequency ranges most relevant in daily life. However, research in acoustic metamaterials mainly focuses on realizations and applications obtained by trial and error approaches, or on theoretical analyses of the novel properties of such metamaterials. A systematic design tool such as a topology optimization method, which enables the direct design of acoustic metamaterials, might provide solutions more easily and effectively.

This dissertation presents a level set-based topology optimization method applied to acoustic wave propagation problems. In this method, the level set function is updated based on a reaction-diffusion equation and the Tikhonov regularization method is used for the relaxation. The method is applied to the structural design of acoustic metamaterials that exploit the phenomenon of local resonance, and obtains optimal configurations that have clear boundaries. The optimization problem is formulated as a two- and three-dimensional wave propagation problem whose objective is to minimize the effective properties at chosen target frequencies. The design of acoustic metamaterials that achieve a negative bulk modulus based on an intrinsic model is presented first, and the design of acoustic metamaterials that achieve a negative mass density based on an inertial model is presented next. Both of the obtained acoustic metamaterial designs have functional dimensions at low frequencies. Several numerical examples for various prescribed target frequencies, initial shapes and material properties are provided to demonstrate the validity of the proposed method. It is hoped that the proposed method may be useful for the design of acoustic metamaterials that exhibit other novel properties that lead to their deployment in innovative applications.

Acknowledgements

First, I would like to thank my supervisor, Professor Shinji Nishiwaki, and two other essential teachers, Associate Professor Kazuhiro Izui and Assistant Professor Takayuki Yamada, for providing me the opportunity to complete my PhD degree at Kyoto University, and for their great support and guidance during my research period.

I would also like to thank Professor Tetsuo Sawaragi in Department of Mechanical Engineering and Science at Kyoto University, and Professor Atsushi Matsubara in Departement of Microengineering at Kyoto University, for their kind help and support to finish my dissertation.

At the same time, I am extremely grateful for the invaluable suggestions and kind help provided to me by Associate Professor Takashi Yamamoto in the Department of Mechanical Engineering at Kogakuin University, and Dr. Masaki Otomori, currently at AISIN AW Co., Ltd. My research would not have been possible without their inspiring guidance and useful discussions about the mechanisms of acoustic metamaterials and the intricacies of the numerical implementations.

I am also very grateful to Professor Daniel A. Tortorelli for his great help during my short internship at his lab in the University of Illinois at Urbana-Champaign, USA. His way of thinking and his working attitude influenced me profoundly and set the direction for my research.

I would also like to thank the graduated and current lab-mates I met when participating in our research group at Kyoto University. Their warmth, kindness, and assistance always lifted my spirits. Working with them was a pleasure no matter how difficult the tasks. I would like to give my special thanks to Mr. John E. Goodman for his patience in helping me improve my English expressions and polish my papers during my doctoral research period.

I owe a deep debt of gratitude to the Ministry of Education, Culture, Sports, Science and Technology of Japan and The China Scholarship Council for their financial support that allowed me to complete my PhD study in Japan. I am also very grateful to the Japan Society for the Promotion of Science for their financial support that enabled me to participate in a

fruitful internship in the United States.

Finally, my deepest appreciation goes to my parents and sister for their never-ending patience and encouragement. Their unflagging support has energized me to vigorously pursue my studies during the past decade. I am greatly indebted to Shijiang Ma for his countless support and company, which made my last few years of hard work possible and my efforts meaningful. I would also like to thank all my friends who bring joy to my life. Their love and attention helped me immeasurably during my stay in Japan. This is especially true for my best friend in Japan, Tabinda Aziz, who was sympathetic to my worries and always full of encouragement.

May, 2014

Lirong Lu

Kyoto University

Contents

List of Figures

Chapter 1

Introduction

1.1 Motivation

One of the most exciting outcomes of the pursuit of lightweight, micro-miniaturized, and multifunctional devices has been the birth of metamaterials. Metamaterials are artificially manufactured materials that demonstrate highly unusual properties not found in natural materials. The first developed metamaterials were designed for electromagnetic applications but during the past decade, analogous studies have explored acoustic metamaterials that enable manipulation of acoustic waves travelling through a medium. The extraordinary properties of acoustic metamaterials can be exploited in diverse acoustic applications in areas such as sound attenuation, wave guidance, and ultrasonic imaging, and impact a variety of industries, such as aerospace, automotive, engineering, and material production. Acoustic metamaterials can also be used to improve the performance of existing designs. Past studies on acoustic metamaterials have mainly focused on numerical or experimental analysis of known composites or structures obtained by trial and error, using methods that are time-consuming and cumbersome when the aim is to obtain optimal designs. Therefore, a systematic acoustic metamaterial design method would streamline the development of novel and effective designs, as well as the improvement of existing acoustic devices. Furthermore, if such a method could flexibly incorporate a variety of constraints and requirements during the design process, it would be an even more powerful tool for creating desirable and useful artificial materials.

This dissertation presents topology optimization methods for the design of acoustic metamaterials based on two different resonance mechanisms. The aim of the systematic approach to the design process is to obtain superior artificially designed materials or composites that have desirable acoustic properties, for advanced technological applications in the field of acoustics.

1.2 Thesis organization

This dissertation presents an investigation of how advanced acoustic metamaterial designs can be successfully obtained with a level set-based topology optimization method, in six chapters. In this chapter, the motivation for this research is briefly introduced. The other five chapters are organized as follows.

In Chapter 2, the theory underlying the fundamental concepts and the properties of phononic crystals and acoustic metamaterials are presented. The differences between the scattering behavior in phononic crystals and the phenomenon of local resonance in acoustic metamaterials are discussed, since the properties of phononic crystals are determined by scatterers and those of acoustic metamaterials by local resonators. These properties are fundamentally related to the novel behaviors observed when the dynamic mass density and bulk modulus in materials composed of periodic structures assume unusual values. In addition, some interesting applications that are enabled by the novel properties of phononic crystals and acoustic metamaterials are described.

Chapter 3 introduces the concepts of structural optimization methods and highlights the characteristics of conventional topology optimization methods (the homogenization method and density approaches) and level set-based topology optimization. The formulation of the level set-based topology optimization method used for the design of acoustic metamaterials in this dissertation is presented.

Chapter 4 discusses the topology optimization method applied for the structural design of acoustic metamaterials that achieve a strongly negative bulk modulus at certain prescribed frequencies. The design of acoustic metamaterials with negative bulk modulus is based on an intrinsic model that exhibits local resonance. Level set-based topology opti-

mization methods such as the presented method can directly obtain optimal configurations that have clear boundaries because the presence of grayscales is avoided. An optimization problem is formulated for an acoustic wave propagation problem, with the objective being to minimize the effective bulk modulus at chosen target frequencies. An effective medium description based on S-parameters is introduced to represent the properties of the acoustic metamaterial. Several numerical examples in two- and three-dimensions with prescribed target frequencies, different initial shapes and material properties are provided to demonstrate that the proposed method can obtain clear, optimized structures for the design of negative bulk modulus acoustic metamaterials.

In Chapter 5, the level set-based topology optimization method for the design of acoustic metamaterials having negative mass density at a certain desired frequency is presented. The design of acoustic metamaterials with negative mass density is based on an inertial model that exhibits local resonance. Effective medium approximation theory is applied to enable a description of the acoustic metamaterial according to its effective mass density, using S-parameters. The developed method is used to obtain grayscale-free optimal configurations representing acoustic metamaterial designs that are appropriate from an engineering viewpoint and thus are suitable for fabrication. Several numerical examples are provided to demonstrate how the algorithm works, and optimal configurations representing acoustic metamaterials that have negative mass density at certain prescribed frequencies are obtained.

Finally, Chapter 6 provides the conclusion of this dissertation, highlights the achievements of this work, and describes promising avenues to explore in future research.

Chapter 2

Acoustic metamaterial

2.1 Introduction

What does the word “metamaterial” mean? Research into metamaterials first began in 1967, when a Russian scholar, Veselago, asked an interesting and unusual question concerning electromagnetic wave propagation in materials, that is, what would happen if the permittivity and permeability of a material both assumed negative values? This was such a “crazy” question that nobody considered it seriously until 30 years later. Researchers found that the results are amazing and the name “metamaterial” is used to represent materials and structures with unusual properties. A metamaterial is an artificial material whose material properties emerge due to its structure, rather than the properties of the material from which the metamaterial is made. Also, a metamaterial has properties that are not found in natural materials. Metamaterials were first created for use in electromagnetic problems. From year 2000 much attention has been paid to the analogue in the acoustic field, creating “acoustic metamaterial” which is designed to solve various acoustic problems of sound propagation.

Waves in acoustic systems and in electromagnetic fields are obviously different. Acoustic waves are longitudinal waves, whereas both electric and magnetic fields are described as transverse waves. However, the two wave systems share certain physical concepts, (such as wave vectors, wave impedance, and power flow,) and the similarity between the electromagnetic wave equations and acoustic wave equations suggests that we should be able to observe similar phenomena in these different fields and use similar approaches when

studying acoustic metamaterials.

2.2 Phononic crystals

Before diverse research activities done for acoustic metamaterials, phononic crystals have attracted far-ranging attentions which can be regarded as the precursor on the way of discovering such novel materials since 1980's [8, 9]. Phononic crystals are artificial composites with the periodic arrangement spatially of inclusions/scatterers embedded in a matrix/host material, showing exceptional phenomena on the control of acoustic waves. As Fig. 2-1 shows, scatterers are embedded in a base material, "a" is the lattice constant, and "d" is the periodic component size. Since such phenomena are generated through Bragg scattering, by which the behaviors of the waves, such as scattering, diffraction and interference, are happened. Thus the dimensions and periodicities of scatterers are comparable to the wavelength.

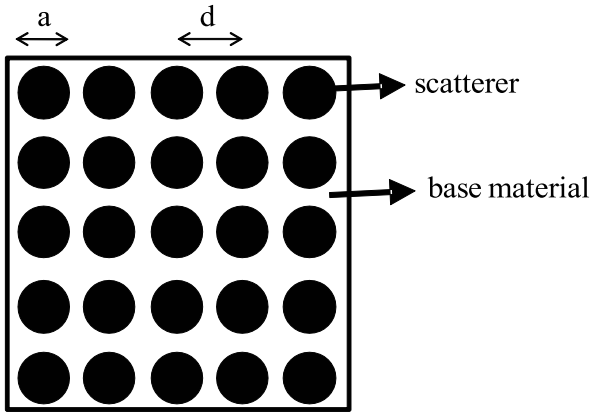

Figure 2-1: Sketches of phononic crystals.

Until now, the progresses and investigations with regard to the unusual behaviors have been focused on bandgaps, negative refraction, waveguides and so on.

2.2.1 Bandgap

Phononic structures composed of different materials in the inclusions and matrix, of which the density and/or the elastic constants are different. This makes the acoustic impedance, then the speed of sound in the different materials change in the crystals. Suppose in a one-dimensional phononic crystal, made up with periodic alternative layers of two different materials, there is an interface between two layers, where the incoming waves reflect and then interfere with each other, ultimately resulting in the bandgaps of the certain range of frequency. The behavior of bandgaps strictly forbids the propagation of waves in the corresponding transmission spectra.

There are two requirements for the formation of acoustic bandgaps. One is the contrast in physical properties between the constituent materials, and the other is a filling fraction of the inclusions. That is, the material properties, the geometry/dimensions and the arrangement of the inclusions and the matrix affect the width and position of the bandgaps. Vasseur et al. has intensively studied this issue through a two-dimensional boron nitride structured periodic composite (the inclusions and matrix are either fluid-fluid or solid-solid) and obtained the conclusion that strong contrast and high filling fraction yield to wider bandgaps [10]. Later Vasseur et al. extended the investigation to two-dimensional mixed periodic composite material (solid-fluid or fluid-solid) and successfully proved that a forbidden band at audible frequency exists in the case of low filling ratio [11].

In the last decade research about the phononic crystals renewed and achieved extensive possibilities of the realizations and applications of phononic crystals, including novel materials and structures, mixed with other physical fields. Robillard et al. actualized a two-dimensional phononic crystal composed of kind of magnetostrictive material inclusions (it expands and contracts in accordance with the change of a magnetic field) and an epoxy matrix with contactless tunable bandgaps [12]. Wu et al. investigated an air-silicon phononic crystal based on layered slanted finger interdigital transducers for the microelectromechanical application in micrometer scale [13]. A phononic crystal was created by etching a hexagonal array of holes in a silicon slab with low rate of energy loss for wireless communication and sensing applications [14]. Zhang et al. were the first team to observe an

bandgap for surface acoustic waves experimentally by thin plates where periodical air-filled holes are made.

As we have known that the sizes/shapes of the inclusions and ratio of the constituents' physical properties decide the position and width of bandgaps, bandgaps can be further divided into two kinds relative to the angle of incident waves, including absolute or complete bandgaps and partial bandgaps. The former one works for waves propagating in any direction and the latter one only terminates the wave-passing in certain directions. This is another popular topic about the behavior of bandgaps [15, 16, 17, 18, 19, 20]. The structures with complete bandgaps specially can be used as insulation partition [21] and have a wide range of applications in the aspects of house interior, construction industry, civil engineering and so on.

2.2.2 Negative refraction and ultrasonic imaging

Natural materials exhibit positive refractive index regardless of electron, photon, and phonon. But the artificially composed phononic crystals show negative refractive index, by which kind of flat and thin lens, so-called superlens is created. The operation frequencies of superlenses are at the ultrasonic range of 20 kHz-100 MHz, accordingly, the lattice constants of such phononic crystals (can be called ultrasonic crystals) are much smaller as 10^{-2}-10^{-5} m.

Traditional lenses have convex or concave surfaces which are difficult to manufacture while those of superlenses are flat and easier to produce. More importantly, ultrasonic imaging based on acoustic superlenses can form images with super-resolution which are as fine as the subwavelength of the acoustic waves being focused. This phenomenon has been observed to beat the diffraction limit. A two-dimensional phononic crystal consisting of coated cylinders embedded in liquid matrix in square arrays has been proved to achieve negative refraction imaging by Li et al. [22]. Ke et al. successfully reported negative refraction imaging with a design of phononic crystals using steel rods immersed in water [23]. Another example about negative refraction index in two-dimensional phononic crystal has been demonstrated and a microsuperlens for acoustic waves has been designed

[24]. Phononic crystal-based wide band acoustic collimation lenses can be used to replace traditional collimation lensed, which are heavy, expensive and hard to fabricate [25]. A three-dimensional phononic crystal exhibiting sound focusing phenomenon has also been claimed [26].

The practical applications of high-resolution ultrasound imaging include diagnostic medical imaging techniques, non-destructive structural testing of buildings and bridges, and novel underwater stealth technology.

2.2.3 Hypersonic phononic crystal

Theoretically if the lattice constant of phononic crystals is decreased to a sufficiently small value, the operation frequencies of phononic crystal will be increased to the gigahertz [27], even terahertz region. We call them hypersonic phononic crystals. Since the frequency region has been raised up to a high level (gigahertz to terahertz) [28] and phonon and photon (terahertz) share the same basic ideas in the bandgap behavior, it is highly possible to consider both types of bandgap in one composite material simultaneously, i.e. this material will be "blind and deaf" to electromagnetic waves and acoustic waves with wavelength of about several hundred nanometers. Maldovan and Thomas at MIT has theoretically proved the feasibility of creating a phononic crystal which has complete phononic and photonic bandgaps by a two-dimensional square and triangular lattice made of air rods arranged in silicon background [29]. This is a very new exploration and may inspire the potential cooperation of phonon and electron. In addition, thermal energy is regarded to be corresponding to the frequency of THz which makes thermal management possible.

Some promising and interesting applications about hypersonic crystals could be phonon-photon interactions [30, 31], acoustic-optical devices and thermal conductivity control [28]. In 2010, one-dimensional hypersonic phononic crystal of periodic SiO_2/poly multilayer film has been observed experimentally to show bandgap at gigahertz frequencies [32]. Single crystalline silicon phononic crystals at submicrometer scale realized a massive reduction in thermal conductivity experimentally [33]. However, it's worth noting that hypersonic crystals with the submicron and nanometer scale are challenging to fabricate com-

pared to sonic and ultrasonic crystals, which are in centimeter, millimeter or sub-millimeter range.

2.2.4 Crystal defects and waveguide

By slightly destroying the perfect phononic crystals, that is, introducing point-like or linear defects (e.g., removing a single inclusion or a row of inclusions, see Fig. 2-2) within the structure, waveguides can be designed. Waveguides are the structures used to guide the propagation of acoustic waves with frequencies inside the bandgaps with minimal energy loss, where the acoustic waves will be trapped near a point or guided along a line according to different defects. Gigahertz frequency phononic crystal has been proved to be well-poised to realize waveguides [27]. Waveguides can lead to a wide range of applications such as frequency filtering, wave guiding, wavelength division multiplexing, and demultiplexing [34]. Frequency filtering is to remove unwanted frequency components from the incoming wave. Multiplexing is a method by which multiple frequencies from different waveguides are combined into one waveguide. Demultiplexing is an inverse method extracting one frequency from one waveguide and sending it to another waveguide.

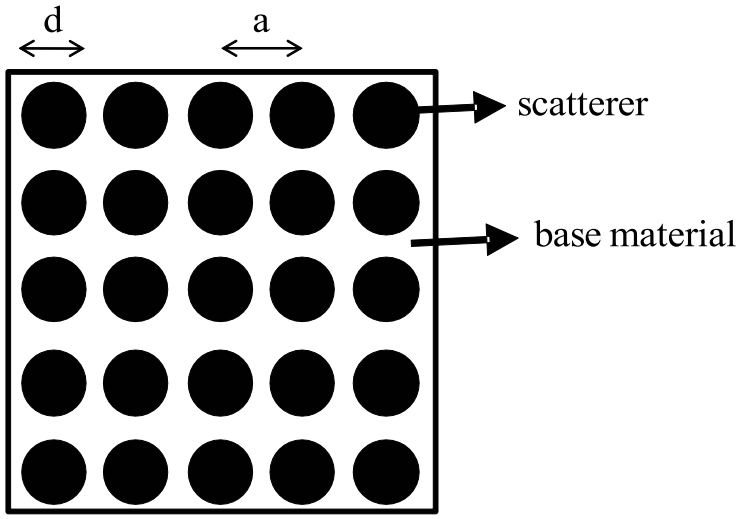

Figure 2-2: Defects of phononic crystals: (a) basic structure; (b) phononic crystals with point-like defect; (c) phononic crystals with linear defect.

Until now various kinds of waveguides have been constructed. Waveguiding in a piezo-

electric phononic crystal is designed by a linear defect created by removing one row of air holes, aiming for telecommunication applications [35]. A linear waveguide, along which a side branch (stub) is attached, is created in a two-dimensional phononic crystal [36]. A sharply bent waveguide is reported and an improved design by adding scatters inside the phononic crystal waveguide is suggested to enhance energy transmission [37]. A tunable waveguide for the filtering purpose is introduced [38].

2.3 Acoustic metamaterials

Acoustic metamaterials are another kind of man-made composite materials, just as phononic crystals, that exhibit novel properties not found in naturally formed substances. However, acoustic metamaterials have the additional feature of local resonance which makes the dispersion characteristics unusual. Same as phononic crystals, acoustic metamaterials are structures often designed in a periodic arrangement as well, however, their novel properties are independent of the periodicity. The structural features of acoustic metamaterials are one order of magnitude lower, even in deep subwavelength range, compared with the wavelength of the incoming waves. Due to this feature, acoustic metamaterial can be analyzed as homogenized materials by effective material properties on one unit cell.

There is no worldwide accepted definition of acoustic metamaterials yet. Someone decide that the materials made artificially and show unusual properties by theirs structures are regarded as acoustic metamaterials. Others call the materials based on Bragg scattering and have comparable sizes of the periodicities as the wavelength as phononic crystals, and the materials mentioned above as acoustic metamaterials. In this dissertation, our descriptions are on the basis of the latter point of view.

Given that the behavior of acoustic metamaterials is determined by the characteristics of the local resonators inside the unit cell, acoustic metamaterials can be classified into two groups according to differences in their structures [39]:

(1) Intrinsic acoustic metamaterials

Such acoustic metamaterials are created by the presence of inclusions embedded in a matrix material. The inclusions are usually soft materials in which the speed of sound is

much lower than that in the matrix material. Local resonances then occur due to the large differences in the speed of sound in these two materials. The combination of rubber and water as the inclusions and matrix, respectively, is a typical example [10, 40].

(2) Inertial acoustic metamaterials

In such acoustic metamaterials, a mass-spring-damper type of oscillating structure is built to trigger local resonances. There are two widely used types of resonators: a coated sphere embedded in background material [1, 2, 3, 4, 41] as shown in Fig. 2-3, and Helmholtz resonators, which often are in the form of a cavity with a neck construction joined to a duct or located in tank, or split ring resonators [5, 6, 7, 42] as shown in Fig. 2-4.

The mechanism of local resonance may bring about revolutionary changes to existing technologies in many fields due to their unusual dispersion characteristics that lead to negative properties, such as negative dynamic mass density, bulk modulus, and refraction.

2.3.1 Single negativity

Among the novel properties/applications that are the subject of research in the field of metamaterials, the most widely applicable property is likely the negative properties that lead to bandgaps that prevent the transmission of waves at some certain frequencies. The definitions of the material properties such as bulk modulus and mass density [39], are shown below:

$$\kappa = -V\frac{\triangle p}{\triangle V} \tag{2.1}$$

$$\rho = \frac{\triangle p}{\triangle V}\frac{F}{V} \tag{2.2}$$

where κ and ρ are the bulk modulus and mass density of the material, respectively. $\triangle p$ represents an infinitesimal pressure change and $\triangle V$ is a volume change, V is the volume, p is the pressure, and F is the applied force. For acoustic waves travelling inside a homogenous medium, the refractive index n is given by

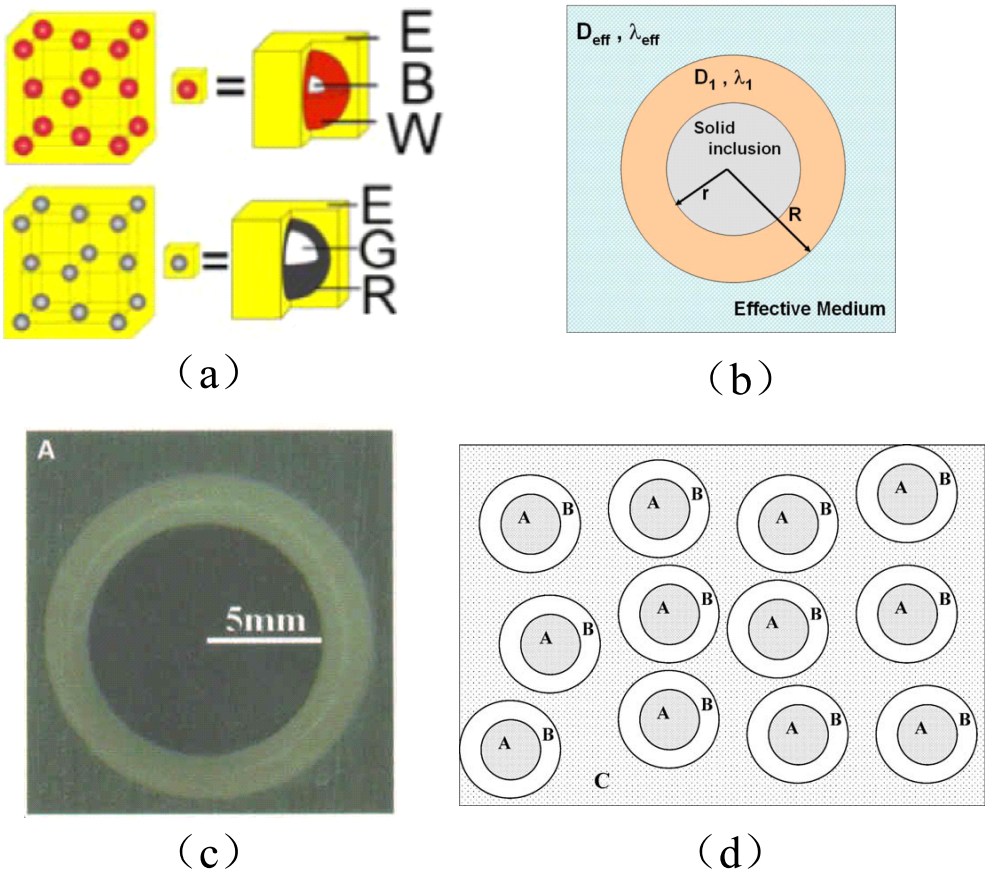

Figure 2-3: Designs of acoustic metamaterials with a coated sphere embedded in background material:(a) A double unit structure which combines an array of bubble-contained water spheres (BWS) with an array of rubber-coated gold spheres (RGS) in epoxy matrix [1]; (b) A structural unit consists of the inclusion and the coating layer, embedded in the effective medium matrix [2]; (c) A micro-structure unit consists of a lead ball as the core material and a layer of silicone rubber as coating material with epoxy as the hard matrix material [3]; (d) A structure geometry is realized by using lead balls coated with silicone rubber and embedded in epoxy [4].

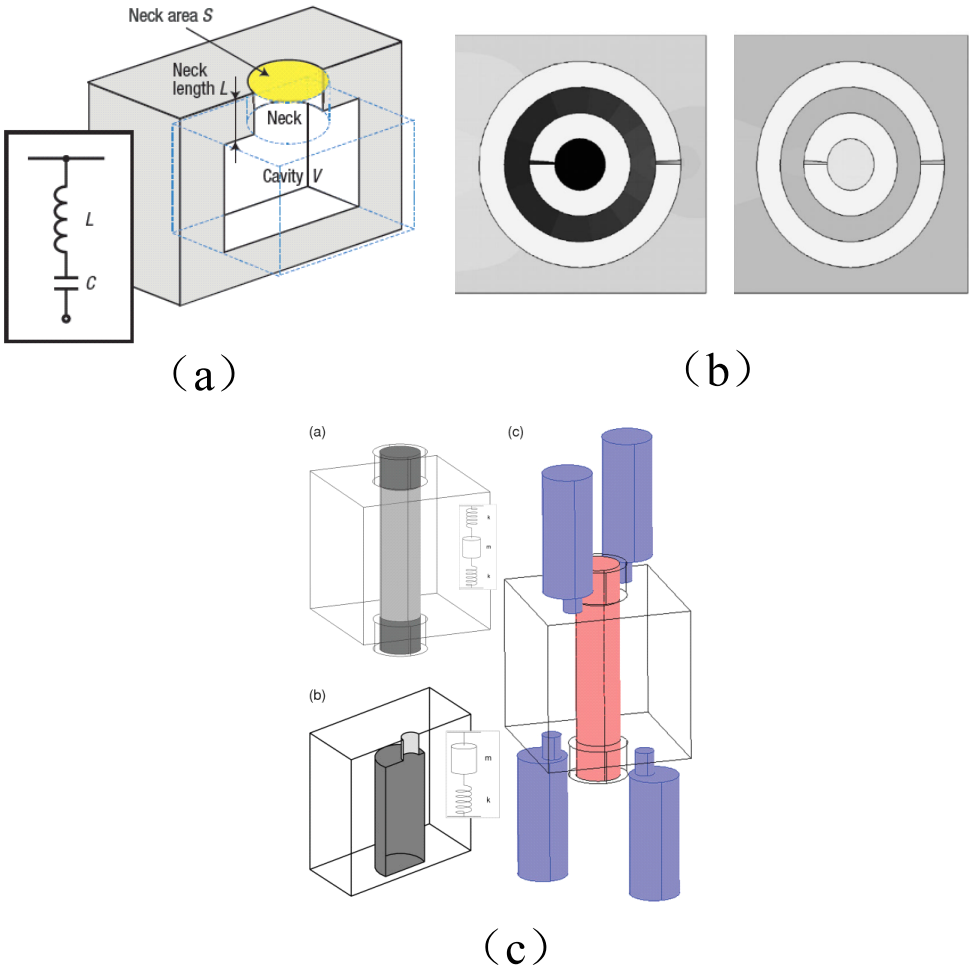

Figure 2-4: Designs of acoustic metamaterials with Helmholtz operators and split ring resonators: (a) A cross-sectional view of a Helmholtz resonator which consists of a rectangular cavity and a cylindrical neck, both of them are made of aluminium, filled with water and connected at the same side to a square water duct [5]; (b) A split-ring resonator, also referred to as “double C” resonator [6]; (c) A unit cell consists of a rod-spring resonator,which is shaded red (light gray) and four Helmholtz resonators shaded blue (gray) [7].

$$n^2 = \frac{\rho}{\kappa} \tag{2.3}$$

The above relationships imply that if either the mass density or the bulk modulus becomes negative (single negativity), then the refractive index becomes imaginary and waves cannot propagate; bandgaps are formed. Negative mass density means that a positive momentum excitation produces a negative total momentum of the composite, and that the composite moves in the direction opposite that of the excitation. Negative bulk modulus appears for composites with an increasing total volume under a compressive stress, or a decreasing volume under a tensile stress [43]. Local resonance-based acoustic metamaterials can realize bandgaps for frequencies in the low kHz range. Ding et al. has presented an acoustic metamaterial based on multi-split hollow spheres that shows a negative bulk modulus bandgap that can be tuned by changing the diameter of the holes [44]. Christensen et al. designed an acoustic metamaterial made of two adjacent plates with arrays of holes, which exhibited a negative bulk modulus leading to a broadband sound blockage [45]. Fang et al. [5] and Huang et al. [46] have also proposed different structures that exhibit negative bulk modulus and achieve bandgaps. Other studies concerning bandgaps in acoustic metamaterials with negative mass density have also been reported, including a membrane-type local resonator [47], simple spring-mass resonant structures [48], and other structures [49, 50]. Theoretical and experimental investigations have demonstrated the strong attenuation of sound waves due to bandgap behavior.

2.3.2 Double negativity

Equation 2.3 above implies that both the bulk modulus and the mass density should be either positive, or negative (double negativity), allowing waves to propagate through the structure. Accordingly, materials with a negative refractive index can be obtained when both the bulk modulus and the mass density are negative [51]. Liang et al. demonstrated a tunable acoustic metamaterial with double negativity [52]. Huang and Sun used a combination of two models, one with negative mass density and the other with negative bulk modulus, to produce a metamaterial that exhibited negative refraction [53]. Ding et al. real-

ized a metamaterial using two types of structural units, water containing spherical bubbles, and rubber-coated gold spheres, to derive double negativity properties [54]. Chen et al. fabricated a three-dimensional acoustic metamaterial based on the coupling of a hollow steel tube with a split hollow sphere, which simultaneously obtained a negative bulk modulus and negative mass density [55].

Analogously to the applications for phononic crystals that achieve negative refraction, acoustic metamaterials that have negative refractive indices resulting from double negativity can also be used for important applications, such as in superlenses (super-resolution imaging, focusing, and localization). Many two-dimensional [56, 57, 58] and three-dimensional designs [59] have been achieved, which have the potential to enhance the performance of devices in the fields of medical ultrasonography, underwater sonar, and non-destructive evaluation.

2.3.3 Cloaking

Another exciting field of investigation in the control of wave propagation in acoustic fields by acoustic metamaterials concerns cloaks. An acoustic cloak is a device enclosing an object that deflects waves that would have interfered with the object, guides them around the object, and makes them return to their original direction of propagation. Thus, the object is shielded from the impinging waves in such a way that its presence cannot be discerned; in other words, the object is deaf to sounds outside. An acoustic cloak can also induce sounds waves to flow like a fluid along an object [60, 61, 62, 63]. One immediate application is to protect objects against undesirable acoustic disturbances.

Acoustic cloaks can be easily realized using acoustic metamaterials that owe their properties to their structure, rather than to the material properties of substances comprising their structure, and can be designed to have properties that are difficult or impossible to find in nature [64]. Zhang et al. were the first to realize a practical low-loss and broadband acoustic cloak for underwater ultrasound, constructed with a network of acoustic circuit elements [65]. Zhu et al. designed a two-dimensional rhombic cylindrical cloak based on homogeneous metamaterials [66]. Cheng et al. designed a two-dimensional acoustic

cloak with a concentric alternating layered structure [67] and later extended the design to a three-dimensional spherical acoustic cloak that can hide an object from detection by acoustic waves impinging from an arbitrary direction [68]. Another three-dimensional acoustic cloak, based on acoustic metamaterials, has also been reported [69].

Acoustic cloaking has attracted great interest since 2006 and has resulted in a number of promising applications in various fields, such as preventing the detection of underwater objects such as submarines, protecting particularly sensitive objects or facilities against blast or shockwaves, acoustic noise reduction using sound-shielding materials, and seismic isolation of civil infrastructure [63].

2.4 Conclusion

Both phononic crystals and acoustic metamaterials, artificially structured composite materials, enable the control of the dispersive properties of acoustic waves and exhibit unusual properties. They also show the following differences.

(1) Phononic crystals are fabricated with periodic distributions of inclusions (scatterers) embedded in a matrix. Although acoustic metamaterials are also fabricated based on a periodic array of unit cells, their novel properties are independent of the periodicity.

(2) Phononic crystals are designed to control the dispersion of waves through Bragg scattering. Acoustic metamaterials have unit cells which exhibit local resonance themselves.

(3) The dimensions and lattice constants of the scatterers in phononic crystals are comparable to the wavelength. Phononic crystals are usually applied in high frequency ranges otherwise their size leads to non-functionality and impracticability. On the other hand, the structure of acoustic metamaterials is at least an order of magnitude smaller than the wavelength of the incoming waves, enabling more practical treatment of the low frequency problems that commonly arise in daily life.

(4) The bandgaps provided by phononic crystals arise due to reflection and refraction from the inclusions as dispersive acoustic waves propagate in the lattice system;

the bandgaps are thus determined by the distribution of the scatterers. In acoustic metamaterials, however, local resonators interact with acoustic waves in the matrix, leading to bandgap behavior, so different unit cell designs create different bandgap behaviors.

In the past few years, phononic crystals and acoustic metamaterials have been used in diverse technological applications, including sound abatement, ultrasonic imaging, telecommunications, thermal management, and others. Additional novel properties and applications can be expected.

In this dissertation, the composite materials based on local resonance will be discussed.

Chapter 3

Topology optimization

3.1 Topology optimization

As described by Christensen and Klarbring [70], structural optimization is “the subject of making an assemblage of materials sustain loads in the best way”. To state this idea in a more general and mathematical way, structural optimization is a method for finding a structural configuration by means of an objective function that is to be minimized or maximized, with boundary conditions and constraints applied. There are three classes of structural optimization that are applied to design problems for mechanical structures: size, shape, and topology optimization.

In a typical sizing optimization problem, first proposed by Schmit in 1962 [71], the structural optimization is conducted mathematically, where the mechanical or structural size elements such as the length, width, or height of a structure, are set as the design variables. The study of shape optimization began in earnest in 1970’s [72, 73], with the goal of finding optimal shapes expressed by the outer boundaries of a structure, which are treated as the design variables. Since the design variables are confined to the shape, the structure’s topology, i.e., the number of holes in the structure, is fixed. In contrast, in topology optimization [74, 75, 76], the topology of the structure can be changed in addition to structure’s shape during the optimization, so this method offers the highest degree of design freedom.

To enable topological changes, Bendsøe and Kikuchi first established the topology op-

timization methodology by introducing a characteristic function [77] in 1988, defined as a discretized value of 0 or 1 in a fixed design domain that includes the original design domain, to obtain an optimal structure. In topology optimization includes two basic concepts. One is the extension of a design domain to a fixed design domain; the other is the replacement of the optimization problem by a material distribution problem, based on the use of the characteristic function.

To clarify this idea, consider a topology optimization problem that aims to find an optimal configuration of a domain Ω that is filled with a solid material, by minimizing an objective functional F under certain constraints. Given a constraint functional, i.e., a volume constraint V, the topology optimization problem can be formulated as follows.

$$\begin{aligned} &\inf_{\Omega} \; F(\Omega) = \int_{\Omega} f(\mathbf{x}) \mathrm{d}\Omega \\ &\text{subject to} \quad V(\Omega) = \int_{\Omega} \mathrm{d}\Omega - V_{\max} \leq 0 \end{aligned} \tag{3.1}$$

where f is a density function of the objective functional, $\mathbf{x}$ represents a point in Ω, and $V_{\max}$ is the upper limit of the material volume. By introducing a fixed design domain D and the characteristic function χ_{Ω} as follows,

$$\chi_{\Omega}(\mathbf{x}) = \begin{cases} 1 & \text{if} \quad \mathbf{x} \in \Omega \\ 0 & \text{if} \quad \mathbf{x} \in D \backslash \Omega \end{cases} \tag{3.2}$$

the original topology optimization problem is replaced with a material distribution problem in the fixed design domain D as follows.

$$\begin{aligned} &\inf_{\chi_{\Omega}} \; F(\chi_{\Omega}(\mathbf{x})) = \int_{D} f(\mathbf{x}) \chi_{\Omega}(\mathbf{x}) \, \mathrm{d}\Omega \\ &\text{subject to} \quad V(\chi_{\Omega}(\mathbf{x})) = \int_{D} \chi_{\Omega}(\mathbf{x}) \, \mathrm{d}\Omega - V_{\max} \leq 0 \end{aligned} \tag{3.3}$$

However, the above topology optimization problem is ill-posed since the characteristic function, defined in L^{∞}, can be discontinuous in infinitesimal intervals in the fixed design domain. The fixed design domain needs to be relaxed. Thus, various approaches such as the homogenization design method (HDM) [78, 79] and density approaches (especially the SIMP method [80, 81]) have been proposed to overcome this problem. However, the in-

troduction of these techniques usually causes the inclusion of grayscales in the obtained optimal configurations, or numerical problems such as checkerboards or mesh-dependency (according to Sigmund and Petersson [82], “the checkerboard problem refers to the formation of regions of alternating solid and void elements ordered in a checkerboard-like fashion. The mesh-dependence problem refers to obtaining qualitatively different solutions for different mesh-sizes or discretizations.”), since the density variable used to represent the optimal configurations can assume a continuous range of values from 0 to 1. Although the existence of grayscales is allowed in the optimal configurations, they are problematic from an engineering viewpoint since such configurations are difficult to regard as practical designs for manufacture. Much work has been done to deal with such problems, such as the application of higher-order finite elements, filters, perimeter controls, and so on. Detailed reviews can be found in the literature [82, 83, 84]. Among these techniques, filtering schemes [85, 86, 87, 88, 89, 90, 91, 92, 93] and restrictions (constraints) [94, 95, 83] are the most popular.

Topology optimization methods have been applied in a large number of problems that incorporate different physics and conditions. Such problems include minimum compliance problems [96, 87, 97], thermal expansion problems [98, 99], fluid problems [100, 101, 102], eigenfrequency problems [103], compliant mechanism design problems [104, 86, 85], and electromagnetic problems [105, 105]. In addition, photonic crystal-based waveguide components have been successfully designed to obtain high-transmission and low-loss over a wide frequency range [106, 107, 108]. Electromagnetic metamaterials with a negative property [109] or in three-dimensions [110] have been designed using topology optimization methods [111].

Topology optimization methods have also been applied in various acoustic problems and applications. Wadbro and Berggern presented a topology optimization design of an acoustic horn with the aim of radiating sound using a scalar function indicating the presence of material [112]. Huang et al. optimized a periodic structure mechanical filter (PSMF) [113] and Zhang et al. optimized a damping layer [114] to reduce vibration transmission and sound radiation. Yamamoto et al. proposed designs for sound-absorbing structures utilizing poroelastic media based on a homogenization method [115] and the

density approach [116]. Lee and Kim optimized the inner layout of partitions inside a muffler by maximizing the transmission loss at target frequencies [117]. Many designs of phononic crystals to achieve bandgaps or waveguide behaviors have also been reported [118, 119, 120, 121, 122, 123, 124, 125].

3.2 Level set-based structural optimization

Level set-based structural optimization methods are another type of structural optimization method used to search for optimal configurations, a combination of structural optimization with the level set method first proposed by Osher and Sethian [126]. Such methods are numerical techniques for tracking moving interfaces and then obtaining certain shapes after evolutionary changes of the level set function . In essence, an n-dimensional object is treated in an n+1-dimensional space. For example, when a three-dimensional cylinder shape in space is intersected by a two-dimensional plane that is perpendicular to the axis of the cylinder, the intersection is a circular disc. One notable feature of level set-based topology optimization methods is that the obtained optimal configurations are free from grayscales.

In the earliest level set-based structural optimization methods, Sethian and Wiegmann [127] pioneered the application of the level set method for structural boundary design, that is, for solving topology optimizations of elastic structures, in which a non-gradient parameter such as the von Mises stress was adopted as the driving direction when updating the level set function. Osher and Santosa [128] proposed a structural optimization method incorporating shape sensitivity in a level set method, which was used as the normal velocity to optimize resonant frequencies or the spectral gaps of a vibrating system. Wang et al. [129] proposed a level set-based topology optimization method where the level set function is updated by the Hamilton-Jacobi equation, based on the shape sensitivities, and successfully applied it to a minimum mean compliance problem. Allaire et al. [130] also proposed a level set-based topology optimization method where the level set function is updated by the Hamilton-Jacobi equation and smoothed shape sensitivities are used as the normal velocity of the moving boundary. Their method was applied to a minimum com-

pliance problem for a model of linear and non-linear elastic material, and the design of compliant mechanism structures. However, since the obtained shape boundaries rely on the updating of the level set function, strictly speaking, the above level set-based structural optimization methods are shape optimization methods that cannot be expected to provide variations in the topology of the fixed design domain; holes can merge or disappear but not emerge. Hence, the obtained optimal configurations can be very dependent on the initial configuration.

To solve this problem, Allaire et al. [131] and Wang et al. [132] proposed an extended level set-based topology optimization method that allows an increase in the number of holes during the optimization process. However, these approaches still have a drawback due to their use of the Hamilton-Jacobi equation. In level set-based shape optimization methods based on Hamilton-Jacobi equation, the moving interfaces usually represented by the zero level set may not be maintained during the evolution. Thus, a periodic reinitialization operation [133] is necessary to maintain the level set function as a signed distance function during the evolution, but this is complicated to conduct and computationally costly. Some variational methods that do without reinitialization have been proposed [134, 135, 136], but new problems arise, such as dependency on the setting of certain parameters that affect the updating of the level set function and then the obtained optimal configurations. Later, Yamada et al. [137] introduced a fictitious interface energy based on the phase field method, the so-called Tikhonov regularization method, to regularize the topology optimization problem, and created a new type of level set-based topology optimization method in which the level set function is updated based on a reaction-diffusion equation. This method allows not only shape but also topological changes in the optimal configurations and enables the adjustment of the complexity of optimal configurations using a regularization parameter. In addition, reinitialization operations during the optimization procedure are not required.

Level set-based structural optimization methods have been successfully applied to a wide range of problems. Based on level set methods, many shape or topology optimization designs for compliant mechanisms have been demonstrated [138, 139, 140, 141]. Hashimoto et al. presented a level set-based topology optimization method for an acoustic problem, designing noise barriers formed by an assembly of scatterers [142]. Maximiza-

tion of heat conduction is another major area of research [143, 144, 145], and minimum mean compliance problems, the most common shape and topology optimization problem, has also been investigated [132]. Other interesting applications include the optimization of structural vibration eigenvalues [146, 147], multiphysics actuators [148], piezoelectric actuators [149], and fluid problems [150, 151, 152].

In this dissertation, a level set-based topology optimization method incorporating a fictitious interface energy derived from the phase field concept [137] is developed for the design of acoustic metamaterials. A brief introduction of this method is presented below.

As shown in Fig. 3-1, the three-dimensional level set function is intersected by a two-dimensional plane, generally at zero height, the so-called iso-surface of the level set function. This iso-surface can be used to represent the structural boundaries of the optimal configuration between a material domain Ω and a non-material or void domain $D\backslash\Omega$ in a fixed design domain Ω. In the level set-based topology optimization method, the boundary is expressed by the level set function as follows.

$$\begin{cases} -1 \leq \phi(\mathbf{x}) < 0 & \text{for} \quad \forall \mathbf{x} \in D\backslash\Omega \\ \phi(\mathbf{x}) = 0 & \text{for} \quad \forall \mathbf{x} \in \partial\Omega \\ 0 < \phi(\mathbf{x}) \leq 1 & \text{for} \quad \forall \mathbf{x} \in \Omega\backslash\partial\Omega \end{cases} \tag{3.4}$$

According to the above mathematical definition, the values of level set function $\phi(\mathbf{x})$ range between -1 and 1. Negative values represent the void domain, positive values represent the material domain, and a value of zero represents a structural boundary.

In the level set-based topology optimization method, the topology optimization problem that determines the optimal configuration of a structure in the fixed design domain can be described as follows.

$$\begin{aligned} &\inf_{\phi} \; F[\chi_\phi, \phi] = \textstyle\int_D f(\mathbf{x})\chi_\phi[\phi]\mathrm{d}\Omega \\ &\text{subject to} \quad V[\chi_\phi] = \textstyle\int_D \chi_\phi[\phi]\mathrm{d}\Omega - V_{\max} \leq 0 \end{aligned} \tag{3.5}$$

The characteristic function $\chi_\phi[\phi]$ which employs the level set function $\phi(\mathbf{x})$ as its variable is introduced as

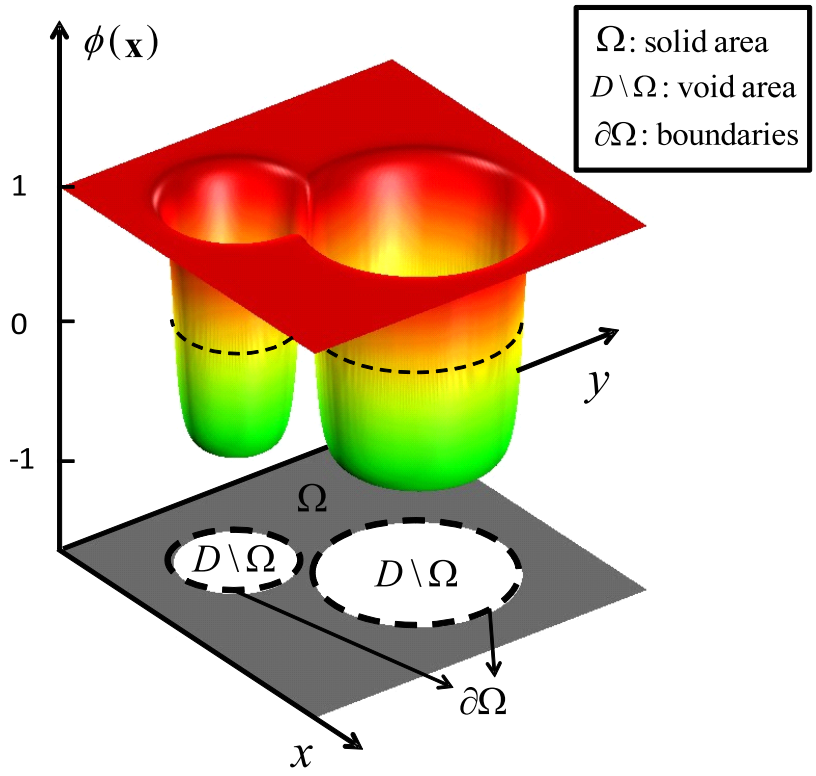

Figure 3-1: Level set function $\phi(\mathbf{x})$

.

$$\chi_\phi[\phi] = \begin{cases} 1 & \text{if} \quad \phi \geq 0 \\ 0 & \text{if} \quad \phi < 0 \end{cases} \tag{3.6}$$

As in Eq. (3.4), values of 1 represent solid material including structural boundaries, and values of 0 represent void domains.

Since the characteristic function $\chi_\phi[\phi]$ can be discontinuous at every point in the fixed design domain, the above topology optimization problem is an ill-posed problem which needs to be regularized. A fictitious interface energy based on the phase field model, the so-called Tikhonov regularization method, is introduced to regularize the optimization problem [137]. By adding a fictitious interface energy term to the original objective functional, the regularized topology optimization problem is defined as follows.

$$\begin{aligned} &\inf_{\phi} \; F_R[\chi_\phi, \phi] = F[\chi_\phi, \phi] + R[\phi] \\ &\text{subject to} \quad V[\chi_\phi] \leq 0 \end{aligned} \tag{3.7}$$

where F_R is the regularized objective functional, $R[\phi]$ is the fictitious interface energy term, expressed as follows.

$$R[\phi] = \int_D \frac{1}{2}\tau |\bigtriangledown \phi|^2 \, \mathrm{d}\Omega \tag{3.8}$$

where $\tau > 0$ is a regularization parameter that represents the extent of the regularization (the ratio of the fictitious interface energy and the value of the objective functional). The optimization problem formulated with constraints is now replaced with an unconstrained formulation using Lagrange's method as follows, assuming that $\bar{F_R}$ is the regularized Lagrangian and λ is the Lagrange multiplier of the volume constraint.

$$\inf_{\phi} \; \bar{F_R}[\chi_\phi, \phi] = F[\chi_\phi] + \lambda V[\chi_\phi] + R[\phi] \tag{3.9}$$

The KKT-conditions for the above problem are now derived as follows.

$$\begin{aligned} &\langle \mathrm{d}\bar{F_R}[\chi_\phi, \phi]/\mathrm{d}\phi, \Phi \rangle = 0 \\ &\lambda V[\chi_\phi] = 0 \\ &\lambda \geq 0 \\ &V[\chi_\phi] \leq 0 \end{aligned} \tag{3.10}$$

where $\langle \mathrm{d}\bar{F_R}[\chi_\phi, \phi]/\mathrm{d}\phi, \Phi \rangle$ represents the Fréchet differential.

A level set function that describes the optimal configuration is a candidate solution to the above KKT conditions, but directly solving Eq. (3.10) is impractical, so we replace the optimization problem with a time evolutional problem that indicates structural changes in the fixed design domain, which progress as time is incremented, as follows.

$$\partial \phi / \partial t = -K[\phi] \bar{F_R'} \tag{3.11}$$

where t is a fictitious time and $K[\phi] > 0$ is a coefficient of proportionality, assuming

that the variation of the level set function with respect to t, $\partial\phi/\partial t$, is proportional to the derivative of the regularized Lagrangian $\bar{F}'_R$.

Then, the variation of the level set function can be replaced by the derivative of Lagrangian $\bar{F}'$ in this method, obtained as follows.

$$\begin{cases} \partial\phi/\partial t = -K[\phi]\left(\bar{F}' - \tau\nabla^2\phi\right) & \text{in} \quad D \\ \partial\phi/\partial n = 0 & \text{on} \quad \partial D \backslash \partial D_N \\ \phi = 1 & \text{on} \quad \partial D_N \end{cases} \tag{3.12}$$

where D_N represents the non-design domain. As a result, the level set function, representing the optimal configuration of the topology optimization problem, is updated by the time evolutionary equation, i.e., the reaction-diffusion equation.

3.3 Level set-based topology optimization for wave propagation problems

During the last few years, much work has been focused on extending level set-based topology optimization approaches to the field of wave propagation designs. Yamasaki et al. [153] and Hirayama et al. [154] obtained optimal designs of waveguides using level set methods applied electric field phenomena. Fujii et al. [155] applied a level set-based topology optimization method [137] for the design of an optical cloaking device. For magnetic field problems, designs for waveguides made of ferrite material that maximize power transmission have been obtained using level set-based topology optimizations [156]. For electromagnetic field problems, many applicable designs have also been obtained using level set-based topology optimizations for dipole antennas [157] and electromagnetic cloaks composed of ferrite material [158]. Designs for novel composite materials, so-called electromagnetic metamaterials that are analogous to acoustic metamaterials, have also been successfully obtained using level set-based topology optimization methods. Yamasaki et al. have designed a composite transmission line consisting of a waveguide and periodically located dielectric resonators to obtain desired dispersion properties [159]. Otomori et al.

[160] and Zhou et al. [161] achieved metamaterial designs that exhibit negative permeability, and Zhou et al. achieved metamaterial designs that show both negative permittivity and negative permeability [162].

Level set-based topology optimization design methods have been much more widely used for electric, magnetic, and electromagnetic field problems than for acoustic problems. In 2011, Shu et al. proposed a level set based structural topology optimization method for the optimal design of a coupled structural-acoustic system for interior noise reduction [163]. But until now, no topology optimization method has been proposed for application to acoustic metamaterial design problems.

3.4 Conclusion

Conventional density-based topology optimization approaches typically encounter the problem of grayscales and other numerical instability problems such as mesh dependencies and checkerboard patterns. On the other hand, level set-based topology optimization, a different type of topology optimization that combines topology optimization and the level set method, can yield optimal shapes free of grayscales and overcome the problems of checkerboard patterns. However, mesh dependencies may still be a factor. Later, a level set-based topology optimization method incorporating a fictitious interface energy derived from the phase field concept was proposed, which does not require reinitialization operations.

The unique characteristics of acoustic metamaterials make it difficult to design such materials based on experience or theoretical analysis, since the relationship between their structures and characteristics is difficult to grasp. Thus, a systematic structural design methodology such as topology optimization is useful to achieve optimal designs of acoustic metamaterials. In this dissertation, designs of acoustic metamaterials based on a level set-based topology optimization method incorporating a fictitious interface energy will be discussed.

Chapter 4

Design of acoustic metamaterial with negative bulk modulus

4.1 Introduction

Materials that can be artificially designed to exhibit special properties have recently generated intense discussion and interest, so-called metamaterials. Metamaterials are generally defined as artificially created composite materials with novel properties that emerge due to their structure, rather than the properties of the materials they are composed of. They initially gained attention in the field of electromagnetic (EM) wave propagation, with novel properties and behavior enabling the design of innovative devices not possible with naturally occurring substances. Research on metamaterials first began in 1967, when a Russian scholar, Viktor G. Veselago, proposed a daring and intriguing question concerning electromagnetic wave propagation in materials: what would happen if both the permittivity and permeability of a material were assumed to be negative [164, 165]? It took roughly 30 years for researchers to treat this question seriously. After considerable theoretical and experimental efforts, Pendry et al. [166, 167] and Smith et al. [168] were able to create artificial materials with negative permittivity and permeability, leading to observations of negative refractive indices. Thenceforward, research concerning the novel properties of metamaterials flourished and diverse applications have been explored and developed, including a superlens [169], waveguides [170], and electromagnetic cloaking [171].

In addition to the study of metamaterials subject to EM waves, materials that display analogous behavior in the acoustic realm have also been explored. Acoustic metamaterials are periodic structures, artificially designed to solve various acoustic problems of sound propagation. This chapter is aimed to design an acoustic metamaterial in which the effective bulk modulus is negative in the sense of an effectively homogeneous medium, by developing a new level set-based topology optimization method. Acoustic and electromagnetic waves are obviously different from the standpoint of their physical properties. Acoustic waves are full-vector waves, a combination of transverse and longitudinal waves, describable in terms of pressures and particle velocities, whereas both electric and magnetic waves are pure transverse waves. However, the two wave systems share certain physical concepts, such as wave vectors, wave impedance, and power flow, implying that approaches used to study electromagnetic metamaterials might also be effective in acoustic metamaterial research. Experience gained through initial investigations of electromagnetic metamaterials led to active research and development of acoustic metamaterials, especially from 2000, when Liu et al. fabricated sonic crystals [3]. In 2003, P. Sheng et al. also fabricated a microscopic composite which displayed localized sonic resonances at 350-2000 Hz [4]. In 2004, split-ring resonators (SRRs) were explored in acoustic metamaterial research [6]. The first flat acoustic metamaterial lens, composed of a planar network of subwavelength Helmholtz resonators, was presented by Shu Zhang et al. in 2009, with practical implications for high-resolution ultrasound imaging, non-destructive structural testing of buildings and bridges, and novel underwater stealth technology [42]. An acoustic cloak, a technology that renders underwater objects invisible to sonar and other ultrasound waves, was demonstrated by a team of Illinois researchers in 2011 [65]. In addition to the above research mainly dealing with experimental development of novel properties and applications, some research has focused on theoretical approaches, such as composites with inclusions having negative bulk modulus [172], modifications of Newton's second law to describe the motion of the bodies whose effective density is anisotropic [50], and the design of cloaking devices by manipulating conventional elastodynamic equations [173].

Prior to 2000, research on artificial materials used to control acoustic wave propagation started with phononic crystals, so-called sonic crystals that are artificial structures

composed of a periodic array of acoustic scatterers embedded in a homogeneous matrix material. Such materials are analogues of photonic crystals. The lattice constant of such materials is comparable to the wavelength, as described in Bragg scattering theory, so the crystals are too large to function in real-world examples. As mentioned above, Liu et al. overcame this obstacle and pioneered the use of localized resonant mechanisms by fabricating a new type of composite, based on 5 mm diameter lead spheres coated with silicone rubber, which behaved as a material with a negative longitudinal elastic modulus and exhibited large elastic wave band gaps in certain sonic frequency ranges. Later, A. B. Movchan et al. presented an asymptotic analysis of a periodic structure composed of split-ring resonators, to control low-frequency bandgaps [6]. M. Hirsekorn performed numerical local interaction simulations of a locally resonant sonic crystal composed of an array of silicone rubber-coated hollow steel cylinders embedded in an epoxy matrix, which exhibited several strong attenuation bands at frequencies between 0.3 and 6.0 kHz [174]. Inspired by Liu et al., Xiaoming Zhou et al. further proposed two composites based on different materials, to examine the physical mechanisms of elastic metamaterials with local resonances [43]. B. S. Lazarov and J. S. Jensen studied wave propagation in a one-dimensional spring-mass system with attached local oscillators, with a bandgap located near the resonant frequency of the oscillators [175]. And H. H. Huang et al. presented a one-dimensional mass-in-mass lattice model to illustrate their method of designing an acoustic metamaterial based on local resonance [176].

After 2000, research on acoustic metamaterials entered a new stage due to an investigation of locally resonant sonic materials by Liu et al., who coated dense metal spheres with soft silicone rubber and encased these in epoxy resin [3]. The resulting metamaterial exhibited strong sound attenuation band gaps in particular sonic frequency ranges, and additionally, the new created structure had a lattice constant an order of magnitude functionally smaller than the corresponding sonic wavelength in air, in contrast to conventional composites that have much larger lattice constants that arise due to Bragg scattering [177]. Moreover, the comparatively minuscule size of the functional components in these acoustic metamaterials enabled numerical analysis using effective parameters.

Similar to electromagnetic metamaterials built from arrays of small structures, acoustic

metamaterials are typically constructed as periodic arrays of acoustically scattering elements embedded in a homogeneous matrix material, with a periodicity that is considerably smaller than the wavelength of the local region (inclusion and background). For analysis, it is meaningful and valid to replace the entire composite by an effective medium. Following this practice, the acoustic metamaterial can be dealt with as a whole rather than as a collection of different components. To date, several methods have been proposed for the extraction of the effective parameters. Nicholas Fang et al. calculated the effective modulus by building an ultrasonic metamaterial composed of resonators, an analogue to an inductor-capacitor circuit [5]. P. Sheng derived formulas for effective parameters using the coherent potential approximation method [178]. Jensen Li et al. extracted the effective surface impedance by using the half-space reflection amplitude [40]. The effective mass density and effective bulk modulus can be easily obtained from the effective impedance. Additionally, reflection and transmission coefficients are also helpful and widely used to compute the effective material properties of acoustic metamaterials. Vladimir Fokin et al. developed a method for extracting the effective material properties of acoustic metamaterials using reflection and transmission coefficients, and discussed the details of this method, including the sign selection of the refractive index and impedance, and the correct branch number of the real part of the refractive index [179].

Here, a topology optimization numerical method, a kind of structural optimization method that determines design features such as the number, location, and shape of holes in a structure, is developed. Among structural optimization approaches, topology optimization offers the highest degree of design freedom, in addition to high levels of performance, since the topology as well as the shape of target structures can be evolved during the optimization process. In topology optimization methods, the optimization problem is replaced by a material distribution problem within a fixed design domain. The fundamental engineered approach was initially proposed by Bendsøe and Kikuchi in 1988 [77] and Bendsøe in 1989 [180]. The material distribution method in topology optimization has been examined in a large number of examples, for acoustic problems [181, 182, 117], fluid problems [100], electromagnetic problems [183], and for electromagnetic metamaterials [109], in which Diaz and Sigmund presented a topology optimization method for the design of

metamaterials with negative permeability. Topology optimization methods can efficiently generate optimal topologies and optimal shapes, facilitate the design of practical structures, and optimize support conditions. Moreover, topology optimization methods have proven to be flexible and reliable design tools. The methodology has, over the last two decades, become fairly widespread in industrial applications, especially among major car manufacturers [116]. But until now, no topology optimization method has been proposed for application to acoustic metamaterial design problems.

To enable topological changes in a structure during optimization, i.e., an increase or decrease in the number of holes, Bendsøe and Kikuchi [77] established a topology optimization methodology by introducing a characteristic function, first proposed by F. Murat and L. Tartar [184]. This characteristic function defined discrete values of 0 or 1 in an expanded fixed design domain that includes the original design domain, to delineate an optimal structure. However, since the function is defined according to discrete values in infinitely small domains, discontinuity is a significant problem; in other words, the design problem becomes ill-posed. To solve this problem, the discontinuous function must be replaced by a continuous one; that is, the design domain must be relaxed. To conduct this relaxation mathematically, relaxation methods based on the homogenization method [77] and the density method [180] have been proposed, but these methods encounter problems of numerical instability, such as mesh dependency, so checkerboard patterns or grayscale areas often are included in optimal configurations, a consequence of intermediate density values between 0 and 1. Much work, including various proposed filtering schemes [85, 86, 84, 185], has been done to deal with the problem of grayscales and provide optimized configurations that have clear boundaries.

Level set-based topology optimization methods can directly provide optimal configurations that do not include grayscales. Wei et al. adopted and updated a level set-based method to obtain sharp corners and clear boundaries [136]. Additionally, level set-based topology optimization methods can avoid distortion of the mesh used in finite element analysis that can be problematic in regular shape optimization methods. In this chapter, a level set-based method for acoustic metamaterial design problems is adopted, where the level set function is updated based on a reaction-diffusion equation developed by Yamada

et al. [137], rather than using an updating scheme based on the Hamilton-Jacobi equation [129, 130]. This level set-based topology optimization method has been successfully applied to a range of material and structural problems, including minimum mean compliance problems, the optimum design of compliant mechanisms, lowest eigenfrequency maximization problems, heat diffusion maximization, and electromagnetic wave propagation. Recently, this level set-based method was successfully applied to design electromagnetic metamaterials [160], who applied it to the design of dielectric metamaterials. Here, a level set-based topology optimization method incorporating a fictitious interface energy derived from the phase field concept is applied to the design of acoustic metamaterials for the first time.

In the following sections of this chapter, a level set-based topology optimization method was proposed for the design of an acoustic metamaterial that achieves a negative bulk modulus, which may lead to interesting applications. First, several essential theories are introduced and the optimization problem is formulated in Section 4.2. The numerical implementation pertaining to the design variables for the acoustic problem and the optimization flowchart are presented in Section 4.3. In Section 4.4, to demonstrate the feasibility of the proposed method, several numerical examples were presented, dealing with different target frequencies, initial configurations and material properties. The final section sums up the results and provides conclusions.

4.2 Formulation

4.2.1 Governing equation of acoustic wave propagation problem

Suppose that p is the acoustic pressure, regarded as the state variable of the governing equation, ρ is the mass density, and κ is the bulk modulus. The Helmholtz equation is adopted as the governing equation for acoustic wave propagation in a single unit cell, Ω, under the assumption that only compressional waves are considered, as follows.

$$\bigtriangledown \cdot \left(\rho^{-1} \bigtriangledown p\right) + \omega^2 \kappa^{-1} p = 0 \tag{4.1}$$

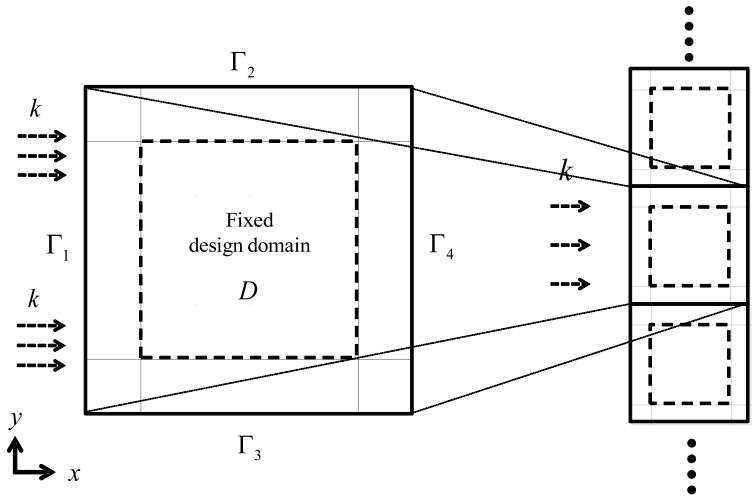

Figure 4-1: Fixed design domain and boundary conditions.

Figure 4-1 shows the analysis model, including the design domain and boundary settings. The design domain was defined to have two parts, i.e., a fixed design domain D and a non-design domain (void areas surrounding D), to simplify the sensitivity analysis, as discussed in subsection 3.1. As shown, this design problem is limited to a row of unit cells, with a single cell in the x direction and the periodic array of the metamaterial extending in the y direction. A longitudinal acoustic incident wave propagates in the direction normal to the left cell face, Γ_1, and the response is observed at the right boundary, indicated as Γ_4. Both Γ_1 and Γ_4 have radiation boundary conditions imposed, with unit pressure and minimal reflection, respectively. The upper and lower boundaries, Γ_2 and Γ_3, are set as periodic boundary conditions.

The boundary conditions are described by equations as follows.

$$\begin{cases} \mathbf{n} \cdot \left(\rho^{-1} \bigtriangledown p\right) = 2ik\rho^{-1}p^i - ik\rho^{-1}p & \text{on} \quad \Gamma_1 \\ \mathbf{n} \cdot \left(\rho^{-1} \bigtriangledown p\right) = -ik\rho^{-1}p & \text{on} \quad \Gamma_4 \\ p|_{\Gamma_2} = p|_{\Gamma_3} & \text{on} \quad \Gamma_2\,\Gamma_3 \end{cases} \tag{4.2}$$

where $\mathbf{n}$ is the normal vector, k is the wave number, i is an imaginary unit and p^i is the pressure of the incident wave. By denoting p^* as the test function corresponding to p, the weak form of Eqs. 4.1 and 4.2 is then derived as follows.

$$a(p,p^*) = l(p^*) \tag{4.3}$$

where

$$a(p,p^*) = \int_\Gamma p^* ik\rho^{-1} p \mathrm{d}\Gamma + \int_D (\bigtriangledown p)\cdot\left(\rho^{-1}\bigtriangledown p^*\right)\mathrm{d}\Omega - \int_D p^*\omega^2\kappa^{-1}p\mathrm{d}\Omega \tag{4.4}$$

$$l(p^*) = 2ik\int_\Gamma \rho^{-1} p^i p^* \mathrm{d}\Gamma \tag{4.5}$$

4.2.2 Effective bulk modulus

As introduced in Section 1, several approaches can be applied to compute the effective properties. In this chapter, an S-parameter-based approach was used, first proposed [186] and later extended to inhomogeneous cases [187] by Smith et al. S-parameters, also called scattering parameters, were first used to describe the electrical behavior of linear electrical networks. Later, C.M. de Blok and R.F.M. van den Brink described how S-parameters can be effectively used when calculating the relationship between input and output in acoustic networks, based on an electronic network analogy [188]. The S-parameters here have the same physical meaning as the reflection and transmission coefficients in [179]. In a two-port system, S_{11} and S_{22} represent the input reflection coefficient and output reflection coefficient, respectively, analogous to the R coefficient. Similarly, S_{21} represents the forward transmission coefficient, analogous to the T coefficient. Because it is expected that the optimal configuration after optimization will be symmetric about the y-axis, S_{22} was used in addition to S_{11}, and three S-parameters were applied to guarantee that the result will be symmetrical. In Smith et al.'s approach, three S-parameters, S_{11}, S_{21}, and S_{22}, were used. Sigmund [111] and Otomori et al. [160] successfully applied this approach to retrieve effective permeability values when designing dielectric metamaterials tailored for use at particular frequencies.

In our proposed method, p^i is the incident field, with p^{i*} as the complex conjugate

transposition of p^i, the S-parameters are expressed as follows.

$$S_{11} = \frac{\int_{\Gamma_1} \left(p - p^i\right) \cdot p^{i*} \mathrm{d}\Gamma}{\int_{\Gamma_1} p^i \cdot p^{i*} \mathrm{d}\Gamma} \tag{4.6}$$

$$S_{21} = \frac{\int_{\Gamma_4} p \cdot p^{i*} \mathrm{d}\Gamma}{\int_{\Gamma_1} p^i \cdot p^{i*} \mathrm{d}\Gamma} \tag{4.7}$$

$$S_{22} = \frac{\int_{\Gamma_4} \left(p - p^i\right) \cdot p^{i*} \mathrm{d}\Gamma}{\int_{\Gamma_4} p^i \cdot p^{i*} \mathrm{d}\Gamma} \tag{4.8}$$

The relative impedance z_e and refractive index n are then derived as follows, using the S-parameters, based on the method of Vladimir Fokin et al. [179].

$$z_e = \pm \sqrt{\frac{\left(1 + S_{11}\right)\left(1 + S_{22}\right) - S_{21}^2}{\left(1 - S_{11}\right)\left(1 - S_{22}\right) - S_{21}^2}} \tag{4.9}$$

$$n = \pm \frac{\cos^{-1}\left(\beta / 2S_{21}\right)}{kd} \tag{4.10}$$

$$\beta = 1 - \left(S_{11}S_{22} - S_{21}^2\right) \tag{4.11}$$

where d is the width of the unit cell. Concerning sign selection in Eqs. 4.9 and 4.10, additional requirements were imposed on the metamaterial properties. This design was aimed to be limited to passive metamaterial structures that exhibit energy losses as acoustic waves are converted into other energy forms, and also exhibit strongly frequency-dependent properties, useful for narrow bandwidth applications. Thus the real part of the impedance z_e is required to be positive. In addition, since the imaginary part of the speed of sound should be positive, the imaginary part of the refractive index n is required to be positive [189]. Thus, the requirements that determine the signs in Eqs. 4.9 and 4.10 are as follows.

$$z_e' \geq 0 \tag{4.12}$$

$$n'' \geq 0 \tag{4.13}$$

where $(\cdot)'$ and $(\cdot)''$ respectively denote the operators for real and imaginary parts of the parameters. Due to the differences between the physical and electromagnetic properties in a metamaterial, a specific expression is needed for the effective bulk modulus K_e for the acoustic metamaterial, but the effective bulk modulus is also expressed by the effective impedance and refractive index, as is the effective permeability. A number of methods for deriving the effective material properties are discussed in the literature, two of which, have been widely used and are easily applied. In one approach, developed by Vladimir Fokin et al. in 2007 [179], the effective material properties of acoustic metamaterials were extracted using reflection and transmission coefficients, and details, including sign selection for the refractive index and impedance, and the correct branch number of the real part of the refractive index, were discussed, using two coefficients, R and T (corresponding to S_{11} and S_{21} in this dissertation). This method was applied to compute the relative impedance z_e and refractive index n from S-parameters. The other approach, developed by Jensen Li et al. [40], can directly handle effective material properties and is applied here to compute the effective bulk modulus κ_e from z_e and n. Three S-parameters were used to ensure that the obtained optimal configurations are symmetrical.

κ_0, ρ_0, and c_0 are respectively represented as the bulk modulus, mass density of the background material, and the speed of sound in the background material. Furthermore, the effective impedance in the fixed design domain and the acoustic impedance of the background material are respectively represented as $Z_e = z_e Z_0$ and z_0. Then, the effective bulk modulus κ_e can then be computed based on three S-parameters, using the following equation:

$$\kappa_e = Z_e \kappa_0 / (c_0 n \rho_0) \tag{4.14}$$

4.2.3 Formulation of optimization problem

Although acoustic metamaterials are regarded as acoustic counterparts of electromagnetic metamaterials, there are nevertheless certain differences that must be taken into account in the design of these two metamaterials. While electromagnetic metamaterials can be engi-

neered by achieving negative permeability, this property is also observed in certain natural materials. For an acoustic metamaterial, however, since no natural material exhibits negative mass density or negative bulk modulus, these properties must be achieved artificially. Physically, a negative mass density implies that force and movement vectors are expressed in opposite directions, and a negative bulk modulus implies that a medium expands in response to compressive forces at a certain frequency.

In this chapter, the optimization problem was formulated so that the real part of the effective bulk modulus is extremely negative at a certain frequency, to achieve an acoustic metamaterial that has novel properties. A single negative property (negative bulk modulus or negative mass density) also can be effective in certain applications, such as achieving an acoustic bandgap (applied for sound barrier etc.) and superlens designs [5]. To obtain this condition through an optimization procedure, the objective of the optimization problem is formulated to find a material distribution within the fixed design domain that minimizes the real part of the effective bulk modulus at a desired frequency. Figure 4-2 shows one example of a typical effective bulk modulus curve, where 'Real' and 'Imag' represent the real and imaginary parts of the effective bulk modulus, respectively. The figure illustrates that the real part of the effective bulk modulus has values that include a positive peak as well as a dip below zero, while the imaginary part of the effective bulk modulus is singly convex. Thus, the desired condition of negative bulk modulus is reflected in the dip of the real part of the effective bulk modulus, where its value is less than zero. Considering the different characteristics of the effective bulk modulus curve, if it was attempted to directly minimize the real part of the effective bulk modulus when the positive peak lies between the initial dip and the target frequency, an optimized configuration cannot be obtained because the level set function must be updated to a smaller value of the objective function compared with that of the previous iteration. Take Fig. 4-2 as an example, if the initial peak lies between the target frequency and the dip, say f_2 as the target frequency in Fig. 4-2, when it was attempted to directly minimize the real part of the effective bulk modulus, the optimization will fail or take an excessively long time to find the desired value. Consequently, the curve of the real part of the effective bulk modulus will be displaced toward the left as a whole because the level set function must be updated to a smaller value of the objective function

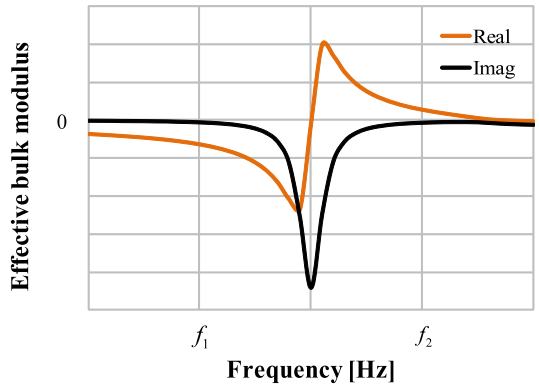

Figure 4-2: A typical effective bulk modulus curve.

compared with that of the previous iteration. There is another case that the initial dip in the real part of the effective bulk modulus line lies between the target frequency and the positive peak, for example, if the target frequency were f_1 in Fig. 4-2, the optimization process could be simplified to minimize the real part of the effective bulk modulus directly in a single step. To allow for all of these possibilities, two-step optimization approach was employed in which the optimization is conducted in two steps, was also successfully applied for the design of dielectric metamaterials with negative permeability [160, 111].

Denote F as the objective functional, and κ_e'' the imaginary part of the effective bulk modulus. In the first step of the optimization procedure, the imaginary part of the effective bulk modulus is minimized:

$$\begin{aligned} &\inf_{\phi} \; F = \kappa_e'' \\ &\text{subject to} \quad \text{Governingequation} \\ &\qquad\qquad\quad \text{Boundaryconditions} \end{aligned} \tag{4.15}$$

After the first step, the obtained results are used as the initial shape for the second step of the optimization procedure, whose objective is to minimize the real part of the effective bulk modulus κ_e'':

$$\begin{aligned} &\inf_{\phi} \; F = \kappa_e' \\ &\text{subject to} \quad \text{Governingequation} \\ &\qquad\qquad\quad \text{Boundaryconditions} \end{aligned} \tag{4.16}$$

4.2.4 Level set-based topology optimization method

Level set methods employ numerical techniques that are used to track moving interfaces, by intersecting the level set function $\phi(\mathbf{x})$ at zero height, with the isocontours of the level set function introduced to implicitly represent the boundary $\partial\Omega$ between the material and the void domains that expresses the structural shape. In this chapter, an improved level set-based topology optimization method was employed, which uses a fictitious interface energy, based on the phase field model [137], which is a combination of topology optimization and the level set method. Suppose that D is the fixed design domain and Ω is a material part in the fixed design domain. A void domain in the fixed design domain is then denoted as $D\backslash\Omega$. The formulation of the boundary expressions of level set method is as follows.

$$\begin{cases} 0 < \phi(\mathbf{x}) \leq 1 & \text{if} \quad \forall \mathbf{x} \in \Omega\backslash\partial\Omega \\ \phi(\mathbf{x}) = 0 & \text{if} \quad \forall \mathbf{x} \in \partial\Omega \\ -1 \leq \phi(\mathbf{x}) < 0 & \text{if} \quad \forall \mathbf{x} \in D\backslash\Omega \end{cases} \tag{4.17}$$

The characteristic function $\chi_\phi(\phi)$ is defined by

$$\chi_\phi(\phi) = \begin{cases} 1 & \text{if} \quad \phi \geq 0 \\ 0 & \text{if} \quad \phi < 0 \end{cases} \tag{4.18}$$

Then the structural optimization problem is replaced by a material distribution problem, and the structural optimization problem was formulated that minimizes the objective functional Fsubject to a volume constraint V as follows, in which f is a density function of the objective functional and $V_{\max}$ is the upper limit of the volume constraint.

$$\begin{aligned} &\inf_{\phi} \; F(\chi_\phi(\phi)) = \textstyle\int_D f(\mathbf{x})\chi_\phi(\phi(\mathbf{x}))\,\mathrm{d}\Omega \\ &\text{subject to} \quad V(\chi_\phi(\phi)) = \textstyle\int_D \chi_\phi(\phi(\mathbf{x}))\mathrm{d}\Omega - V_{\max} \leq 0 \end{aligned} \tag{4.19}$$

However, the above formulation is an ill-posed problem, due to the discontinuity of the characteristic function in the fixed design domain, so the Tikhonov regularization method [137] was used to regularize the optimization problem. The original optimization problem is therefore replaced with an energy minimization problem, namely, minimization of the sum of the original objective function and the fictitious interface energy. Let F_R be the regularized objective functional and τ be a regularization parameter that represents the extent of the regularization. The optimization problem is then regularized as follows.

$$\begin{aligned} &\inf_{\phi} \; F_R(\chi_\phi(\phi)) = \textstyle\int_D f(\mathbf{x})\chi_\phi(\phi(\mathbf{x}))\,\mathrm{d}\Omega + \int_D \frac{1}{2}\tau\,|\bigtriangledown\phi|^2\,\mathrm{d}\Omega \\ &\text{subject to} \quad V(\chi_\phi(\phi)) = \textstyle\int_D \chi_\phi(\phi(\mathbf{x}))\mathrm{d}\Omega - V_{\max} \leq 0 \end{aligned} \tag{4.20}$$

Next, the optimization problem is reformulated, using Lagrange's method of undetermined multipliers, without constraints. Suppose that F_R is the regularized Lagrangian and that λ is the Lagrange multiplier of the volume constraint.

$$\inf_{\phi} \; \bar{F_R}(\chi_\phi(\phi)) = \int_D f(\mathbf{x})\chi_\phi(\phi(\mathbf{x}))\,\mathrm{d}\Omega + \lambda V + \int_D \frac{1}{2}\tau\,|\bigtriangledown\phi|^2\,\mathrm{d}\Omega \tag{4.21}$$

Now, the KKT-conditions for the above problem are derived by making $\langle \mathrm{d}\bar{F_R}\left(\chi_\phi(\phi)\right)/\mathrm{d}\phi, \Phi\rangle$ represent the Fréchet differential of the regularized Lagrangian $\bar{F_R}$ with respect to ϕ in the direction of Φ, as follows.

$$\left\langle \frac{\mathrm{d}\bar{F_R}\left(\chi_\phi(\phi)\right)}{\mathrm{d}\phi}, \Phi \right\rangle = 0, \lambda V\left(\chi_\phi(\phi)\right) = 0, \lambda \geq 0, G \leq 0 \tag{4.22}$$

To find a solution to this level set function, which represents an optimized configuration, the KKT-conditions are derived, but solving them directly is impossible, so the optimization problem is replaced by a time evolutional problem, as follows. By introducing a fictitious time t and assuming that the variation of the level set function with respect to t is proportional to the gradient of the regularized Lagrangian F_R, it is obtained

$$\frac{\partial \phi}{\partial t} = -K(\phi)\frac{\mathrm{d}\bar{F_R}}{\mathrm{d}\phi} \tag{4.23}$$

where $K(\phi) > 0$ is a coefficient of proportionality. It was noted that the derivative of $\bar{F_R}$ with respect to ϕ is equivalent to its topological derivative, $\mathrm{d}\bar{F}\left(\chi_\phi\right)/\mathrm{d}\chi_\phi$. Finally, the variation of the level set function used to obtain the optimized configuration can be replaced by the derivative of Lagrangian $\mathrm{d}\bar{F}\left(\chi_\phi\right)/\mathrm{d}\chi_\phi$, so that the time evolutionary equation, i.e., the reaction-diffusion equation with boundary conditions, is obtained as follows.

$$\begin{cases} \frac{\partial \phi}{\partial t} = -K(\phi)\left(\frac{\mathrm{d}\bar{F}}{\mathrm{d}\chi_\phi} - \tau|\bigtriangledown\phi|^2\right) & \text{in} \quad D \\ \frac{\partial \phi}{\partial n} = 0 & \text{on} \quad \partial D \backslash \partial D_N \\ \phi = 1 & \text{on} \quad \partial D_N \end{cases} \tag{4.24}$$

4.2.5 Sensitivity analysis

The adjoint variable method (AVM) was used for the sensitivity analysis of the effective bulk modulus minimization problem. With p_{ij}^* as the adjoint variable with respect to S_{ij}, the Lagrangian of the optimization problem is

$$\bar{F} = F - \sum_{ij}\left[a\left(p, p_{ij}^*\right) - l\left(p_{ij}^*\right)\right] + \lambda V, \; ij = 11, 21, 22 \tag{4.25}$$

The evolution of the optimized structure boundary is conducted by updating the level set function based on the variation of the Lagrangian, using a reaction diffusion equation. The variation of the Lagrangian is obtained by the AVM as follows.

$$\begin{aligned} \left\langle \frac{\mathrm{d}\bar{F}}{\mathrm{d}\chi_\phi}, \chi_\phi^* \right\rangle = & \sum_{ij}\left\langle \frac{\partial F}{\partial S_{ij}}, S_{ij}^* \right\rangle \left\langle \frac{\partial S_{ij}}{\partial p}, p_{ij}^* \right\rangle \left\langle \frac{\partial p}{\partial \chi_\phi}, \chi_\phi^* \right\rangle \\ & - \sum_{ij}\left(\left\langle \frac{\partial a}{\partial p}, p_{ij}^* \right\rangle \left\langle \frac{\partial p}{\partial \chi_\phi}, \chi_\phi^* \right\rangle + \left\langle \frac{\partial a}{\partial \chi_\phi}, \chi_\phi^* \right\rangle\right) \\ & + \lambda \left\langle \frac{\partial V}{\partial \chi_\phi}, \chi_\phi^* \right\rangle, \; ij = 11, 21, 22 \end{aligned} \tag{4.26}$$

where $\mathrm{d}\bar{F}/\mathrm{d}\chi_\phi$ is the Fréchet differential of the Lagrangian with respect to the characteristic function.

In order to cancel out the $\langle \partial p/\partial \chi_\phi, \chi_\phi^* \rangle$ term, make $\alpha_{ij} = \langle \partial F/\partial S_{ij}, S_{ij}^* \rangle$. Rewriting Eq. (4.26) it is obtained

$$\begin{aligned}\left\langle \frac{\mathrm{d}\bar{F}}{\mathrm{d}\chi_\phi}, \chi_\phi^* \right\rangle =& \sum_{ij} \left(\left\langle \frac{\partial F}{\partial S_{ij}}, S_{ij}^* \right\rangle \left\langle \frac{\partial S_{ij}}{\partial p}, p_{ij}^* \right\rangle - \left\langle \frac{\partial a}{\partial p}, p_{ij}^* \right\rangle \right) \left\langle \frac{\partial p}{\partial \chi_\phi}, \chi_\phi^* \right\rangle \\ & - \sum_{ij} \left\langle \frac{\partial a}{\partial \chi_\phi}, \chi_\phi^* \right\rangle + \lambda \left\langle \frac{\partial V}{\partial \chi_\phi}, \chi_\phi^* \right\rangle,\ ij = 11, 21, 22\end{aligned} \tag{4.27}$$

To obtain the solution for p_{ij}^*, solve the following equation.

$$\left\langle \frac{\partial a}{\partial p}, p_{ij}^* \right\rangle = \left\langle \frac{\partial F}{\partial S_{ij}}, S_{ij}^* \right\rangle \left\langle \frac{\partial S_{ij}}{\partial p}, p_{ij}^* \right\rangle,\ ij = 11, 21, 22 \tag{4.28}$$

Finally, the variation of the Lagrangian is calculated using the following equation.

$$\left\langle \frac{\mathrm{d}\bar{F}}{\mathrm{d}\chi_\phi}, \chi_\phi^* \right\rangle = -\sum_{ij} \left\langle \frac{\partial a}{\partial \chi_\phi}, \chi_\phi^* \right\rangle + \lambda \left\langle \frac{\partial V}{\partial \chi_\phi}, \chi_\phi^* \right\rangle,\ ij = 11, 21, 22 \tag{4.29}$$

Here, $\langle \mathrm{d}\bar{F}/\mathrm{d}\chi_\phi, \chi_\phi^* \rangle$ is a complex function with real and imaginary parts, equal to the sensitivities of the real and imaginary parts of the objective function, respectively.

4.3 Numerical implementations

4.3.1 Design variables

In a level set-based topology optimization method, the level set function is used to describe the distribution of material and void areas inside a fixed design domain. Unlike an electromagnetic metamaterial design problem in which a single material property, electric permittivity, is used to define the fixed design domain, two acoustic properties were applied in this chapter, the mass density ρ and the bulk modulus κ. The speed of sound, c, can then be easily obtained using the relation $c = \sqrt{\kappa/\rho}$. By denoting ρ_1 and κ_1 as the properties of material areas, and ρ_0 and κ_0 as the properties of void areas (background areas), a reciprocal function was used to define the mass density and bulk modulus as the material properties to be optimized, using the characteristic function, χ_ϕ, as follows.

$$\rho^{-1} = \left(\rho_1^{-1} - \rho_0^{-1}\right)\chi_\phi(\phi) + \rho_0^{-1} \tag{4.30}$$

$$\kappa^{-1} = \left(\kappa_1^{-1} - \kappa_0^{-1}\right)\chi_\phi(\phi) + \kappa_0^{-1} \tag{4.31}$$

In the optimization implementation, the characteristic function χ_ϕ is approximated by the following Heaviside function, $H(\phi)$.

$$H(\phi) = \begin{cases} 0 & (\phi < -w) \\ \frac{1}{2} + \frac{\phi}{w}\left[\frac{15}{16} - \frac{\phi^2}{w^2}\left(\frac{5}{8} - \frac{3}{16}\frac{\phi^2}{w^2}\right)\right] & (-w \le \phi \le w) \\ 1 & (w \le \phi) \end{cases} \tag{4.32}$$

where w is the transition width of the Heaviside function which represents the width of the interface between two materials, set to a sufficiently small and real value.

Based on the definition of the material properties in Eqs. (4.30) and (4.31), the term in the variation of the Lagrangian in Eq. (4.29) can be derived as follows.

$$\begin{aligned} \left\langle \frac{\partial a}{\partial \chi_\phi}, \chi_\phi^* \right\rangle =& 2\int_D \left(\rho_1^{-1} - \rho_0^{-1}\right) \bigtriangledown p \cdot \bigtriangledown p^* \chi_\phi^* \mathrm{d}\Omega \\ & - \int_D \left(\kappa_1^{-1} - \kappa_0^{-1}\right) p \cdot p^* \cdot \omega^2 \cdot \chi_\phi^* \mathrm{d}\Omega \\ & + ik\int_\Gamma \left(\rho_1^{-1} - \rho_0^{-1}\right) p p^* \chi_\phi^* \mathrm{d}\Gamma \end{aligned} \tag{4.33}$$

In the calculation of $\langle \partial a/\partial \chi_\phi, \chi_\phi^* \rangle$, the third term to the right of the equals sign is defined on the exterior boundaries, beyond the fixed design domain, and thus can be ignored in the global expression. It was noted that, due to the adoption of a reciprocal function, the expression of the derivative of a is independent of the mass density ρ and the bulk modulus κ, the values of which change suddenly near the structural boundaries to achieve the clear boundaries that characterize level set-based topology optimization methods. This means that the sensitivities remain stable near these boundaries, and discontinuous sensitivity distributions are avoided. In short, the reciprocal formulation guarantees a continuous material distribution and the stability of the optimization procedure.

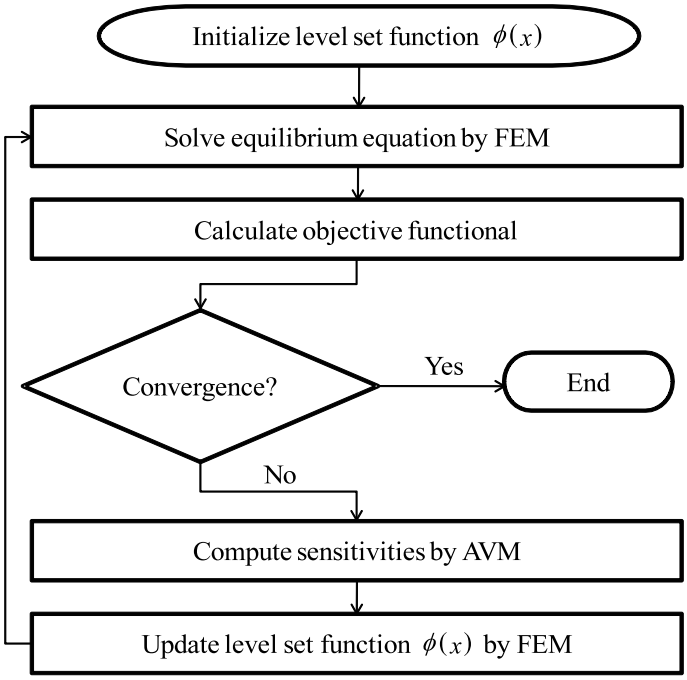

Figure 4-3: Flowchart of optimization procedure.

4.3.2 Optimization algorithm

The special characteristics of the effective bulk modulus curve of an acoustic metamaterial impel us to conduct a two-step optimization approach to achieve the target, which is to find the minimum of the effective bulk modulus at a desired frequency. In the first step, the imaginary part of the effective bulk modulus is minimized and the obtained result is then used as the initial configuration in the second step, during which the real part of the effective bulk modulus is minimized. The flowchart of the optimization procedure for these two steps is shown in Fig. 4-3.

4.4 Numerical examples

In this section, several numerical examples for the design of acoustic metamaterials are presented to illustrate how the proposed method finds material distributions that function as acoustic metamaterials with extremely negative bulk modulus at a desired frequency. Furthermore, it is observed that different low point position, initial configurations and material

properties have effects on the optimal results.

In all examples, the transition width of the Heaviside function w is set to 0.001. The regularization parameter τ is set to 0.0002. There is no volume constraint applied in the numerical examples.

4.4.1 Example 1: Effect of low point position in the initial configuration

In this subsection, negative effective bulk modulus minimization problems are presented considering frequencies that are either high or lower than that of the positive peak of the initial configuration in the graph of the real part of the effective bulk modulus versus the frequency. It is aimed to show the effectiveness of proposed method in finding an optimized distribution of materials in the fixed design domain, that is, the optimal shape of an acoustic metamaterial unit cell.

Figure 4-4 shows the design model with size indication. As with the model shown in Fig. 4-1, the size of the analysis domain is set to 30 mm $\times$ 30 mm and the fixed design domain is set to 20 mm $\times$ 20 mm. The fixed design domain D is discretized with a fine mapped mesh of 80 $\times$ 80 quadrilateral elements, which is used for the FEM analysis. Two different materials, the solid and background material, are used in the optimization. The bulk modulus of the solid material and the background material are set to 6.27×10^5 Pa and 2.15×10^9 Pa, respectively, and the mass densities are set to 1300 kg/m^3 and 1000 kg/m^3, respectively. In this example, the imaginary part of the bulk modulus of the solid material, namely, damping coefficients, was set as equal to 1% of the real part of the bulk modulus. An annular shape with a 2:1 outer/inner radius ratio and an inner radius of 4 mm is used as the initial configuration.

Minimization of effective bulk modulus at 1550 Hz

First, minimization of the effective bulk modulus is conducted with the target frequency set as 1550 Hz (target wavelength equal to 31.7 times of the width of unit cell d), which is lower than that of the positive peak of the initial configuration in the real part of the

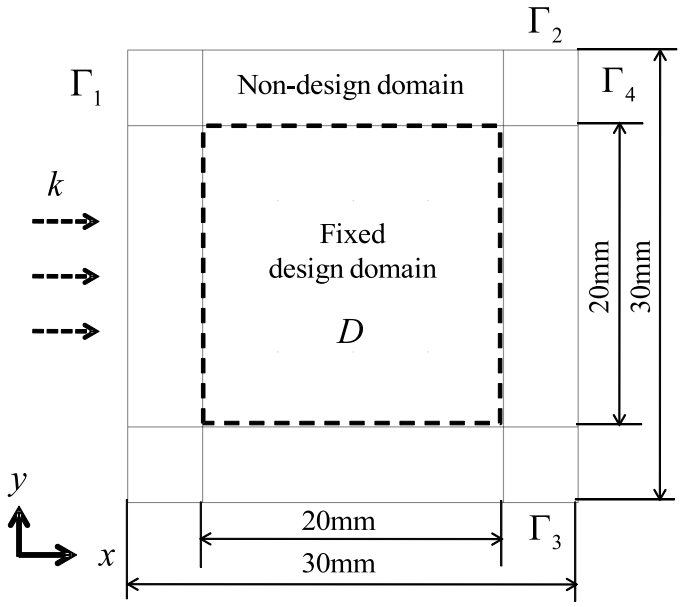

Figure 4-4: Analysis model, with size indications (Example 1, 2)

effective bulk modulus graph.

As introduced in the previous section, the optimization is conducted in two steps: the imaginary part of the effective bulk modulus is minimized first and then the real part is minimized. Figure 4-5 shows the initial configuration and the optimized configuration of the first step. In the figure, blue represents the solid material and white represents the background material. The effective bulk modulus curves for the initial configuration and the optimized distribution obtained after the first step are shown in Fig. 4-6. The imaginary part of the effective bulk modulus decreases gradually during the optimization process and reaches the low point at the desired frequency. The value of the imaginary part of the effective bulk modulus of the initial configuration at 1550 Hz is -7.78 Pa. After the 1st step optimization, this value at 1550 Hz is -4.14×10^4 Pa. Figure 4-7 shows the convergence history of changes in the imaginary part of the effective bulk modulus.

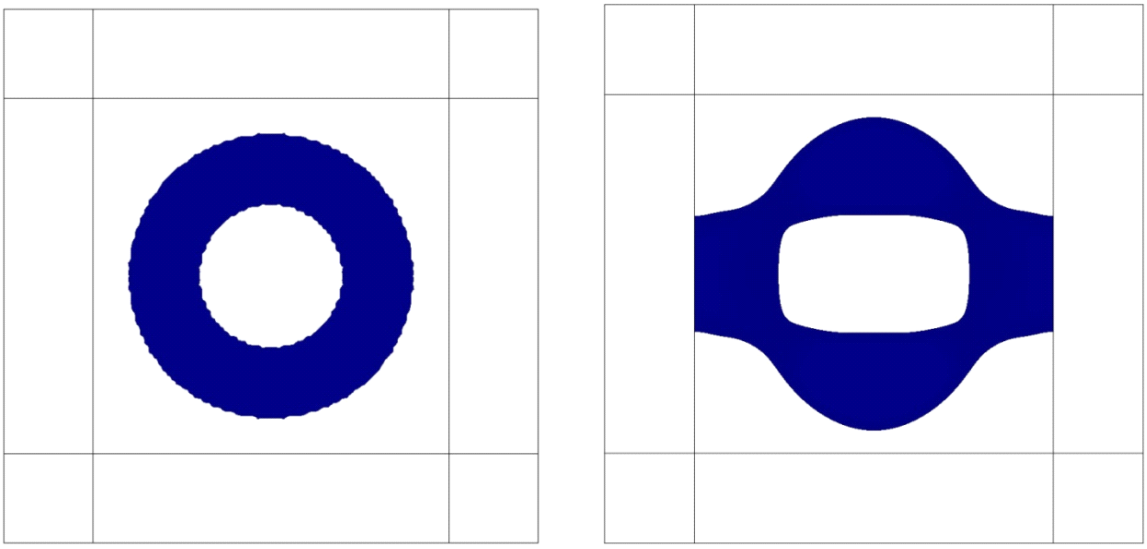

(a) initial; (b) the first step optimized.

Figure 4-5: Configurations of 1st step optimization in effective bulk modulus minimization problem based on ring initial shape targeting 1550 Hz: (a) initial; (b) the first step, optimized.

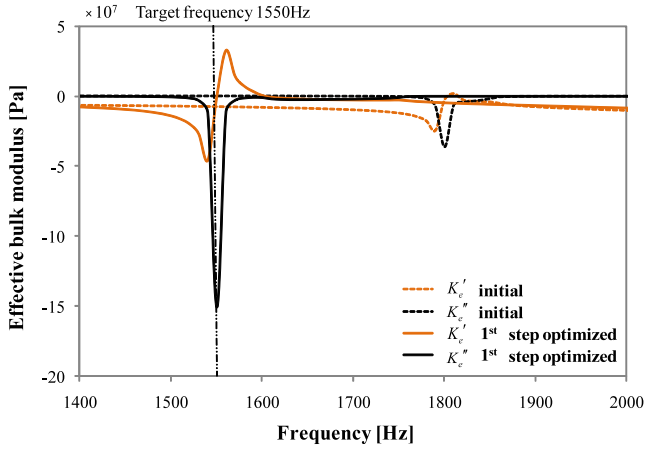

Figure 4-6: Effective bulk modulus curves for 1st step optimization of effective bulk modulus minimization problem based on ring initial shape targeting 1550 Hz.

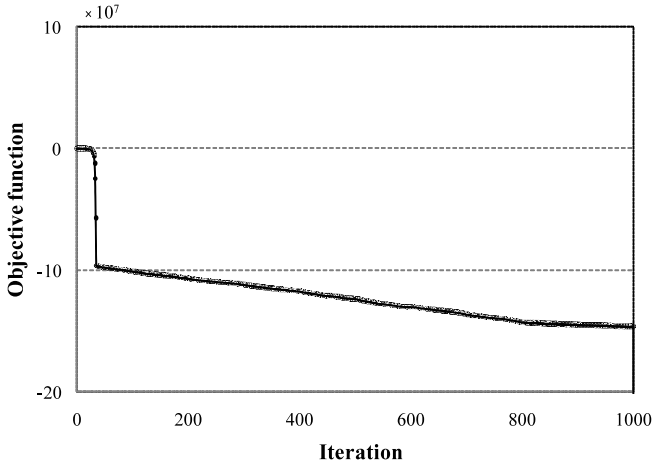

Figure 4-7: Convergence history of objection function of 1st step optimization for effective bulk modulus minimization problem based on ring initial shape targeting 1550 Hz.

After the 1st step optimization is finished, the real part of the effective bulk modulus was minimized targeting 1550 Hz in the 2nd step optimization, using the optimized configuration obtained in the 1st step as the initial configuration. Figure 4-8 shows the initial configuration and the optimized configuration for the 2nd step. Figure 4-9 shows the effective bulk modulus curves for the initial configuration of the 2nd step optimization, and the optimized distribution after the optimization. The real part of the effective bulk modulus decreases gradually during the optimization process and reaches a minimum at 1550 Hz. The value of the real part of the effective bulk modulus of the initial configuration at 1550 Hz was 181.85 Pa. After the 2nd step optimization, this value at 1550 Hz was -2.53×10^4 Pa. Figure 4-10 shows the convergence history of the real part of the effective bulk modulus, which reaches a minimum soon after the start of the optimization and then remains essentially stable, with minor oscillation. This result implies that the optimization successfully found a minimized and negative effective bulk modulus at the desired frequency, and produced an appropriate material distribution.

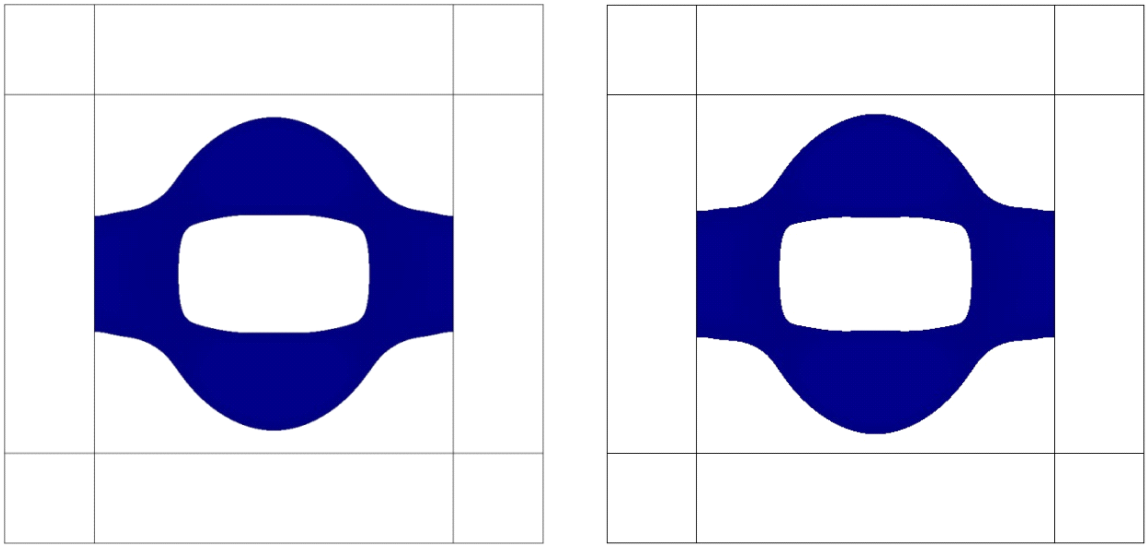

(a) initial (the first step, optimized); (b) the second step, optimized.

Figure 4-8: Configurations of the second step optimization of effective bulk modulus minimization problem based on ring initial shape targeting 1550 Hz: (a) initial (the first step, optimized); (b) the second step, optimized.

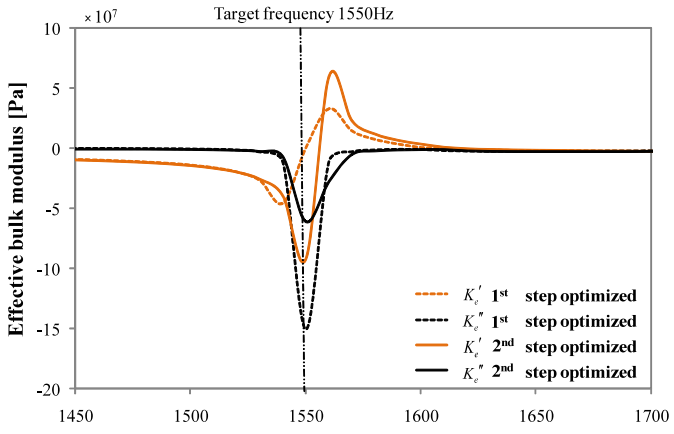

Figure 4-9: Effective bulk modulus curves for the second step optimization of effective bulk modulus minimization problem based on ring initial shape targeting 1550 Hz.

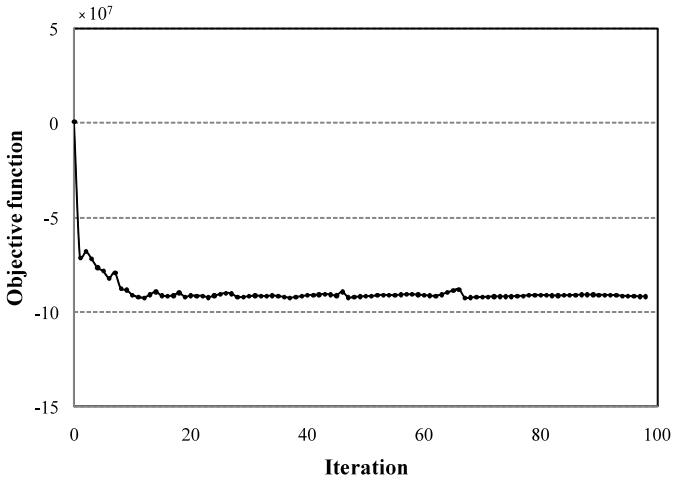

Figure 4-10: Convergence history of objection function of the second step optimization for effective bulk modulus minimization problem based on ring initial shape targeting 1550 Hz.

Bulk modulus κ is defined as the ratio of an infinitesimal pressure change $\triangle P$ to the resulting relative change in the volume $\triangle V$, and it is proportional to volume V as in Eq. (4.34).

$$\kappa = -V\frac{\triangle P}{\triangle V} \tag{4.34}$$

In a natural material that has a positive bulk modulus κ, an applied pressure gradient increases the force inside the material, which causes a decrease in volume. However, in an acoustic metamaterial, increases in a pressure gradient increase the volume, and decreases in a pressure gradient decrease the volume, a condition that creates a negative bulk modulus, shown in the relationship expressed in Eq. (4.34). The sound pressure change over the design domain and the displacements over the boundaries are integrated. The results show that the signs of the normal displacements of the right and left boundaries are both positive, which means that the volume of the design domain has increased. Concurrently, the pressure integration of the design domain is also positive, indicating that the bulk modulus has become negative at 1550 Hz.

Minimization of effective bulk modulus targeting 2200 Hz

A case in which the effective bulk modulus minimization has a target frequency of 2200 Hz (target wavelength equal to $22.3d$), which is higher than that of the positive peak of the initial configuration in the real part of the effective bulk modulus graph, is examined. The material settings and initial configuration are same as those described in the above example. The optimization in this problem is also conducted in two steps. Figure 4-11 shows the initial configuration for the 1st step and the optimized configuration after the 2nd step. The effective bulk modulus curves for the initial configuration and the optimized distribution obtained after the second step are shown in Fig. 4-12. The minimum value of the real part of the effective bulk modulus was reached at 2200 Hz. The value of the real part of the effective bulk modulus of the initial configuration at 2200 Hz was -3.98×10^3 Pa. After the 2nd step optimization, this value at 2200 Hz was -3.66×10^4 Pa. Figure 4-13 shows the convergence history during the first and second steps of the optimization.

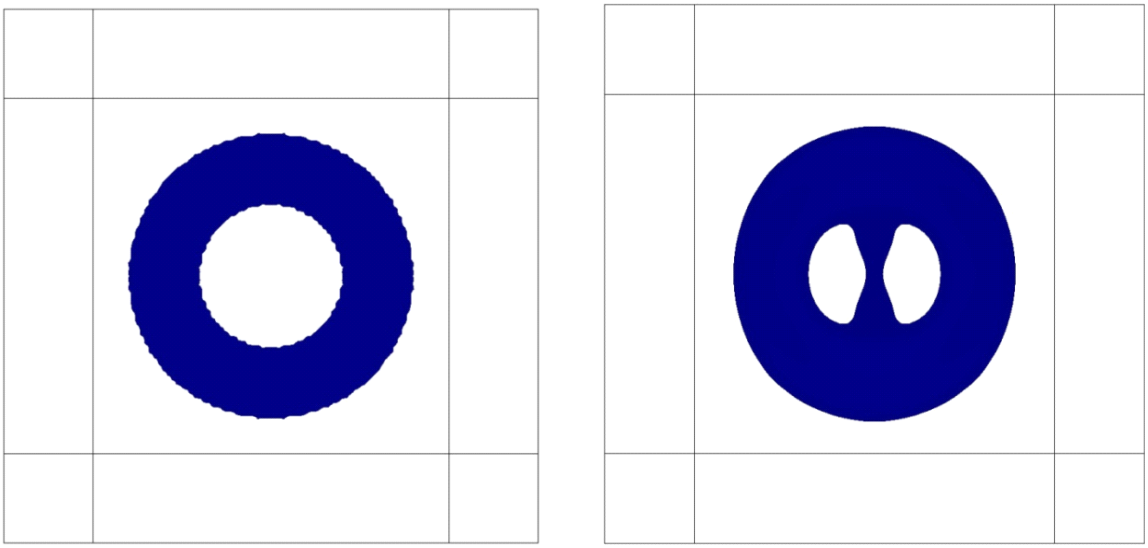

(a) initial; (b) the second step optimized.

Figure 4-11: Configurations of effective bulk modulus minimization problem based on ring initial shape targeting 2200 Hz: (a) initial; (b) the second step, optimized.

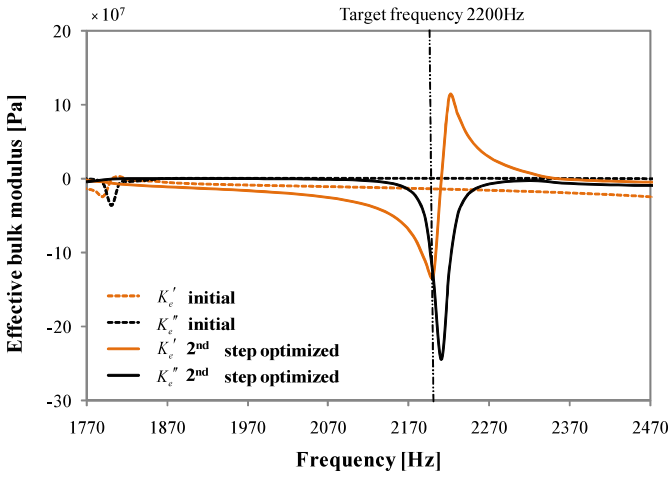

Figure 4-12: Effective bulk modulus curves of effective bulk modulus minimization problem based on ring initial shape targeting 2200 Hz.

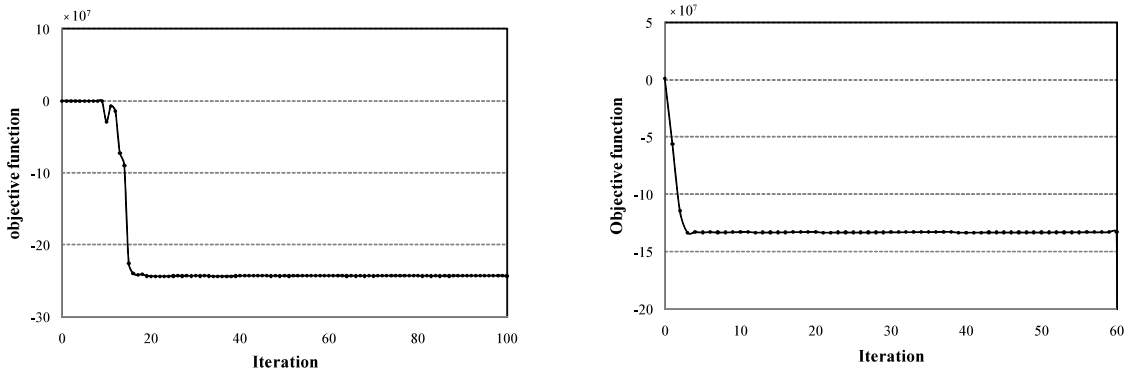

(a) the first step; (b) the second step.

Figure 4-13: [13] Convergence histories of objection function of effective bulk modulus minimization problem based on ring initial shape targeting 2200 Hz (a) the first step; (b) the second step.

Applying integrations to the sound pressure changes over the design domain and the displacements over the boundaries, the positive pressure change and resulting volume increase are responsible for the obtained negative bulk modulus achieved in the optimized configuration of the 2nd step.

4.4.2 Example 2: Effect of the initial configuration

Having solved effective bulk modulus minimization problems at different desired frequencies, effective bulk modulus minimization problems based on different initial configurations is examined in this section, to further verify the practicality of our proposed method and to discover if optimized results are dependent upon the initial configuration. The analysis model and material properties are same as for Example 1 above.

A problem to minimize the effective bulk modulus based on a circular shape with a volume ratio of 0.4 as the initial configuration for the optimization is described. The target frequency is set to 2200 Hz (target wavelength equal to 22.3d), and the optimization is conducted in two steps. Figure 4-14 shows the initial configuration for the 1st step and the optimized configuration after the 2nd step. The effective bulk modulus curves for the initial configuration and the optimized distribution obtained after the second step are shown in Fig. 4-15. The minimum of the real part of the effective bulk modulus was reached at

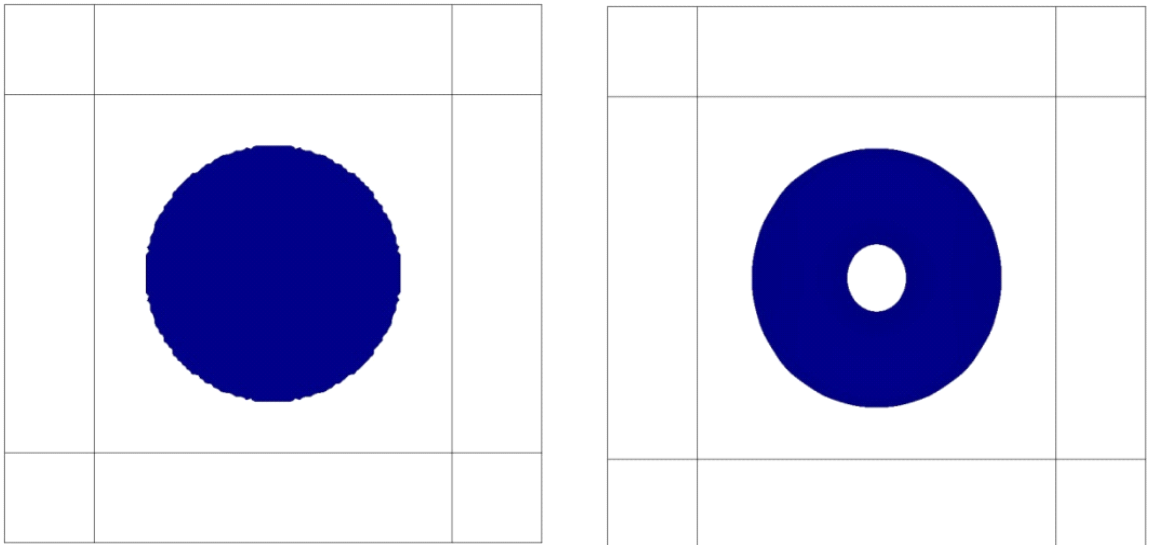

(a) initial; (b) the second step optimized.

Figure 4-14: Configurations of effective bulk modulus minimization problem based on circular initial shape targeting 2200 Hz: (a) initial; (b) the second step, optimized.

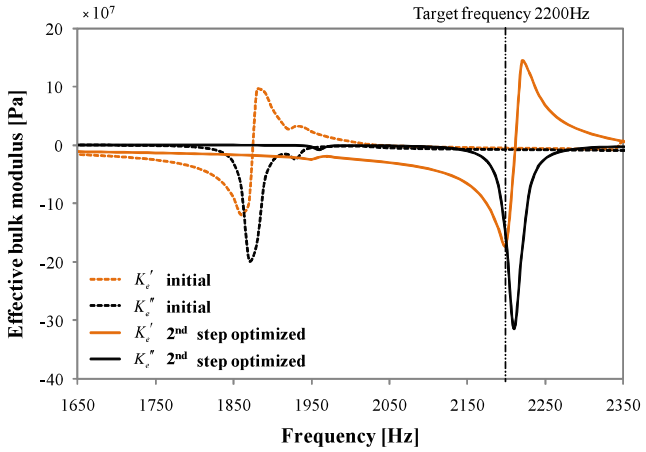

Figure 4-15: Effective bulk modulus curves of effective bulk modulus minimization problem based on circular initial shape targeting 2200 Hz.

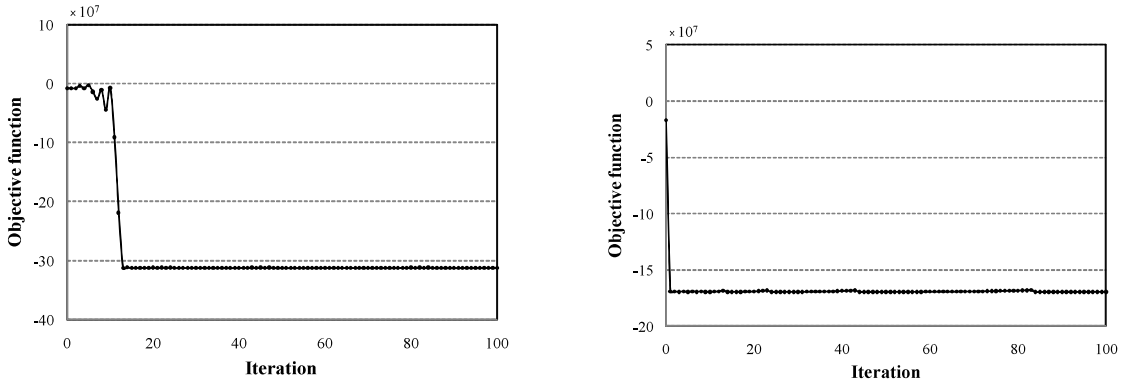

(a) the first step; (b) the second step.

Figure 4-16: Convergence histories of objection function of effective bulk modulus minimization problem based on circular initial shape targeting 2200 Hz: (a) the first step; (b) the second step.

2200 Hz. The value of the real part of the effective bulk modulus of the initial configuration at 2200 Hz was -1.37×10^3 Pa. After the 2nd step optimization, this value at 2200 Hz was -4.67×10^4 Pa. This result indicates that the optimization successfully found an optimized distribution at 2200 Hz, given the initial configuration. Figure 4-16 shows the convergence history during the first and second steps of the optimization. With the sound

pressure changes integrated over the design domain and the displacements integrated over the boundaries, the positive pressure change and resulting volume increase result in a negative bulk modulus.

Next, this result is compared with the example shown in 4.4.1 where the initial configuration used in the first step is a ring shape and the target frequency is also set to 2200 Hz, to show the effect of different initial configurations on the optimal configuration results. A comparison of the optimized configurations obtained based on different initial configurations, namely, a circular shape and an annular shape, shows that both initial configurations lead to optimized material distributions at the target frequency, where the effective bulk modulus is minimized. From Fig. 4-12 and Fig. 4-15 the data for the circular and annular initial configuration shapes show that the real part of the effective bulk modulus at 2200 Hz had a value of -3.66×10^4 Pa and -4.67×10^4 Pa, respectively. Although the difference in the obtained optimized values implies that this design problem has many local optima, clear optimized configurations that achieve an extremely negative effective bulk modulus at a desired frequency were obtained in both cases, confirming that the proposed method yields appropriate designs of acoustic metamaterials with minimized and negative bulk modulus.

4.4.3 Example 3: Effect of material properties

Here, different materials are applied for the design of acoustic metamaterials that exhibit negative bulk modulus. The solid material and the background material are same as the ones applied in the previous examples, but the constituent in the domain outside the fixed design domain (the non-design domain) is different from the background material. The bulk modulus of the solid material, the background material and the material in the non-design domain are respectively set as 6.27×10^5 Pa, 5.49×10^9 Pa and 1.47×10^5 Pa, in which damping coefficients are set to 0.3% of the real part of the bulk modulus. The mass density of the solid material, the background material and the material in the non-design domain are respectively set as 1300 kg/m^3, 1180 kg/m^3 and 1.25 kg/m^3, in which damping coefficients are set to -0.3% of the real part of the mass density. A configuration filled

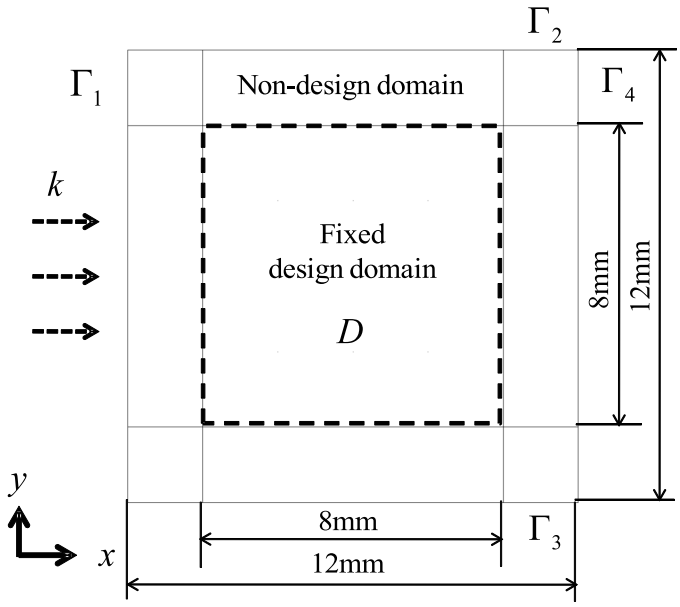

Figure 4-17: Analysis model, with size indications (Example 3)

with the solid material in the fixed design domain is used as an initial configuration in this example. The design is conducted based on two different target frequencies.

The analysis domain used in this example is 12 mm $\times$ 12 mm in size and the fixed design domain is 8 mm $\times$ 8 mm, as shown in Fig. 4-17. The analysis domain is discretized using 120 $\times$ 120 square elements.

Minimization of effective bulk modulus at 3000 Hz

First, a design problem that has a target frequency of 3000 Hz is addressed. Figure 4-18 shows the initial configuration (a) used in the first step and the optimal configuration (b) obtained after the 2nd step. The effective bulk modulus curves for the initial configuration and the optimized configuration obtained after the second step are shown in Fig. 4-19. The value of the real part of the effective bulk modulus gradually decreases during the optimization process and reaches a minimum at the target frequency. The values of the effective bulk modulus for the initial and optimal configuration at 3000 Hz are 2.50×10^9 Pa and -1.61×10^10 Pa, respectively. The value of the real part of the effective bulk modulus reached a minimum and was negative at the target frequency.

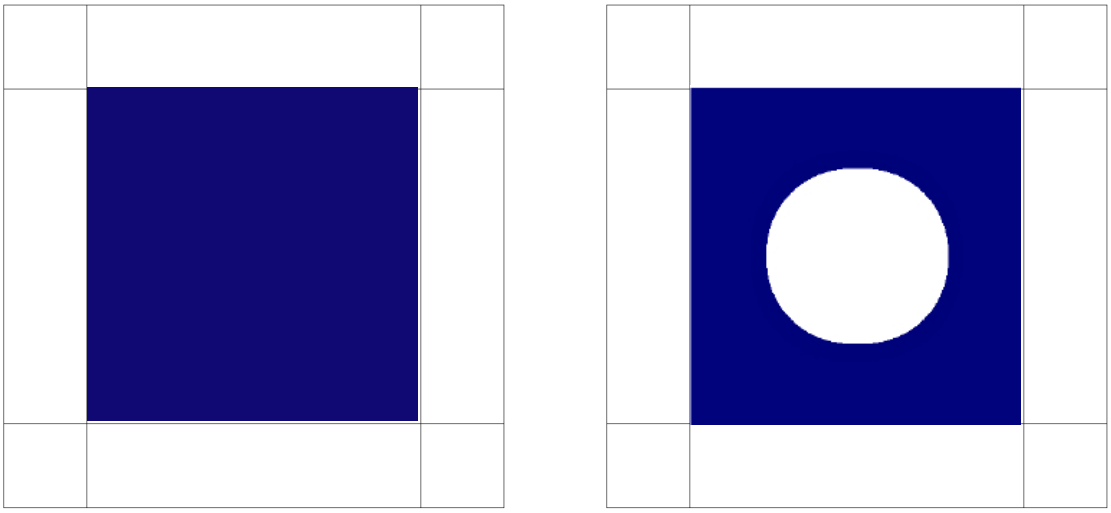

(a) initial; (b) the second step optimized.

Figure 4-18: Configurations of effective bulk modulus minimization problem targeting 3000 Hz: (a) initial; (b) the second step, optimized.

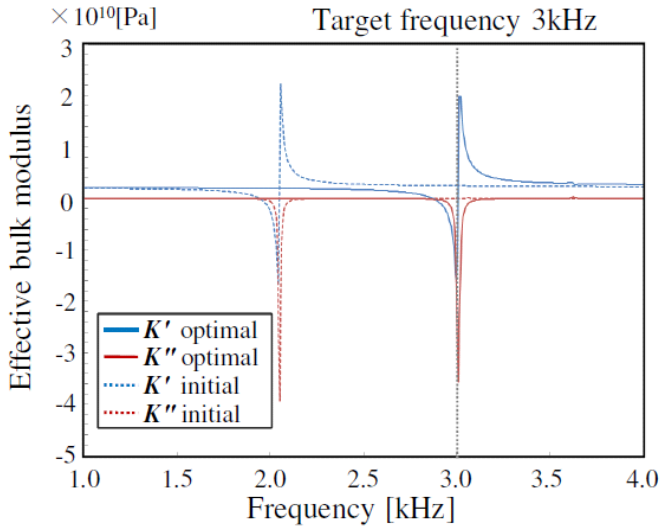

Figure 4-19: Effective bulk modulus curves for effective bulk modulus minimization problem targeting 3000 Hz.

Minimization of effective bulk modulus at 5000 Hz

Next, a design problem with a target frequency of 5000 Hz is considered. Figure 4-20 shows the initial configuration (a) used in the first step and the optimal configuration (b) obtained after the 2nd step. The corresponding effective bulk modulus curves for the initial configuration and the optimized configuration obtained after the second step are shown in Fig. 4-21. The effective bulk modulus values at 5000 Hz for the initial configuration were 2.83×10^9 Pa and gradually decreased to -5.24×10^9 Pa for the optimal configuration. Again, the negative peak of the real part of the effective bulk modulus was reached at the target frequency.

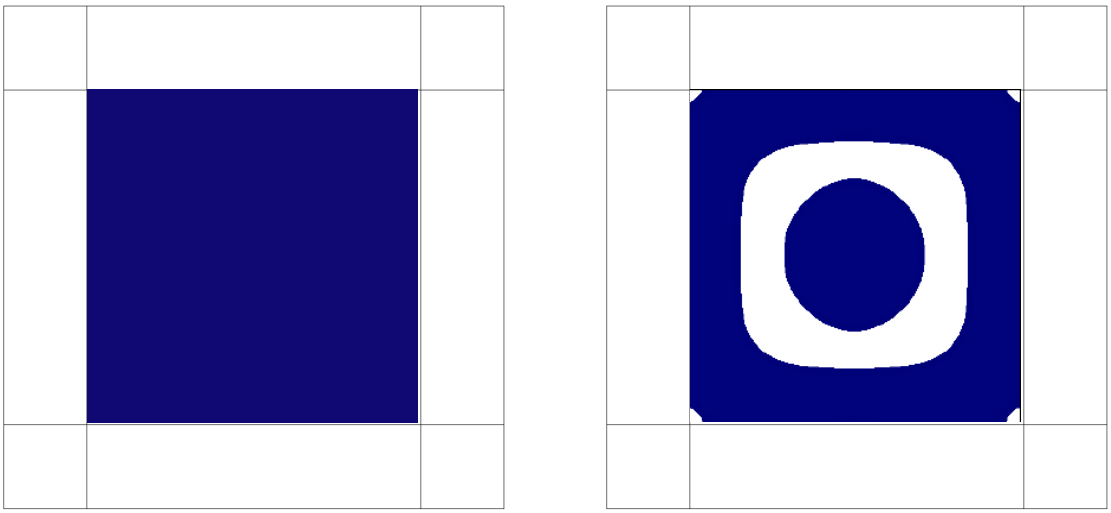

(a) initial; (b) the second step optimized.

Figure 4-20: Configurations of effective bulk modulus minimization problem targeting 5000 Hz: (a) initial; (b) the second step, optimized.

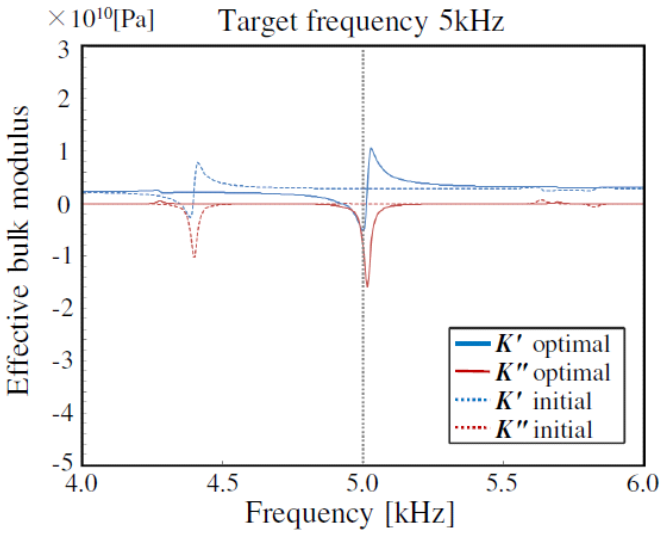

Figure 4-21: Effective bulk modulus curves for effective bulk modulus minimization problem targeting 5000 Hz.

4.4.4 Example 4: Three-dimensional design

In this section, a three-dimensional design example is presented using two cases in which the target frequencies are above or below that of the positive peak of the initial configuration . The analysis domain is shown in Fig. 4-22. The analysis domain is 12 mm $\times$ 12 mm $\times$ 12 mm in extent, and the fixed design domain is 8 mm $\times$ 8 mm $\times$ 8 mm. The analysis domain is discretized using 48 $\times$ 48 $\times$ 48 cubic elements. The applied materials are same as those used in Example 3, including the solid material, the background material and the material in the domain outside the fixed design domain. A configuration filled with the solid material in the fixed design domain is used as the initial configuration in this example.

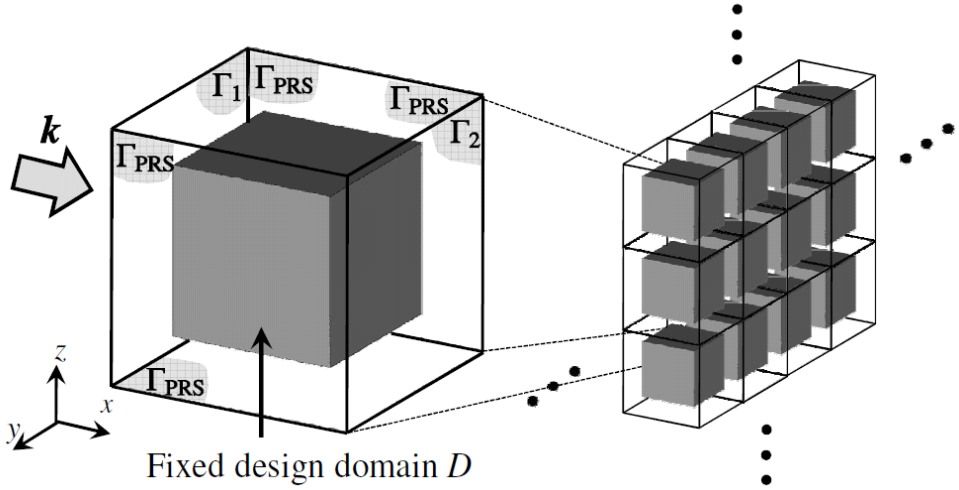

Figure 4-22: Analysis model (Example 4)

Minimization of effective bulk modulus at 3000 Hz

Here, a three-dimensional design problem with a target frequency of 3000 Hz is addressed. Figures 4-23(a) and (b) show the optimal configuration and the cross-sectional view of the interior, respectively, obtained after the 2nd step. Figure 4-24 shows a graph of frequency versus the effective bulk modulus for the initial and optimal configurations. The value of the real part of the effective bulk modulus gradually decreases during the optimization process and reaches a minimum at the target frequency. The values of the effective bulk modulus for the initial and optimal configuration at 3000 Hz are 1.98×10^9 Pa and -6.20×10^9 Pa, respectively. The value of the real part of the effective bulk modulus reached a minimum and was negative at the target frequency.

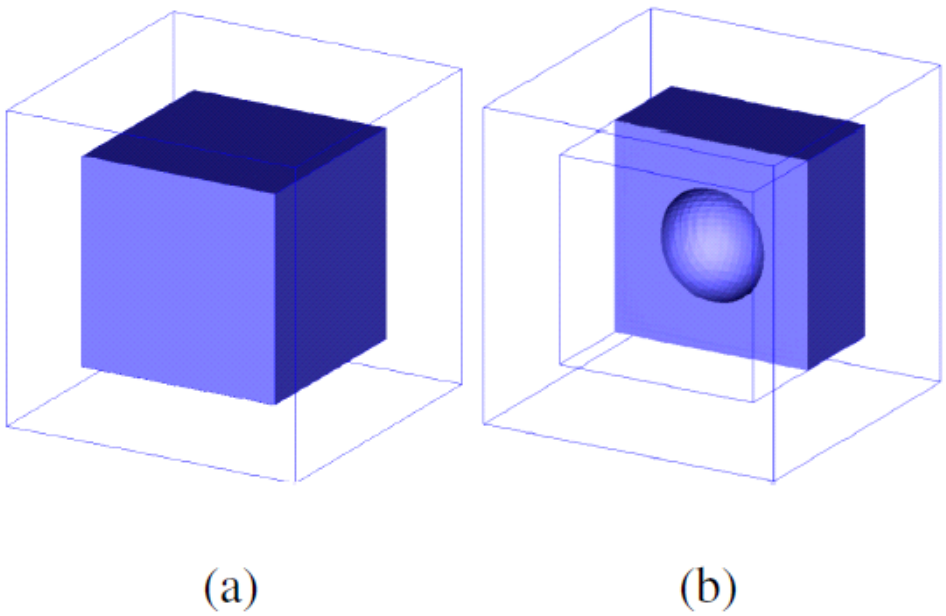

Figure 4-23: Optimal configuration for three-dimensional effective bulk modulus minimization problem targeting 3000 Hz: (a) optimal configuration; (b) cross-sectional view.

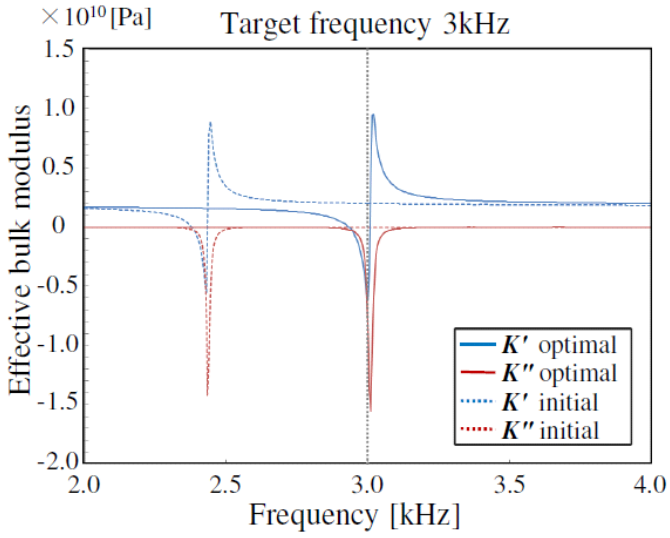

Figure 4-24: Effective bulk modulus curves for effective bulk modulus minimization problem targeting 3000 Hz.

Minimization of effective bulk modulus at 5000 Hz

Finally, a three-dimensional design problem with a target frequency of 5000 Hz is described. Figures 4-25(a) and (b) show the optimal configuration and a corresponding cross-sectional view, respectively, obtained after the 2nd step. Figure 4-26 shows a graph of frequency versus the effective bulk modulus for the initial and optimal configurations. The value of the real part of the effective bulk modulus gradually decreases during the optimization process and reaches a minimum at the target frequency. The values of the effective bulk modulus for the initial and optimal configuration at 5000 Hz are 2.12×10^9 Pa and -1.40×10^9 Pa, respectively. The value of the real part of the effective bulk modulus reached a minimum and was negative at the target frequency.

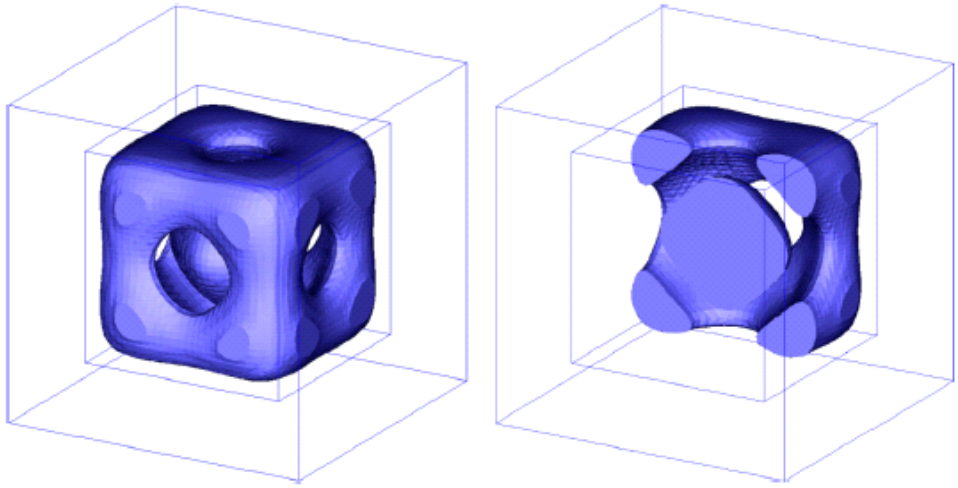

Figure 4-25: Optimal configuration for three-dimensional effective bulk modulus minimization problem targeting 5000 Hz: (a) optimal configuration; (b) cross-sectional view.

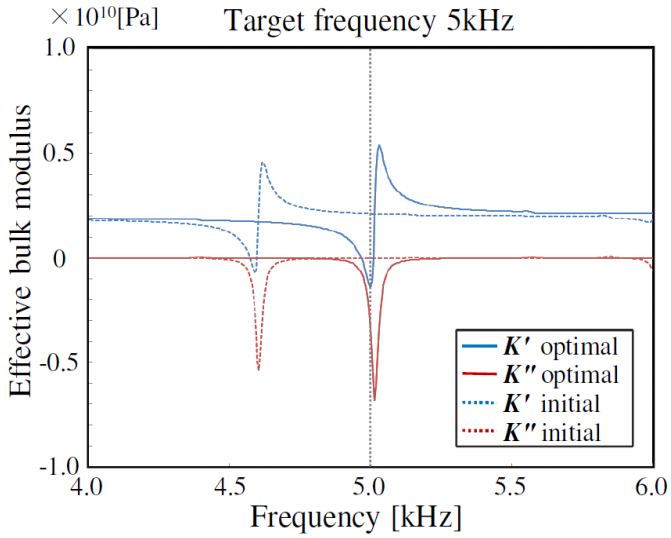

Figure 4-26: Effective bulk modulus curves for effective bulk modulus minimization problem targeting 5000 Hz.

4.5 Conclusions

This chapter presented a level set-based topology optimization method applied to the design of negative bulk modulus acoustic metamaterials based on local resonance phenomena, using a functional scale in both two- and three-dimensional cases. The following results were obtained.

(1) The optimization problem was formulated to minimize the effective bulk modulus. A homogenization method based on S-parameters was applied to compute the effective bulk modulus of the metamaterials. A level set-based topology optimization method using a reaction-diffusion equation was successfully applied to obtain clear boundary expressions in the optimal configurations.

(2) Based on the formulation of the optimization problem, an optimization algorithm was constructed. The FEM was used to solve the governing equation of acoustic wave propagations, and to update the level set function. The Adjoint Variable Method was used when computing sensitivity analyses.

(3) Several examples were presented to confirm that the proposed method successfully finds optimized material distributions at different target frequencies, and with different initial configurations. It was also confirmed that a two-step optimization approach enabled the handling of effective bulk modulus curves with unusual characteristics. The proposed method should facilitate the design of acoustic metamaterials without the need for physical experiments or trial and error approaches.

It is hoped that the current two-material-phase cases can be extended to three-material-phase problems in the future, which may broaden and improve the prospects for developing effective applications of acoustic metamaterials.

Chapter 5

Design of acoustic metamaterial with negative mass density

5.1 Introduction

The advent of photonic and phononic crystals, and electromagnetic and acoustic metamaterials, has attracted extensive attention and profoundly affected researchers, since such do not appear in nature and exhibit novel characteristics unavailable with natural materials. Phononic crystals and acoustic metamaterials were developed following on photonic crystals and electromagnetic metamaterials by conceived with different forms of waves, and they respectively exhibit analogous behavior. Acoustic metamaterials are regarded as a new type of artificial composite acoustic material that is closely related to the concept of phononic crystals at a subwavelength scale. The fact that the unit cell dimensions in acoustic metamaterials is roughly one tenth that of the acoustic wavelength, or even smaller, makes these materials especially promising in a broad range of applications, since their size is far smaller than that in phononic crystals which are impractically huge and unapplicable in real life, and triggering intensive research on a variety of topics since Liu et al. [3]. They first engineered a cubic array of bi-layer coated spheres in water that show a complete band gap as a result of effective negative elastic constants, in 2000. The other two novel properties of acoustic metamaterials include a negative mass density and a negative refractive index.

After the pioneering work of Liu et al., much research was subsequently carried out on experimental fabrication and theoretical analysis of acoustic metamaterials. Fox and Zhang developed a metamaterial that combines water-filled unit cells composed of four 12.5 mm-long aluminum rod-spring resonators and one 10 mm-long aluminum Helmholtz resonator, and demonstrated that the real component of the acoustic index was negative [7]. Fang et al. presented an ultrasonic metamaterial with a negative modulus, consisting of an array of Helmholtz resonators analogous to inductor-capacitor circuits operating in a narrow frequency band from 31 to 35 kHz [5]. Furthermore, a multi-resonator mass-in-mass system has been used to fabricate an acoustic metamaterial that displays multiple band gaps due to its negative effective mass density [190]. In the above research, the acoustic metamaterials were obtained using different kinds of resonators to achieve negative bulk modulus or negative mass density (single negativity).

The novel property of single negativity can be exploited to design devices that exhibit bandgap behavior, and acoustic waveguides that guide, block, or manipulate the transmission of sound waves at prescribed frequencies. Double negativity (negative bulk modulus and negative mass density) leading to a negative refractive index is another unusual phenomenon attracting much research attention, with development of devices that include acoustic metamaterial lenses and cloaking devices. A variety of acoustic superlenses and magnifying hyperlenses have been demonstrated using locally resonant or non-resonant acoustic elements to focus ultrasound waves, in devices with enhanced capabilities tailored for high-resolution medical imaging, non-destructive structural testing, and underwater sonar sensing [191, 42, 192]. In 2011, Zhang et al. was the first to design a low-loss broadband acoustic metamaterial cloak for underwater ultrasound, using a network of acoustic circuit elements [65]. Garía-Chocano et al. designed a non-symmetric acoustic metamaterial cloak based on a dispersed distribution of cylinders with an operating frequency of 3061 Hz by inverse design [193]. Acoustic cloak applications include underwater stealth technologies and the soundproofing of areas.

Several structural designs have been proposed to achieve the design of acoustic metamaterials that have negative effective mass density. Mei et al. rigorously derived effective dynamic mass density expressions for an inhomogeneous structure consisting of a matrix

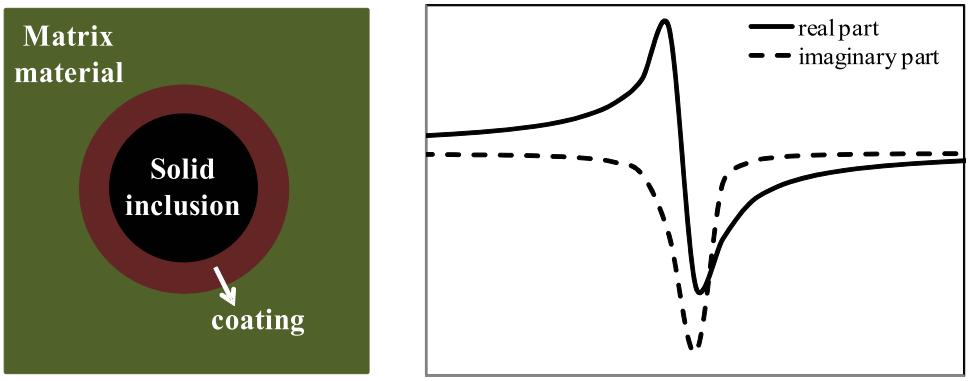

Figure 5-1: (a) Typical resonance structure; (b) Typical effective mass density curve.

and inclusions, which exhibited negative dynamic mass density at a finite frequency [2]. The mechanism of wave propagation in an acoustic metamaterial with negative effective mass density has been studied and the results are expected to be applied to the design of metamaterials [194]. A number of designs of acoustic metamaterials with negative mass density resulting from local resonances have been achieved experimentally and analyzed theoretically [3, 4, 195, 2, 49, 194]. Additionally, a membrane-type acoustic metamaterial with negative dynamic mass density, experimentally realized by Yang et al. [196] and Lee et al. [197], has also been reported.

In the case of acoustic metamaterials with negative mass density, most of the realizations have been based on a mass-in-mass system, a so-called local dipole resonance structure (Fig. **??**(a)), which has a typical effective mass density curve (Fig. **??**(b)). As shown in Fig. **??**(a), the composite consists of a solid inclusion coated with a different material, embedded in a matrix material. Generally, the matrix and inclusion are hard materials, and the coating is softer [195]. The density of the coating is sufficiently high and that of the inclusion is higher than that of the matrix [49]. Relatively incompressible materials such as water or epoxy are typically used as the matrix material, and soft materials such as rubber or silicone rubber are applied over solid shapes made of lead or other metal.

In most of the above-mentioned research, however, the designs of the metamaterial structures were developed using an intuitive and experimental approach. Nevertheless, to obtain metamaterial designs that optimally achieve specified targets, and to explore this

realm with greater freedom and potential for discovery, a powerful and systemic design method is desirable. To achieve such systemic design approach, here, a level set-based topology optimization method for the design of acoustic metamaterials that have negative effective mass density and achieve specified performance targets is presented.

Topology optimization is a mature structural optimization method, an outgrowth of the size and shape structural optimization methods that have been studied for roughly 50 years. Compared with the earlier two approaches, topology optimization offers the highest degree of design freedom, as well as an infinite range of potential designs, since any initial design can be used. Topology optimization allows changes in the structure's outer shape. Topology optimization is therefore advantageous for achieving designs that have specific targets, and is often used in manufacturing industries to obtain optimal structures that minimize weight.

The fundamental concept of topology optimization is the replacement of an optimization problem with a material distribution problem within a fixed design domain, first proposed by Bendsøe and Kikuchi in 1988 [77]. Currently, there are two popular approaches used in topology optimization design problems. The first and the most widely-used one is a density-based approach that uses the normalized density as the design variable to achieve a material distribution of two or more phases (generally, a material and non-material/void phases). The density-based approach led to the development of SIMP (solid isotropic material with penalization) methods [198]. Well-developed density-based approaches have been successfully applied in a wide range of topics, as described in the work of Dühring et al. [181], Lee et al. [117], and Yamamoto et al. [116] for acoustic design problems, Wiker et al. [100] for fluid problems, and Cox et al. [199] and Dühring et al. [183] for electromagnetic wave propagation problems. However, this approach produces the optimal configurations which suffer from numerical instability problems, such as grayscales and mesh-dependency.

The second widely-used topology optimization approach in level set-based topology optimization methods that employ an intersected evolving contour to implicitly represent the interfaces between different material phases [133, 200, 201, 129, 130]. Such methods can provide clear optimal configurations directly and conveniently, which avoid intermediate material phases (grayscales) and mesh-dependent spatial oscillations (checkerboarding

or staircasing). In this level set-based topology optimization method, the evolution of the level set function is governed by a Hamilton-Jacobi equation. In 2000, Yamada et al. [137] developed a level set-based topology optimization, which incorporates a reaction-diffusion equation for updating the level set function during the optimization. This scheme differs from updating schemes based on the Hamilton-Jacobi equation [201, 129, 130] that were first explored some years ago. This method allows topological changes, i.e., the increment of the number of the holes, and the control of the complexity of optimal configuration by a regularization parameter, to the optimal configurations, whereas Wang et al.'s [129] and Allaire et al.'s [130] methods change the boundaries of the structures and decrease the number of the holes.

Level set-based topology optimization methods usually require regularization to deal with the ill-posed nature of most structural optimization problems and to improve performance [129, 202, 203]. Over the past decade, level set-based topology optimization methods have been applied to a variety of problems, using various design constraints and physics. Initially, such methods were applied to structural mechanics problems [201, 204]. Subsequently, application was extended to electromagnetic wave propagation [205, 162], heat conduction [145, 206], fluid problems [151, 150, 207], electro-mechanical systems [149], and optical structures [208, 209].

In this chapter, a level set-based topology optimization method developed by Yamada et al. [137] is applied for the design of an acoustic metamaterial. Level set-based topology optimization methods incorporating Yamada et al.'s updating scheme have been applied to a range of design problems in various physical systems, including compliance minimization [137], compliant mechanisms [137], eigenfrequency problems [137], heat conduction [210], electromagnetic metamaterials [160], and acoustic metamaterials [211].

Here, a level set-based topology optimization method is proposed for the design of an acoustic metamaterial that displays negative mass density, by making structures locally resonate at target frequencies. The rest of this chapter has the following outline. The topology optimization problem is formulated in Section 5.2 and the numerical implementations, including the design variables to be optimized and the optimization flowchart, are described in Section 5.3. Several numerical examples are then presented to demonstrate the operation

of the proposed method, and verify its feasibility. Finally, conclusion is offered and future avenues for research is proposed.

5.2 Formulation

5.2.1 Level set-based topology optimization method

In this chapter, the same level set-based topology optimization method [137] applied in the design of Chapter 4 is used. Detailed introduction can be found in section 3.3 and subsection 4.14.

In the level set-based topology optimization method, the structural boundaries are expressed by the level set function. The variation of the level set function can be obtained as follows.

$$\begin{cases} \partial\phi/\partial t = -K[\phi]\left(\bar{F}' - \tau\left|\bigtriangledown\phi\right|^2\right) & \text{in} \quad D \\ \partial\phi/\partial n = 0 & \text{on} \quad \partial D \backslash \partial D_N \\ \phi = 1 & \text{on} \quad \partial D_N \end{cases} \tag{5.1}$$

where D_N represents the non-design domain. As a result, the level set function, representing the optimal configuration of the topology optimization problem, is updated by the time evolutionary equation, i.e., the reaction-diffusion equation.

5.2.2 Acoustic wave propagation problem

Here, a problem of acoustic wave propagation in an acoustic metamaterial is considered under the assumption that the problem is two-dimensional (2D). This paper is limited to a problem dealing with longitudinal waves only. The governing equation is the Helmholtz equation that includes two material properties, namely the mass density ρ and the bulk modulus κ of the acoustic medium, both of which are dependent on position $\mathbf{x}$. The speed of sound, ζ, is expressed as the square root of the ratio of the bulk modulus and the mass density, i.e., $\zeta = \sqrt{\kappa/\rho}$. Suppose that the state variable is the sound pressure p, which

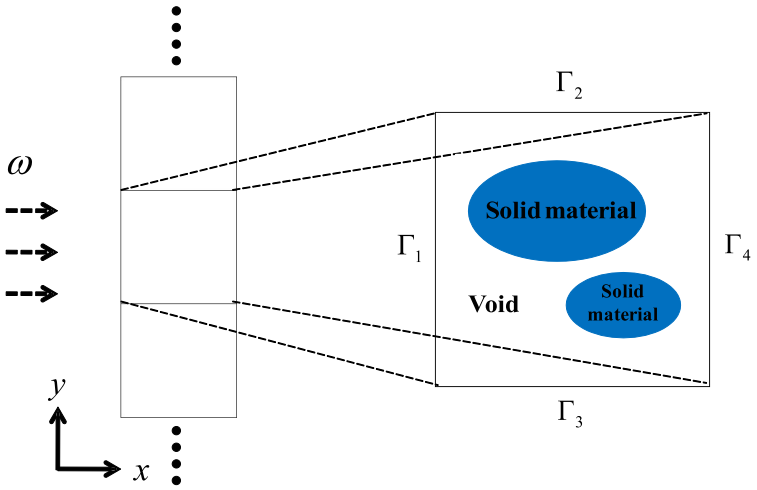

Figure 5-2: Periodic acoustic metamaterial and a basic unit cell.

also depends on position **x**, and ω is angular frequency of sinusoidal acoustic waves. Then, it is obtained that

$$\nabla \cdot \left(\rho^{-1} \nabla p\right) + \omega^2 \kappa^{-1} p = 0 \tag{5.2}$$

The acoustic metamaterial here has a periodic structure, designed as a periodic array of basic unit cells in the y direction, with longitudinal incident waves impinging at an angle normal to the left side with the response observed at the right side (Fig. 5-2). Each unit cell consists of a distribution of solid material and void domains. After optimization of the basic unit cell, the periodic array of unit cells forming the metamaterial will exhibit the same properties as those of the unit cell, so-called inverse homogenization approach by Sigmund [111].

In this design problem, the waves travel through the domain boundaries from the left to the right side. Thus, the following boundary conditions are imposed:

$$\begin{cases} \mathbf{n} \cdot \left(\rho^{-1} \nabla p\right) = 2ik\rho^{-1} p^i - ik\rho^{-1} p & \text{on} \quad \Gamma_1 \\ \mathbf{n} \cdot \left(\rho^{-1} \nabla p\right) = -ik\rho^{-1} p & \text{on} \quad \Gamma_4 \\ p|_{\Gamma_2} = p|_{\Gamma_3} & \text{on} \quad \Gamma_2\, \Gamma_3 \end{cases} \tag{5.3}$$

where **n** is the normal vector, k is the wave number, i is an imaginary unit, and p^i

is the pressure of the incident wave. The first boundary condition describes an absorbing boundary condition with incident pressure p^i applied normal to the left boundary. The second boundary condition indicates an absorbing boundary condition with minimal reflection, applied at the right boundary, and the third boundary condition expresses a periodic boundary condition applied at the upper and lower boundaries of the design domain.

By denoting p^* as the test function corresponding to p, the weak form of Eqs. (5.2) and (5.3) is then derived as follows.

$$a(p, p^*) = l(p^*) \tag{5.4}$$

where

$$a(p, p^*) = \int_\Gamma p^* ik\rho^{-1} p \mathrm{d}\Gamma + \int_D (\bigtriangledown p) \cdot \left(\rho^{-1} \bigtriangledown p^*\right) \mathrm{d}\Omega - \int_D p^* \omega^2 \kappa^{-1} p \mathrm{d}\Omega \tag{5.5}$$

$$l(p^*) = 2ik \int_\Gamma \rho^{-1} p^i p^* \mathrm{d}\Gamma \tag{5.6}$$

The above weak form of the governing equation is obtained for the analysis of sensitivities. The physical problem, expressed by the Helmholtz equation in Eq. (5.2) and the related boundary conditions in Eq. (5.3), can be solved using the finite element method (FEM).

5.2.3 Effective mass density

An acoustic metamaterial is an inhomogeneous medium with a multilayered structure composed of at least two kinds of homogeneous material, each having distinct values of its material parameters. It is difficult to solve a metamaterial unit cell design problem by considering the characteristics of each homogeneous material individually, and one practical approach is to compute the effective properties based on S-parameters. Thus, the original inhomogeneous material can be conceptually replaced by an equivalent continuous medium which, in terms of wave propagation characteristics, behaves in the same way as the multi-

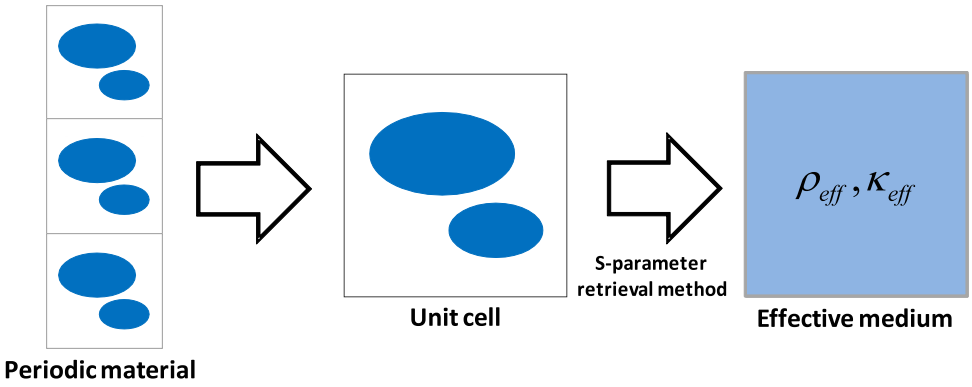

Figure 5-3: The application of the S-parameter retrieval method, ρ_{eff}, κ_{eff} are the effective mass density and bulk modulus, respectively.

layer medium. Note that this approach is effective when the unit cell is at least 1 order of magnitude smaller than the free-space wavelength of excitation. Thus, the S-parameter retrieval method to the description of the acoustic metamaterial in the current design problem is applied (Fig. 5-3).

Based on the work of Li and Chan [40] and following the S-parameter retrieval method, the effective mass density of a metamaterial design is derived using the relative impedance z_e and refractive index n, as follows:

$$\rho_e = Z_0 z_e n / \zeta_0 \tag{5.7}$$

where Z_0 and ζ_0 are the acoustic impedance and the sound speed of the background material, respectively.

Calculation of relative impedance z_e and refractive index n can be accomplished by calculating reflection and transmission coefficients (equivalent to S-parameters). Initial trials for the formulation of z_e and n were conducted for an electromagnetic metamaterial in order to obtain effective constitutive parameters [186, 189, 187]. Later, Fokin proposed an extended procedure to obtain expressions of z_e and n for an acoustic metamaterial [179] and discussed the selection of z_e and n signs; Fokin's approach is adopted here. For our design, the optimal configuration has a symmetric structure, oriented normally to the direction of the wave propagation. Two reflection coefficients are used, so that Eq. (5.8) is symmetric

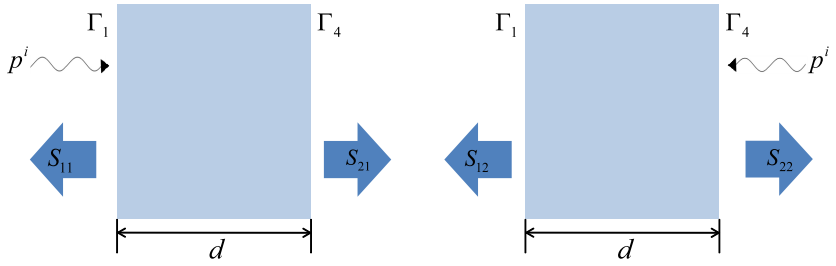

Figure 5-4: The illustrations of S-parameters.

with respect to S_{11} and S_{22}, and a single transmission coefficient, S_{21}, for the expression of z_e and n, as follows.

$$z_e = \pm\sqrt{\frac{(1+S_{11})(1+S_{22})-S_{21}^2}{(1-S_{11})(1-S_{22})-S_{21}^2}} \tag{5.8}$$

$$n = \pm\frac{\cos^{-1}\{[1-(S_{11}S_{22}-S_{21}^2)]/2S_{21}\}}{kd} \tag{5.9}$$

where d represents the width of a single unit cell of the structure. As Fig. 5-4 illustrates, S_{11} represents the reflection coefficient, a measure of waves reflected from Γ_1 as incident waves strike in this boundary. Likewise, S_{22} represents the reflection coefficient that is a measure of waves reflected from Γ_4 in response incident waves applied thereto. S_{21} represents the transmission coefficient of waves transmitted from Γ_1 to Γ_4 through the design domain. With p^i as the incident field and its complex conjugate transposition as p^{i*}, the reflection and transmission coefficients are expressed as follows, based on their standard definitions.

$$S_{11} = \frac{\int_{\Gamma_1}(p-p^i)\cdot p^{i*}\mathrm{d}\Gamma}{\int_{\Gamma_1} p^i\cdot p^{i*}\mathrm{d}\Gamma} \tag{5.10}$$

$$S_{21} = \frac{\int_{\Gamma_4} p\cdot p^{i*}\mathrm{d}\Gamma}{\int_{\Gamma_1} p^i\cdot p^{i*}\mathrm{d}\Gamma} \tag{5.11}$$

$$S_{22} = \frac{\int_{\Gamma_4}(p-p^i)\cdot p^{i*}\mathrm{d}\Gamma}{\int_{\Gamma_4} p^i\cdot p^{i*}\mathrm{d}\Gamma} \tag{5.12}$$

5.2.4 Design variables and material interpolation

In a level set-based topology optimization problem, the value of each finite element of the fixed design domain is interpolated according to the material properties of the solid material and void domains that express an optimal configuration. For the acoustic wave propagation problem here, two material properties, namely the mass density ρ and bulk modulus κ, are used as the variables to be changed by level set function for the material distribution. For the void domains, the material properties are represented as $(\rho, \kappa) = (\rho_0, \kappa_0)$ and for material areas, the material properties are represented as $(\rho, \kappa) = (\rho_1, \kappa_1)$. As previously described, the introduction of the characteristic function χ_ϕ prevents the appearance of intermediate values for the material properties in the optimal configurations. Here, the two material variables are constructed using reciprocal formulations as Eq. (5.13) and Eq. (5.14). Compared with the linear formulations, they would guarantee the numerical continuity near the structural boundaries. Detailed explanation can be found in the next subsection.

$$\rho^{-1} = \left(\rho_1^{-1} - \rho_0^{-1}\right)\chi_\phi + \rho_0^{-1} \tag{5.13}$$

$$\kappa^{-1} = \left(\kappa_1^{-1} - \kappa_0^{-1}\right)\chi_\phi + \kappa_0^{-1} \tag{5.14}$$

where $\begin{cases} \rho = \rho_0 \\ \kappa = \kappa_0 \end{cases}$ at $\chi_\phi = 0$ and $\begin{cases} \rho = \rho_1 \\ \kappa = \kappa_1 \end{cases}$ at $\chi_\phi = 1$.

In the numerical implementation, the characteristic function χ_ϕ is replaced by a smoothed Heaviside function, $H(\phi)$, as follows.

$$H(\phi) = \begin{cases} 0 & (\phi < -w) \\ \frac{1}{2} + \frac{\phi}{w}\left[\frac{15}{16} - \frac{\phi^2}{w^2}\left(\frac{5}{8} - \frac{3}{16}\frac{\phi^2}{w^2}\right)\right] & (-w \le \phi \le w) \\ 1 & (w \le \phi) \end{cases} \tag{5.15}$$

where w is the transition width of the Heaviside function, set to a sufficiently small and real value.

5.2.5 Sensitivity formulation

In the proposed topology optimization procedure, the level set function is updated at each iteration, using a reaction-diffusion equation, and the sensitivity analysis is derived using the adjoint variable method (AVM).

The Lagrangian of the optimization problem is formulated as

$$\bar{F} = F - \sum_{ij} \left[a\left(p, p_{ij}^*\right) - l\left(p_{ij}^*\right) \right] + \lambda V,\ ij = 11, 21, 22 \tag{5.16}$$

where p_{ij}^* is the adjoint sound pressure field with respect to S_{ij}.

The variation of the Lagrangian is obtained as follows.

$$\begin{aligned} \left\langle \frac{\mathrm{d}\bar{F}}{\mathrm{d}\chi_\phi}, \chi_\phi^* \right\rangle =& \sum_{ij} \left\langle \frac{\partial F}{\partial S_{ij}}, S_{ij}^* \right\rangle \left\langle \frac{\partial S_{ij}}{\partial p}, p_{ij}^* \right\rangle \left\langle \frac{\partial p}{\partial \chi_\phi}, \chi_\phi^* \right\rangle \\ & - \sum_{ij} \left(\left\langle \frac{\partial a}{\partial p}, p_{ij}^* \right\rangle \left\langle \frac{\partial p}{\partial \chi_\phi}, \chi_\phi^* \right\rangle + \left\langle \frac{\partial a}{\partial \chi_\phi}, \chi_\phi^* \right\rangle \right) \\ & + \lambda \left\langle \frac{\partial V}{\partial \chi_\phi}, \chi_\phi^* \right\rangle,\ ij = 11, 21, 22 \end{aligned} \tag{5.17}$$

where the term $\langle \partial l / \partial \chi_\phi, \chi_\phi^* \rangle$ is excluded because $l(\tilde{p})$ is evaluated on the exterior boundaries which are outside the fixed design domain, and thus can be ignored in the global expression in which the sensitivity is distributed.

Rewriting Eq. (5.17), it is obtained

$$\begin{aligned} \left\langle \frac{\mathrm{d}\bar{F}}{\mathrm{d}\chi_\phi}, \chi_\phi^* \right\rangle =& \sum_{ij} \left(\left\langle \frac{\partial F}{\partial S_{ij}}, S_{ij}^* \right\rangle \left\langle \frac{\partial S_{ij}}{\partial p}, p_{ij}^* \right\rangle - \left\langle \frac{\partial a}{\partial p}, p_{ij}^* \right\rangle \right) \left\langle \frac{\partial p}{\partial \chi_\phi}, \chi_\phi^* \right\rangle \\ & - \sum_{ij} \left\langle \frac{\partial a}{\partial \chi_\phi}, \chi_\phi^* \right\rangle + \lambda \left\langle \frac{\partial V}{\partial \chi_\phi}, \chi_\phi^* \right\rangle,\ ij = 11, 21, 22 \end{aligned} \tag{5.18}$$

The solution of p_{ij}^* can be obtained by solving the following adjoint equation.

$$\left\langle \frac{\partial a}{\partial p}, p_{ij}^* \right\rangle = \left\langle \frac{\partial F}{\partial S_{ij}}, S_{ij}^* \right\rangle \left\langle \frac{\partial S_{ij}}{\partial p}, p_{ij}^* \right\rangle,\ ij = 11, 21, 22 \tag{5.19}$$

The variation of the Lagrangian is now calculated by the following equation.

$$\left\langle \frac{\mathrm{d}\bar{F}}{\mathrm{d}\chi_\phi}, \chi_\phi^* \right\rangle = -\sum_{ij} \left\langle \frac{\partial a}{\partial \chi_\phi}, \chi_\phi^* \right\rangle + \lambda \left\langle \frac{\partial V}{\partial \chi_\phi}, \chi_\phi^* \right\rangle,\ ij = 11, 21, 22 \tag{5.20}$$

Based on the definition of the material properties in Eqs. (5.13) and (5.14), $\langle \partial a / \partial \chi_\phi, \chi_\phi^* \rangle$ in Eq. (5.20) is derived as follows:

$$\begin{aligned} \left\langle \frac{\partial a}{\partial \chi_\phi}, \chi_\phi^* \right\rangle =& 2 \int_D \left(\rho_1^{-1} - \rho_0^{-1} \right) \bigtriangledown p \cdot \bigtriangledown p^* \chi_\phi^* \mathrm{d}\Omega \\ & - \int_D \left(\kappa_1^{-1} - \kappa_0^{-1} \right) p \cdot p^* \cdot \omega^2 \cdot \chi_\phi^* \mathrm{d}\Omega \end{aligned} \tag{5.21}$$

Employing the same treatment as for $l(\tilde{p})$ in Eq. (5.6), the first term of $a(p, \tilde{p})$ in Eq. (5.5), namely $\int_\Gamma \tilde{p} i k \rho^{-1} p d\Gamma$, which lies outside the fixed design domain, is also ignored in the calculation of the variation of the Lagrangian. Therefore, the time evolutionary expression in Eq. (5.1) is obtained as follows:

$$\begin{aligned} \frac{\partial \phi}{\partial t} =& -K(\phi) \{ -[2 \left(\rho_1^{-1} - \rho_0^{-1} \right) \bigtriangledown p \cdot \bigtriangledown p^* \\ & - \left(\kappa_1^{-1} - \kappa_0^{-1} \right) p \cdot p^* \cdot \omega^2] - \tau \bigtriangledown^2 \phi \} \end{aligned} \tag{5.22}$$

Note that both variables of the mass density ρ and bulk modulus κ, whose values change suddenly in the vicinity of structural boundaries, are not included in the time evolutionary expression, which prevents calculation instabilities. Thus, the sensitivity distributions are continuous and stable near such boundaries, and smooth structural boundaries. Therefore it is appropriate to use reciprocal functions in Eq. (5.13) and (5.14) to define design variables ρ and κ [160].

5.2.6 Optimization scheme

Here, the level set-based topology optimization scheme is constructed, which provides the unit cell design for an acoustic metamaterial that has negative mass density at a desired frequency. A successful design depends on the mechanism of local resonance occurring in an artificial structure, based on the model shown in Fig. 5-1. That is, a resonance phenomenon leads to a negative effective property such as a negative effective mass density or effective bulk modulus, which is the hallmark of an acoustic metamaterial. An acoustic

metamaterial with negative mass density ρ_e at a target frequency f_t will display a resonance response at frequency f_t. Thus, a successful unit cell design will be obtained and the metamaterial will displays a negative mass density at the particular resonance frequency, if make the objective functional $\rho_e < 0$ at f_t.

As shown in Fig. 5-1, the effective mass density ρ_e is a complex function which has a real part ρ_e' and an imaginary part ρ_e''. Furthermore, a plot of ρ_e'' versus frequency is non-convex and has a single minimal point, whereas that of ρ_e' is concave-convex and has both a peak and a minimum. Thus, from a computational point of view, minimization of ρ_e'' is preferable. The optimization problem is now formulated as follows.

$$\begin{aligned} &\inf_{\phi} \; F = \rho_e'' \\ &\text{subject to} \quad \text{Governing equation} \\ &\qquad\qquad\quad \text{Boundary conditions} \end{aligned} \tag{5.23}$$

Since the above optimization only deals with the imaginary part of the effective mass density, it must be ensured that the real part of the effective mass density, ρ_e', is also negative, to obtain the desired acoustic metamaterial. When the imaginary part, ρ_e'', is minimized at the target frequency, the frequency at the graphed minimum and the target frequency coincide. After optimization of the imaginary part, the real part, ρ_e', is also close to the position of the target frequency. Now, it is easy to obtain the minimum of the real part in the second step optimization, without the worry that the optimization would proceed in an undesirable direction and yield an inappropriate value of the real part of the effective mass density.

In the second step, the real part of the effective mass density, ρ_e', is minimized using the result obtained in the previous step as the initial value.

$$\begin{aligned} &\inf_{\phi} \; F = \rho_e' \\ &\text{subject to} \quad \text{Governing equation} \\ &\qquad\qquad\quad \text{Boundary conditions} \end{aligned} \tag{5.24}$$

For the effective mass density curve like the one shown in Fig. 5-1(b), the above

two-step optimization approach is required when the target frequency is smaller than the frequency corresponding to the peak of the real part. If this two-step optimization approach were not employed, the optimization procedure would likely fail when using standard gradient-based algorithms because the optimization is designed to search for smaller values. It is noted that, although it might be possible to minimize the real part directly in a single optimization in the case when the target frequency is larger than the frequency corresponding to the peak of the real part, nevertheless the two-step optimization approach is used for both cases to limit the scope of this dissertation. Additionally, it is noted that, except for certain simple bounds on the design variables, the design problem is unconstrained, so a volume constraint is not applied.

In the two-step optimization approach, the sensitivities used in the first and second steps are derived using $\langle \mathrm{d}\bar{L}/\chi_\phi, \chi_\phi^* \rangle$, which is a complex function with real and imaginary parts that respectively correspond to the sensitivities of the real and imaginary parts of the objective function.

5.3 Optimization flowchart

In this chapter, a reaction-diffusion equation is adopted to update the level set function using the FEM. With the goal of the two-step optimization approach being to achieve a unit cell design for an acoustic metamaterial that has minimal and negative effective mass density at a desired frequency, the imaginary part of the complex effective mass density is minimized first in the first step, and then the obtained result is used as the initial value for the second step in which the real part of the effective mass density is minimized. Both steps use identical optimization routines. First, the level set function in the fixed design domain D is initialized. The equilibrium equations are then solved using the FEM and the objective functional is then computed. If the objective functional is converged, the optimization process is finished and the optimal configuration is obtained, otherwise the sensitivity analysis is conducted and the level set function ϕ is updated based on Eq. (5.1), again using the FEM. The process then returns to the first step of the iteration loop, which is repeated until the objective functional converges (Fig. 5-5).

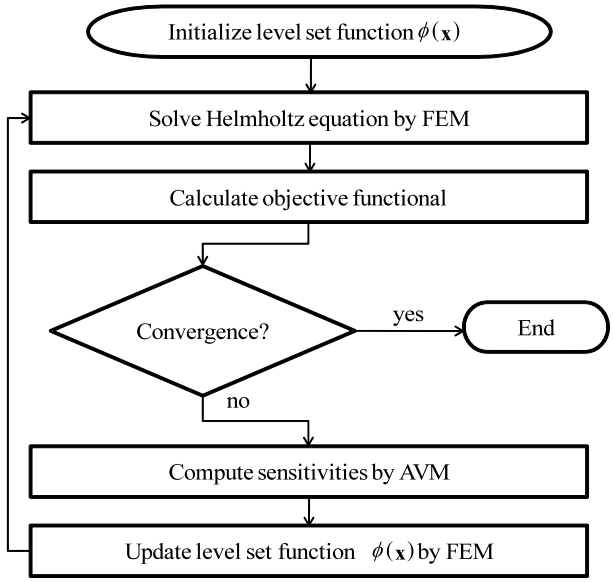

Figure 5-5: Flowchart of the optimization procedure.

5.4 Numerical examples

Two examples are presented here for the design of an acoustic metamaterial with negative mass density at a desired frequency, where a clear material layout is to be found which results in a local resonance. As described in Section 2.6, the design is based on a mass-in-mass structure. The appearance and dimensions of the unit cell to be designed are illustrated in Fig. 5-6. The design domain is divided into two parts, i.e., a fixed design domain D and a non-design domain, to simplify the sensitivity analysis, as discussed in subsection 5.2.5. The entire analysis domain is 30 mm $\times$ 30 mm in the (x,y) plane. The fixed design domain D is 20 mm $\times$ 20 mm, with a 5 mm-radius circle positioned at the center that is a non-design domain area, as are the areas surrounding D. The entire analysis domain is finely discretized using triangular finite elements initially 0.25 mm on an edge, for the FEM analysis.

Two different materials are used in the optimization for the solid and background material, respectively. The bulk modulus of the solid and background materials are set so that κ_1=6.27 $\times 10^5$ Pa and κ_0=2.15 $\times 10^9$ Pa, respectively. The mass density of the solid and background materials are set so that ρ_1=1300 kg/m^3 and ρ_0=1000 kg/m^3, respectively. The material used in the non-design domain is same as the background material. The material

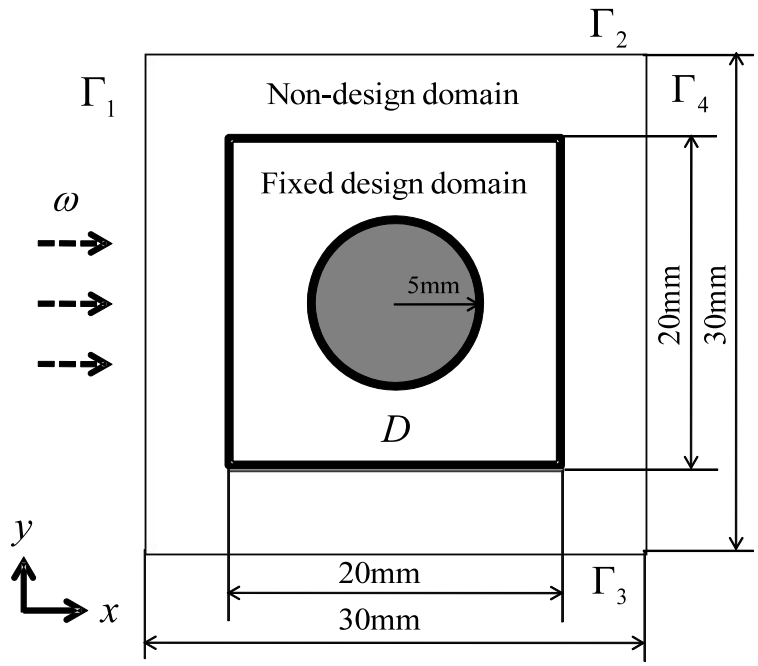

Figure 5-6: Design domain with boundary conditions and size indications.

for the central gray circle is set to have bulk modulus of 46 $\times 10^9$ Pa, with a mass density of 11600 kg/m^3. All the materials used in the design are specified according to their mass density and bulk modulus. A new kind of pentamode metamaterial, a so-called "metafluid", has recently been realized that can theoretically obtain any conceivable mechanical properties by varying the relevant parameters [212]. Furthermore, a liquid state is the ideal state of such materials, which avoids the need to consider transverse waves. The transition width of the Heaviside function w is set to 0.001 in this chapter and the regularization parameter τ is set to 2 $\times 10^{-4}$. No volume constraint is applied in the numerical examples. An annular ring with 7 mm outer and a 5 mm inner radii, surrounding the central circle, is used as the initial configuration (Fig. 5-7)(a).

5.4.1 Example 1: Target frequency set lower than the resonance frequency

This example shows a case in which the target frequency is 800 Hz, lower than the frequency corresponding to the peak of the effective mass density of the initial configuration.

For this target frequency, the target wavelength λ is roughly 1850 mm in the background material ($\lambda/d = 61.7$).

Due to the special characteristic of the effective mass density curve, minimization of the imaginary part of the effective mass density is conducted first, as described above. The optimized configuration of the first step has the solid material represented in black and the void material in white (Fig. 5-7)(b). Accordingly, the effective mass density curves for the initial and optimized configuration are shown in Fig. 5-8. The imaginary part of the

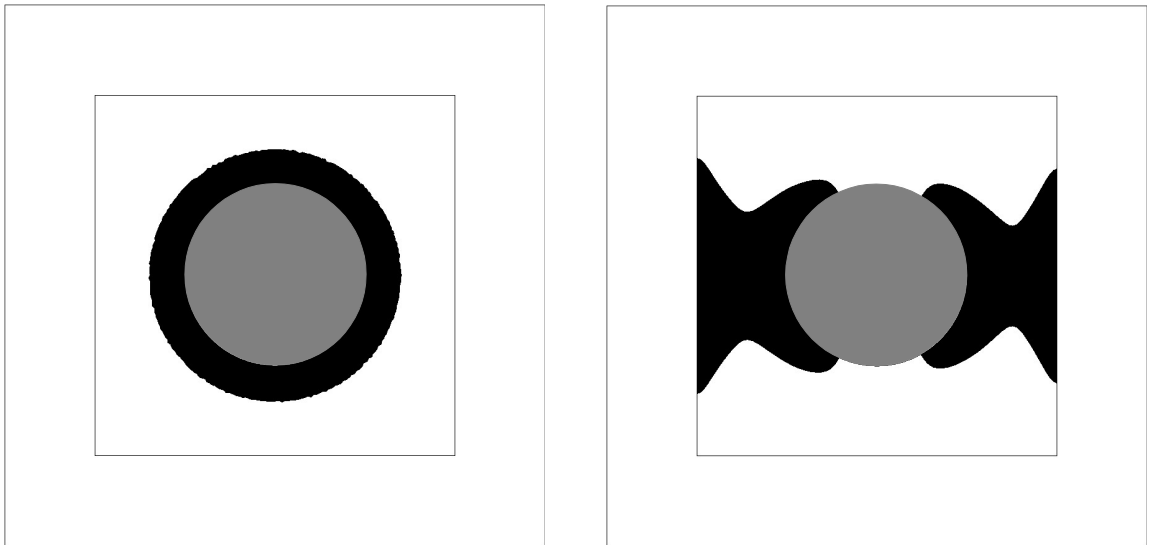

(a) initial; (b) the first step, optimized.

Figure 5-7: Configurations of the first step optimization in effective mass density minimization problem targeting 800 Hz.

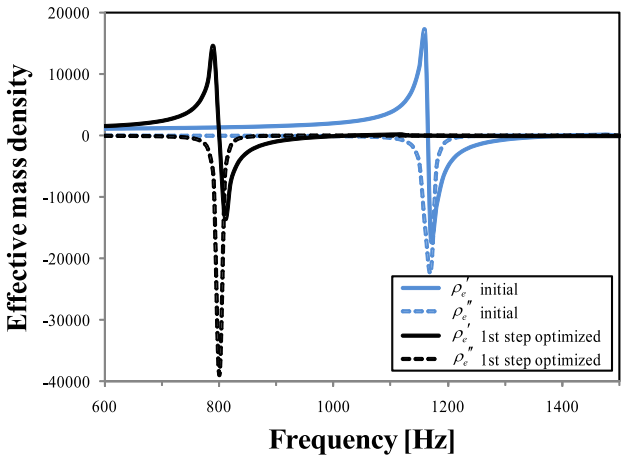

Figure 5-8: Effective mass density curves for the first step of effective mass density minimization problem targeting 800 Hz.

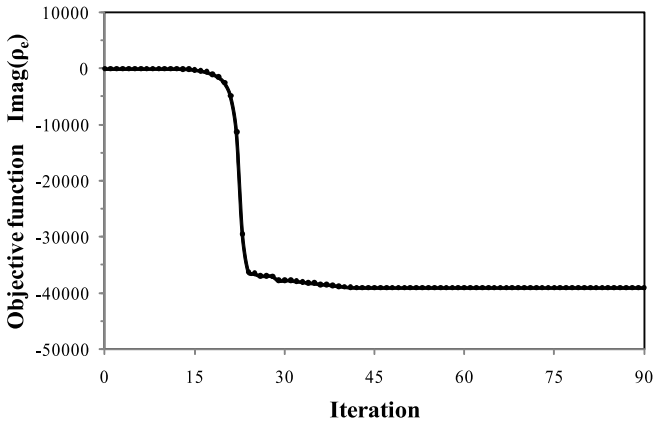

Figure 5-9: Convergence history of objective function (Imag(ρ_e)) of the first step optimization for effective mass density minimization problem targeting 800 Hz.

effective mass density (the dashed line) decreases gradually during the optimization process, i.e., the curve of the imaginary part moves toward the left, and ultimately reaches the minimum value at the desired frequency of 800 Hz. The value of the imaginary part of the effective mass density decreases from -37.27 kg/m^3 for the initial configuration to -3.91×10^4 kg/m^3 in the optimized configuration at 800 Hz. The convergence history for imaginary part of the effective mass density in the first step is shown in Fig.5-9.

The second step is then applied to minimize the real part of the effective mass density, using the optimized configuration obtained in the first step as the initial configuration, to achieve the goal of obtaining a negative mass density at 800 Hz. Following the optimization procedure described in Section 3, the optimized configuration for the second step is shown in Fig. 5-10)(b). Likewise, black area is filled with the solid material and white area area the background material. The effective mass density curves for the 2nd step are shown in Fig. 5-11. The real part of the effective mass density (the solid line) decreases sharply and reaches a minimum at 800 Hz. Finally, the value of the real part of the effective mass density at 800 Hz becomes -1.80×10^4 kg/m^3. The convergence history of the real part of the effective mass density shows some oscillations at the start, then reaches a minimum and remains essentially stable thereafter (Fig. 5-12). Sound pressure distributions and local velocity of the initial configuration (a) and the optimal configuration (b) at 800Hz at certain time are shown in Fig. 5-13, where the contours represent sound pressure distributions with different scales in the (a) and (b) illustrations and the black arrows indicate local velocity. Known from the pressure contours in both illustrations, the pressure increases from about 0 Pa (7.0×10^{-3} Pa exactly) in the initial configuration to 1.5 Pa in the optimal configuration, where the location has the highest pressure indicates the resonance happens. The arrows indicate the direction of movement of the materials. Negative mass density means that a medium accelerates to the left when being forced to the right. When integrate the acceleration of the left and right boundaries of the optimal configuration with the phase of incident pressure of 0°, we obtain the integrated value of the acceleration of the left boundary Γ_1 is $2.45\times10^{-5}-1.13\times10^{-4}i\ m^2/s^2$ and that of the right boundary Γ_4 is $-2.46\times10^{-5}-9.98\times10^{-5}i\ m^2/s^2$, which indicate the left boundary moves to the left and right boundary moves to the left as well. As in this example the applied force (corresponding to incidence pressure in this paper) points to the right, thus the mass density becomes negative. Half a period later, both the applied force and the integrated acceleration values at boundaries change the signs, so that the mass density remains negative. This example implies that the optimization successfully found a minimized and negative effective mass density at the desired frequency, and a smooth and symmetric material distribution was obtained.

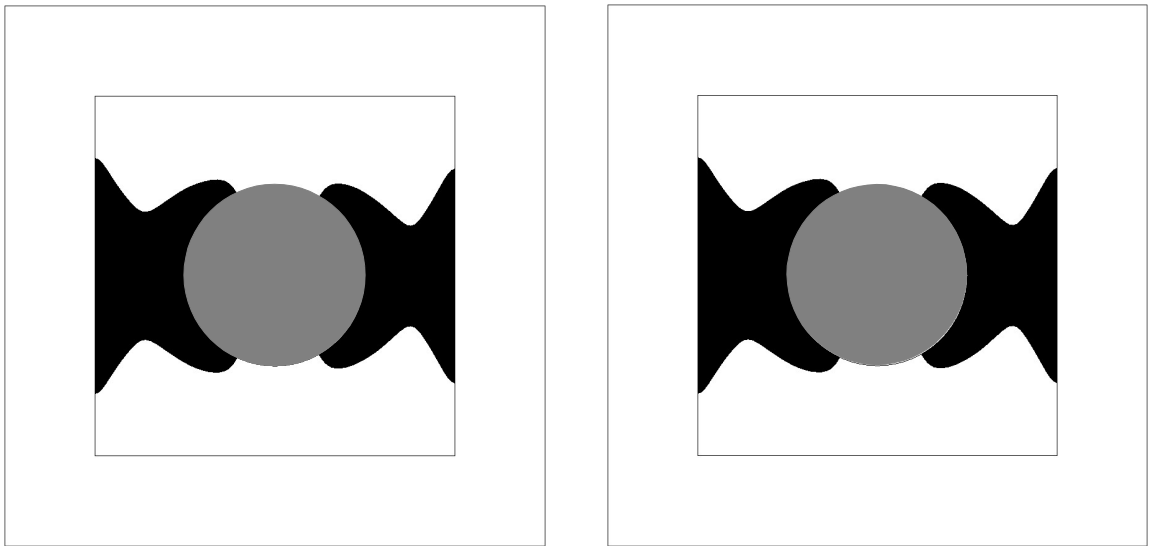

(a) initial (the first step, optimized); (b) the second step, optimized.

Figure 5-10: Configurations of the second step optimization of effective mass density minimization problem targeting 800 Hz.

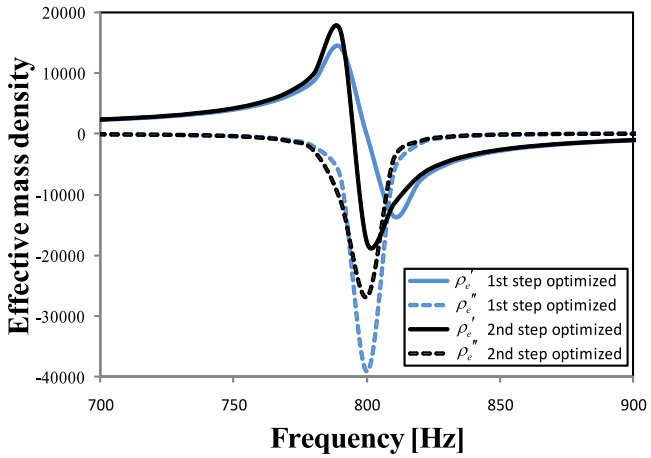

Figure 5-11: Effective mass density curves for the second step of effective mass density minimization problem targeting 800 Hz.

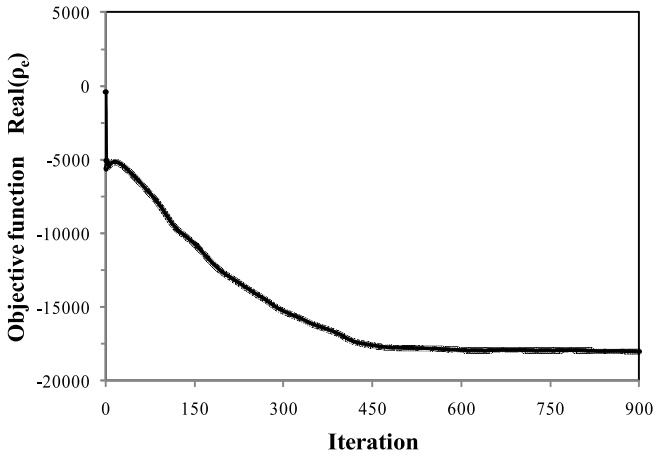

Figure 5-12: Convergence history of objective function (Real(ρ_e)) of the second step optimization for effective mass density minimization problem targeting 800 Hz.

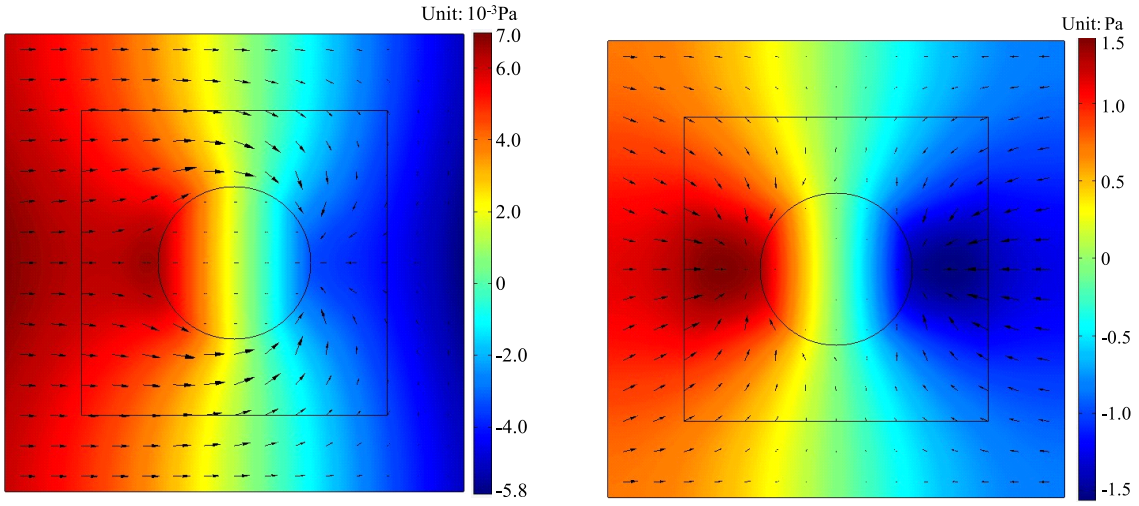

(a) the initial configuration; (b) the optimal configuration.

Figure 5-13: Sound pressure distributions and local velocity of effective mass density minimization problem targeting 800 Hz.

5.4.2 Example 2: Target frequency set higher than the resonance frequency

Here a case in which the target frequency is 1300 Hz, higher than the frequency corresponding to the peak of the effective mass density of the initial configuration, is presented. The initial configuration is same as that for Example 1. For this target frequency, the target wavelength λ is roughly 1140 mm in the background material ($\lambda/d = 38$).

Again the two-step optimization approach is applied, although directly minimizing the real part of the effective mass density might theoretically be effective in this case. The initial configuration used for the first step, and the optimized configuration obtained after the second step, are shown in Fig. 5-14, where black area represents the solid material and white area the background material. The corresponding curves of the effective mass density are shown in Fig. 5-15. The minimum value of the real part of the effective mass density was reached at the 1300 Hz target frequency, and deceased to -1.37×10^4 kg/m^3 at the end of the second optimization procedure. The entire curve was displaced toward the right side, due to the occurrence of the resonance at 1300 Hz. The convergence history during the first and second steps of the optimization is shown in Fig. 5-16. Figure 5-17 shows the sound pressure distributions and local velocity of the initial configuration (a) and the optimal configuration (b), at 1300Hz at a certain time. As in the previous example, the color gradients represent sound pressure distributions over the entire fixed design domain, with different scales in the (a) and (b) illustrations. The pressure increases from about 0 Pa (8.9×10^{-3} Pa exactly) in the initial configuration to 1.7 Pa in the optimal configuration where the resonance happens. The black arrows indicate local velocity and the material movement and accumulation lead to the optimal configuration. Applying integration to the acceleration of the left and right boundaries of the obtained optimal configuration, the integrated acceleration of the left boundary Γ_1 is $1.65\times10^{-5}-1.46\times10^{-4}i\ m^2/s^2$ and that of the right boundary Γ_4 is $-2.38\times10^{-5}-1.77\times10^{-4}i\ m^2/s^2$, which indicate both of the left and the right boundaries move to the left. In this example, the applied force (corresponding to incidence pressure) points to the right, finally it leads to negative mass density. After the phase has changed 180 degrees, the acceleration values integrated at the boundaries will

have opposite signs and the applied force will change its sign as well, so that the sign of the mass density remains negative. The smooth and

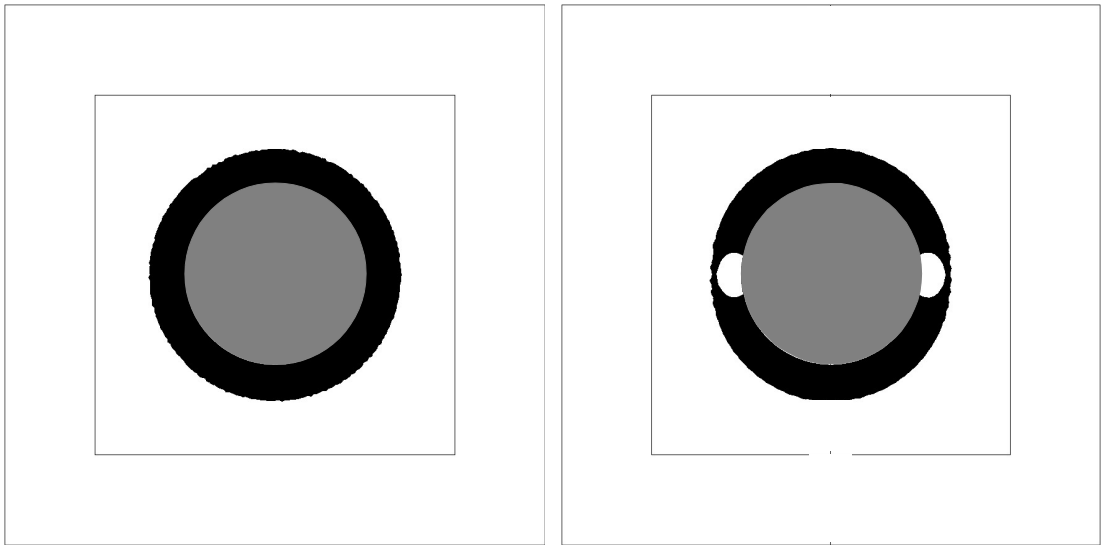

(a) initial; (b) the second step, optimized.

Figure 5-14: Configurations of the optimization in effective mass density minimization problem targeting 1300 Hz.

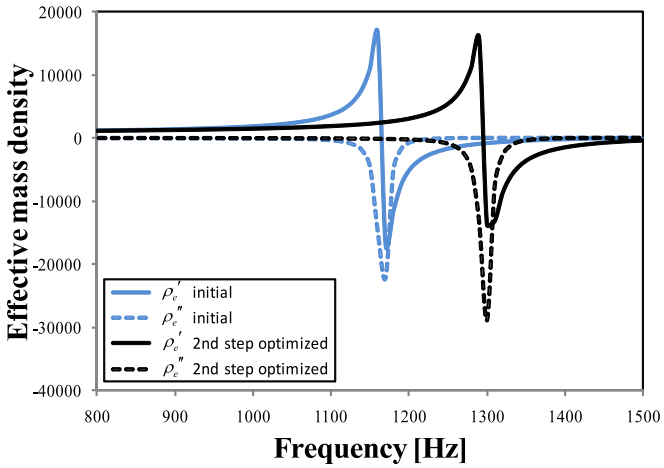

Figure 5-15: Effective mass density curves for the of effective mass density minimization problem targeting 1300 Hz.

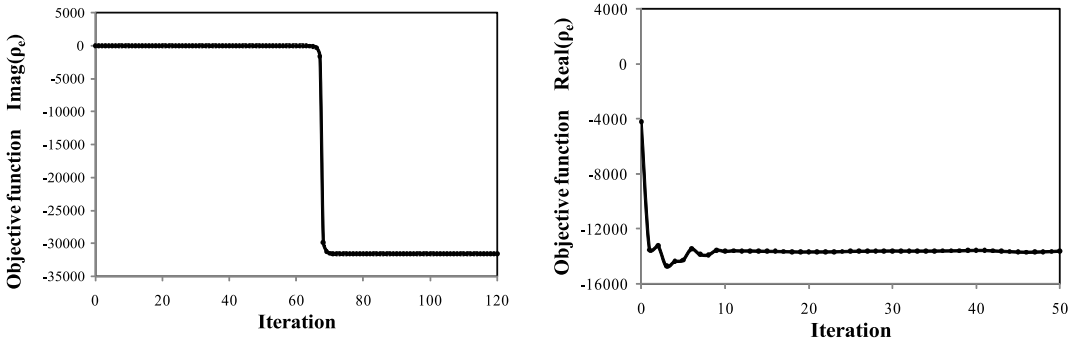

(a) the first step; (b) the second step.

Figure 5-16: Convergence history of objective function, (Imag(ρ_e))) and (Real(ρ_e)), of the effective mass density minimization problem targeting 1300 Hz.

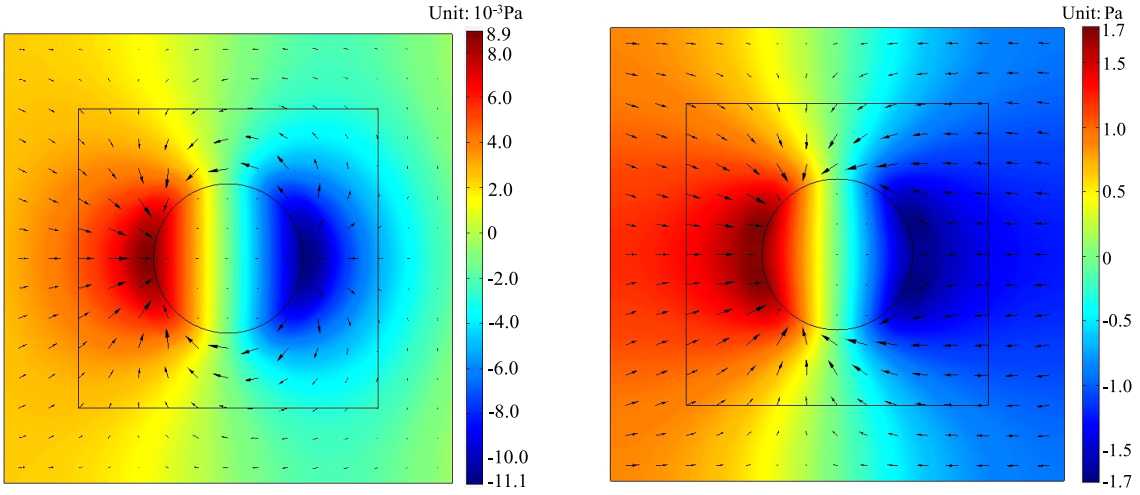

(a) the initial configuration; (b) the optimal configuration.

Figure 5-17: Sound pressure distributions and local velocity of effective mass density minimization problem targeting 1300 Hz.

symmetric result again implies that an acoustic metamaterial with a minimized and negative effective mass density at a different frequency was achieved by the optimization procedure.

Thus, the proposed method effectively achieves unit cell designs for an acoustic metamaterial that exhibits negative mass density in cases regardless of whether the target fre-

quency is higher or lower than the target frequency corresponding to the peak of the effective mass density of the initial configuration.

5.5 Conclusion

A level set-based topology optimization method applied to the design of acoustic metamaterials with negative mass density based on a mass-in-mass system is presented. The following results were obtained.

(1) Two designs for subwavelength unit cells for an acoustic metamaterial constructed as an artificial composite were obtained. The S-parameter retrieval method was applied for the homogenization of the unit cell. The effective material property of the metamaterials was computed based on S-parameters.

(2) The designs of the acoustic metamaterial unit cells were achieved by minimizing the effective mass density, leading to a resonance at a desired frequency. A level set-based topology optimization method, using a reaction-diffusion equation, was successfully applied to obtain optimized configurations with smooth boundaries.

(3) A mass-in-mass system was effective in achieving acoustic metamaterials with a negative mass density. A two-step optimization approach enabled the handling of effective mass density curves that have concave-convex shape.

(4) During the optimization procedure, the FEM was used to solve the equilibrium equation of acoustic wave propagations, and to update the level set function. Moreover, the FEM was also applied to perform sensitivity analyses in both steps, combined with the Adjoint Variable Method.

(5) The proposed method successfully found optimized material distributions for different target frequencies, and provided a flexible and reliable means for the design of acoustic metamaterials, without relying on physical experiments or trial and error approaches.

(6) This research was limited to case having two material phases. In future research, we hope to apply the proposed method to cases with three material phases so that the novel properties and potential applications of acoustic metamaterials can be more easily realized. It would also be beneficial to verify the optimal results through experiments and cooperation with other researchers. This might increase the reliability of the design results and stimulate a wider interest in these novel manmade materials.

Chapter 6

Thesis Conclusions

6.1 Conclusions

A topology optimization method based on a level set method and incorporating the concept of the phase field method was applied for the design of acoustic metamaterials. The systematic design approach incorporating topology optimization was more efficient and effective for developing acoustic metamaterials than a trial and error approach. The following results were achieved.

(1) A level set-based topology optimization method with the level set function updated via a reaction-diffusion equation and regularized using the Tikhonov regularization method was applied to acoustic wave propagation problems, and optimized configurations having clear boundaries were obtained.

(2) Subwavelength scale acoustic metamaterial designs were successfully realized by achieving a single negativity property (negative bulk modulus or negative mass density) due to local resonance. The acoustic metamaterial designs exhibiting single negativity were based on two different structures with locally resonant unit cells. Specifically, an intrinsic model comprising a solid material inclusion embedded in a soft material matrix achieved acoustic metamaterial designs that provide a negative bulk modulus, and an inertial model comprising a solid material sphere coated with a soft material embedded in a soft matrix material achieved acoustic metamaterial

designs that provide a negative mass density.

(3) The S-parameter retrieval method was applied for the homogenization of the unit cell with respect to the effective bulk modulus and effective mass density. Computations of the effective material properties of the metamaterials were based on the use of S-parameters. Three S-parameters, namely, two reflection coefficients S_{11} and S_{22}, and a single transmission coefficient S_{21}, were adopted to guarantee the symmetry of the obtained optimal configurations that are oriented normally to the direction of the wave propagation.

(4) The designs of the acoustic metamaterial unit cells were achieved by minimizing the effective properties, leading to local resonance at desired frequencies. Due to the special characteristics of the curves of the effective properties, a two-step optimization approach was used. In this approach, the imaginary part of the effective properties is optimized first and then the real part of the effective properties is optimized. This enables the handling of effective bulk modulus and effective mass density curves that have a combination of concave-convex shapes.

(5) Several numerical examples, for two- and three-dimensional problems, were provided to verify the validity of the presented method. The proposed method successfully obtained acoustic metamaterial designs that minimize the effective properties at desired frequencies.

6.2 Prospects

My research presented in this dissertation is the beginning of the topology optimization design of acoustic metamaterials. Concerning the continuing research in the near future, the following points could be taken into account.

(1) My research was limited to cases involving compressional waves only. An aim of future research will be to extend the application of the proposed method to cases in which compressional and transverse waves are coupled.

(2) Trying to design problems that include three material phases (or even multiphase scenarios) would help explore new and unusual properties.

(3) It would also be promising to verify the optimal results through experiments and explore cooperations with other researchers.

(4) Apply constraints considering the manufacturing processes and real applications, which may improve the optimal results.

I hope that this research will stimulate increased interest in the field of acoustic metamaterials and related periodic composite materials, and help trigger new developments that exploit the novel properties of these materials for potential applications, such as the hyperlenses applications, and the interaction and coupling of photon and phonon, etc.

Bibliography

[1] Y. Ding, Z. Liu, C. Qiu, and J. Shi, "Metamaterial with simultaneously negative bulk modulus and mass density," *Physical Review Letters*, vol. 99, no. 9, p. 093904, 2007.

[2] J. Mei, Z. Liu, W. Wen, and P. Sheng, "Effective dynamic mass density of composites," *Physical Review B*, vol. 76, no. 13, p. 134205, 2007.

[3] Z. Liu, X. Zhang, Y. Mao, Y. Zhu, Z. Yang, C. Chan, and P. Sheng, "Locally resonant sonic materials," *Science*, vol. 289, no. 5485, pp. 1734–1736, 2000.

[4] P. Sheng, X. Zhang, Z. Liu, and C. Chan, "Locally resonant sonic materials," *Physica B: Condensed Matter*, vol. 338, no. 1, pp. 201–205, 2003.

[5] N. Fang, D. Xi, J. Xu, M. Ambati, W. Srituravanich, C. Sun, and X. Zhang, "Ultrasonic metamaterials with negative modulus," *Nature Materials*, vol. 5, no. 6, pp. 452–456, 2006.

[6] A. Movchan and S. Guenneau, "Split-ring resonators and localized modes," *Physical Review B*, vol. 70, no. 12, p. 125116, 2004.

[7] L. Fok and X. Zhang, "Negative acoustic index metamaterial," *Physical Review B*, vol. 83, no. 21, p. 214304, 2011.

[8] R. Camley, B. Djafari-Rouhani, L. Dobrzynski, and A. Maradudin, "Transverse elastic waves in periodically layered infinite and semi-infinite media," *Physical Review B*, vol. 27, no. 12, p. 7318, 1983.

[9] L. Dobrzynski, B. Djafari-Rouhani, and O. H. Duparc, "Theory of surface phonons in superlattices," *Physical Review B*, vol. 29, no. 6, p. 3138, 1984.

[10] J. Vasseur, B. Djafari-Rouhani, L. Dobrzynski, and P. Deymier, "Acoustic band gaps in fibre composite materials of boron nitride structure," *Journal of Physics: Condensed Matter*, vol. 9, no. 35, p. 7327, 1997.

[11] J. Vasseur, P. Deymier, A. Khelif, P. Lambin, B. Djafari-Rouhani, A. Akjouj, L. Dobrzynski, N. Fettouhi, and J. Zemmouri, "Phononic crystal with low filling fraction and absolute acoustic band gap in the audible frequency range: A theoretical and experimental study," *Physical Review E*, vol. 65, no. 5, p. 056608, 2002.

[12] J.F. Robillard, O. B. Matar, J. Vasseur, P. Deymier, M. Stippinger, A.C. Hladky-Hennion, Y. Pennec, and B. Djafari-Rouhani, "Tunable magnetoelastic phononic crystals," *Applied Physics Letters*, vol. 95, no. 12, pp. 124104–124104, 2009.

[13] T. T. Wu, L. C. Wu, and Z. G. Huang, "Frequency band-gap measurement of two-dimensional air/silicon phononic crystals using layered slanted finger interdigital transducers," *Journal of Applied Physics*, vol. 97, no. 9, pp. 094916–094916, 2005.

[14] S. Mohammadi, A. A. Eftekhar, W. D. Hunt, and A. Adibi, "High-¡ equation¿ q¡/equation¿ micromechanical resonators in a two-dimensional phononic crystal slab," *Applied Physics Letters*, vol. 94, no. 5, pp. 051906–051906, 2009.

[15] S. Mohammadi, A. A. Eftekhar, A. Khelif, W. D. Hunt, and A. Adibi, "Evidence of large high frequency complete phononic band gaps in silicon phononic crystal plates," *Applied Physics Letters*, vol. 92, no. 22, pp. 221905–221905, 2008.

[16] A. Khelif, B. Aoubiza, S. Mohammadi, A. Adibi, and V. Laude, "Complete band gaps in two-dimensional phononic crystal slabs," *Physical Review E*, vol. 74, no. 4, p. 046610, 2006.

[17] S. Mohammadi, A. Eftekhar, A. Khelif, H. Moubchir, R. Westafer, W. Hunt, and A. Adibi, "Complete phononic bandgaps and bandgap maps in two-dimensional silicon phononic crystal plates," *Electronics Letters*, vol. 43, no. 16, pp. 898–899, 2007.

[18] V. Laude, M. Wilm, S. Benchabane, and A. Khelif, "Full band gap for surface acoustic waves in a piezoelectric phononic crystal," *Physical Review E*, vol. 71, no. 3, p. 036607, 2005.

[19] J. Vasseur, P. Deymier, B. Djafari-Rouhani, Y. Pennec, and A. Hladky-Hennion, "Absolute forbidden bands and waveguiding in two-dimensional phononic crystal plates," *Physical Review B*, vol. 77, no. 8, p. 085415, 2008.

[20] S. Benchabane, A. Khelif, J. Rauch, L. Robert, and V. Laude, "Evidence for complete surface wave band gap in a piezoelectric phononic crystal," *Physical Review E*, vol. 73, no. 6, p. 065601, 2006.

[21] C. Goffaux, F. Maseri, J. Vasseur, B. Djafari-Rouhani, and P. Lambin, "Measurements and calculations of the sound attenuation by a phononic band gap structure suitable for an insulating partition application," *Applied Physics Letters*, vol. 83, no. 2, pp. 281–283, 2003.

[22] J. Li, Z. Liu, and C. Qiu, "Negative refraction imaging of acoustic waves by a two-dimensional three-component phononic crystal," *Physical Review B*, vol. 73, no. 5, p. 054302, 2006.

[23] M. Ke, Z. Liu, C. Qiu, W. Wang, J. Shi, W. Wen, and P. Sheng, "Negative-refraction imaging with two-dimensional phononic crystals," *Physical Review B*, vol. 72, no. 6, p. 064306, 2005.

[24] X. Zhang and Z. Liu, "Negative refraction of acoustic waves in two-dimensional phononic crystals," *Applied Physics Letters*, vol. 85, no. 2, pp. 341–343, 2004.

[25] J. Shi, S.C. S. Lin, and T. J. Huang, "Wide-band acoustic collimating by phononic crystal composites," *Applied Physics Letters*, vol. 92, no. 11, pp. 111901–111901, 2008.

[26] S. Yang, J. Page, Z. Liu, M. Cowan, C. Chan, and P. Sheng, "Focusing of sound in a 3d phononic crystal," *Physical Review Letters*, vol. 93, no. 2, p. 024301, 2004.

[27] M. Su, R. Olsson, Z. Leseman, and I. El-Kady, "Realization of a phononic crystal operating at gigahertz frequencies," *Applied Physics Letters*, vol. 96, no. 5, pp. 053111–053111, 2010.

[28] T. Gorishnyy, C. Ullal, M. Maldovan, G. Fytas, and E. Thomas, "Hypersonic phononic crystals," *Physical Review Letters*, vol. 94, no. 11, p. 115501, 2005.

[29] M. Maldovan and E. Thomas, "Simultaneous complete elastic and electromagnetic band gaps in periodic structures," *Applied Physics B*, vol. 83, no. 4, pp. 595–600, 2006.

[30] P. Dainese, P. S. J. Russell, N. Joly, J. Knight, G. Wiederhecker, H. L. Fragnito, V. Laude, and A. Khelif, "Stimulated brillouin scattering from multi-ghz-guided acoustic phonons in nanostructured photonic crystal fibres," *Nature Physics*, vol. 2, no. 6, pp. 388–392, 2006.

[31] M. Trigo, A. Bruchhausen, A. Fainstein, B. Jusserand, and V. Thierry-Mieg, "Confinement of acoustical vibrations in a semiconductor planar phonon cavity," *Physical Review Letters*, vol. 89, no. 22, p. 227402, 2002.

[32] N. Gomopoulos, D. Maschke, C. Koh, E. Thomas, W. Tremel, H. Butt, and G. Fytas, "One-dimensional hypersonic phononic crystals," *Nano Letters*, vol. 10, no. 3, pp. 980–984, 2010.

[33] P. E. Hopkins, C. M. Reinke, M. F. Su, R. H. Olsson III, E. A. Shaner, Z. C. Leseman, J. R. Serrano, L. M. Phinney, and I. El-Kady, "Reduction in the thermal conductivity of single crystalline silicon by phononic crystal patterning," *Nano Letters*, vol. 11, no. 1, pp. 107–112, 2010.

[34] Y. Pennec, J. O. Vasseur, B. Djafari-Rouhani, L. Dobrzyński, and P. A. Deymier, "Two-dimensional phononic crystals: Examples and applications," *Surface Science Reports*, vol. 65, no. 8, pp. 229–291, 2010.

[35] J. Vasseur, A.C. Hladky-Hennion, B. Djafari-Rouhani, F. Duval, B. Dubus, Y. Pennec, and P. Deymier, "Waveguiding in two-dimensional piezoelectric phononic crystal plates," *Journal of Applied Physics*, vol. 101, no. 11, pp. 114904–114904, 2007.

[36] A. Khelif, B. Djafari-Rouhani, J. Vasseur, P. Deymier, P. Lambin, and L. Dobrzynski, "Transmittivity through straight and stublike waveguides in a two-dimensional phononic crystal," *Physical Review B*, vol. 65, no. 17, p. 174308, 2002.

[37] J. H. Sun and T. T. Wu, "Propagation of surface acoustic waves through sharply bent two-dimensional phononic crystal waveguides using a finite-difference time-domain method," *Physical Review B*, vol. 74, no. 17, p. 174305, 2006.

[38] A. Khelif, P. Deymier, B. Djafari-Rouhani, J. Vasseur, and L. Dobrzynski, "Two-dimensional phononic crystal with tunable narrow pass band: Application to a waveguide with selective frequency," *Journal of Applied Physics*, vol. 94, no. 3, pp. 1308–1311, 2003.

[39] L. Zigoneanu, "Design and experimental applications of acoustic metamaterials," 2013.

[40] J. Li and C. Chan, "Double-negative acoustic metamaterial," *Physical Review E*, vol. 70, no. 5, p. 055602, 2004.

[41] C. Goffaux, J. Sánchez-Dehesa, A. L. Yeyati, P. Lambin, A. Khelif, J. Vasseur, and B. Djafari-Rouhani, "Evidence of fano-like interference phenomena in locally resonant materials," *Physical Review Letters*, vol. 88, no. 22, p. 225502, 2002.

[42] S. Zhang, L. Yin, and N. Fang, "Focusing ultrasound with an acoustic metamaterial network," *Physical Review Letters*, vol. 102, no. 19, p. 194301, 2009.

[43] X. Zhou and G. Hu, "Analytic model of elastic metamaterials with local resonances," *Physical Review B*, vol. 79, no. 19, p. 195109, 2009.

[44] C. Ding, H. Chen, S. Zhai, and X. Zhao, "Acoustic metamaterial based on multi-split hollow spheres," *Applied Physics A*, pp. 1–9, 2013.

[45] J. Christensen, L. Martin-Moreno, and F. J. Garcia-Vidal, "All-angle blockage of sound by an acoustic double-fishnet metamaterial," *Applied Physics Letters*, vol. 97, no. 13, pp. 134106–134106, 2010.

[46] H. Huang and C. Sun, "Theoretical investigation of the behavior of an acoustic metamaterial with extreme young's modulus," *Journal of the Mechanics and Physics of Solids*, vol. 59, no. 10, pp. 2070–2081, 2011.

[47] C. J. Naify, C.M. Chang, G. McKnight, and S. R. Nutt, "Scaling of membrane-type locally resonant acoustic metamaterial arrays," *The Journal of the Acoustical Society of America*, vol. 132, p. 2784, 2012.

[48] E. P. Calius, X. Bremaud, B. Smith, and A. Hall, "Negative mass sound shielding structures: Early results," *Physica Status Solidi (b)*, vol. 246, no. 9, pp. 2089–2097, 2009.

[49] P. Sheng, J. Mei, Z. Liu, and W. Wen, "Dynamic mass density and acoustic metamaterials," *Physica B: Condensed Matter*, vol. 394, no. 2, pp. 256–261, 2007.

[50] G. W. Milton and J. R. Willis, "On modifications of newton's second law and linear continuum elastodynamics," *Proceedings of the Royal Society A: Mathematical, Physical and Engineering Science*, vol. 463, no. 2079, pp. 855–880, 2007.

[51] S. H. Lee, C. M. Park, Y. M. Seo, Z. G. Wang, and C. K. Kim, "Composite acoustic medium with simultaneously negative density and modulus," *Physical Review Letters*, vol. 104, no. 5, p. 054301, 2010.

[52] Z. Liang, M. Willatzen, J. Li, and J. Christensen, "Tunable acoustic double negativity metamaterial," *Scientific Reports*, vol. 2, 2012.

[53] H. Huang and C. Sun, "Anomalous wave propagation in a one-dimensional acoustic metamaterial having simultaneously negative mass density and youngs modulus," *The Journal of the Acoustical Society of America*, vol. 132, p. 2887, 2012.

[54] Y. Ding, Z. Liu, C. Qiu, and J. Shi, "Metamaterial with simultaneously negative bulk modulus and mass density," *Physical Review Letters*, vol. 99, p. 093904, 2007.

[55] H. Chen, H. Zeng, C. Ding, C. Luo, and X. Zhao, "Double-negative acoustic metamaterial based on hollow steel tube meta-atom," *Journal of Applied Physics*, vol. 113, no. 10, pp. 104902–104902, 2013.

[56] J. Wen, H. Shen, D. Yu, and X. Wen, "Exploration of amphoteric and negative refraction imaging of acoustic sources via active metamaterials," *Physics Letters A*, 2013.

[57] A. Liu, X. Zhou, G. Huang, and G. Hu, "Super-resolution imaging by resonant tunneling in anisotropic acoustic metamaterials," *The Journal of the Acoustical Society of America*, vol. 132, p. 2800, 2012.

[58] D. Bigoni, S. Guenneau, A. Movchan, and M. Brun, "Elastic metamaterials with inertial locally resonant structures: Application to lensing and localization," *Physical Review B*, vol. 87, no. 17, p. 174303, 2013.

[59] J. Zhu, J. Christensen, J. Jung, L. Martin-Moreno, X. Yin, L. Fok, X. Zhang, and F. Garcia-Vidal, "A holey-structured metamaterial for acoustic deep-subwavelength imaging," *Nature Physics*, vol. 7, no. 1, pp. 52–55, 2010.

[60] J. B. Pendry, D. Schurig, and D. R. Smith, "Controlling electromagnetic fields," *Science*, vol. 312, no. 5781, pp. 1780–1782, 2006.

[61] S. A. Cummer and D. Schurig, "One path to acoustic cloaking," *New Journal of Physics*, vol. 9, no. 3, p. 45, 2007.

[62] A. N. Norris, "Acoustic cloaking theory," *Proceedings of the Royal Society A: Mathematical, Physical and Engineering Science*, vol. 464, no. 2097, pp. 2411–2434, 2008.

[63] A. V. Amirkhizi, A. Tehranian, and S. Nemat-Nasser, "Stress-wave energy management through material anisotropy," *Wave Motion*, vol. 47, no. 8, pp. 519–536, 2010.

[64] H. Shen, J. Wen, M. P. Païdoussis, D. Yu, L. Cai, and X. Wen, "Parameter derivation for an acoustic cloak based on scattering theory and realization with tunable metamaterials," *Modelling and Simulation in Materials Science and Engineering*, vol. 21, no. 6, p. 065011, 2013.

[65] S. Zhang, C. Xia, and N. Fang, "Broadband acoustic cloak for ultrasound waves," *Physical Review Letters*, vol. 106, no. 2, p. 024301, 2011.

[66] W. Zhu, C. Ding, and X. Zhao, "A numerical method for designing acoustic cloak with homogeneous metamaterials," *Applied Physics Letters*, vol. 97, no. 13, pp. 131902–131902, 2010.

[67] Y. Cheng, F. Yang, J. Y. Xu, and X. J. Liu, "A multilayer structured acoustic cloak with homogeneous isotropic materials," *Applied Physics Letters*, vol. 92, no. 15, pp. 151913–151913, 2008.

[68] Y. Cheng and X. Liu, "Three dimensional multilayered acoustic cloak with homogeneous isotropic materials," *Applied Physics A*, vol. 94, no. 1, pp. 25–30, 2009.

[69] H. Chen and C. Chan, "Acoustic cloaking in three dimensions using acoustic metamaterials," *Applied Physics Letters*, vol. 91, no. 18, pp. 183518–183518, 2007.

[70] P. W. Christensen and A. Klarbring, *An introduction to structural optimization*, vol. 153. Springer, 2009.

[71] L. Schmit, "Structural design by systematic synthesis," in *Proceedings of the Second ASCE Conference on Electronic Computation*, pp. 105–122, 1960.

[72] K. Dems and Z. Mróz, "Multiparameter structural shape optimization by the finite element method," *International Journal for Numerical Methods in Engineering*, vol. 13, no. 2, pp. 247–263, 1978.

[73] T. D. Norum and J. M. Seiner, "Shape optimization of pressure-gradient microphones," *The Journal of the Acoustical Society of America*, vol. 62, p. S71, 1977.

[74] C. Ramakrishnan and A. Francavilla, "Structural shape optimization using penalty functions," *Journal of Structural Mechanics*, vol. 3, no. 4, pp. 403–422, 1974.

[75] P. Duysinx and M. P. Bendsøe, "Topology optimization of continuum structures with local stress constraints," *International Journal for Numerical Methods in Engineering*, vol. 43, no. 8, pp. 1453–1478, 1998.

[76] M. M. Neves, O. Sigmund, and M. P. Bendsøe, "Topology optimization of periodic microstructures with a penalization of highly localized buckling modes," *International Journal for Numerical Methods in Engineering*, vol. 54, no. 6, pp. 809–834, 2002.

[77] M. P. Bendsøe and N. Kikuchi, "Generating optimal topologies in structural design using a homogenization method," *Computer Methods in Applied Mechanics and Engineering*, vol. 71, no. 2, pp. 197–224, 1988.

[78] K. Suzuki and N. Kikuchi, "A homogenization method for shape and topology optimization," *Computer Methods in Applied Mechanics and Engineering*, vol. 93, no. 3, pp. 291–318, 1991.

[79] G. Allaire, E. Bonnetier, G. Francfort, and F. Jouve, "Shape optimization by the homogenization method," *Numerische Mathematik*, vol. 76, no. 1, pp. 27–68, 1997.

[80] R. Yang and C. Chuang, "Optimal topology design using linear programming," *Computers & Structures*, vol. 52, no. 2, pp. 265–275, 1994.

[81] M. Bendsøe, *Optimization of Structural Topology, Shape, And Material*. Springer, 1995.

[82] O. Sigmund and J. Petersson, "Numerical instabilities in topology optimization: a survey on procedures dealing with checkerboards, mesh-dependencies and local minima," *Structural Optimization*, vol. 16, no. 1, pp. 68–75, 1998.

[83] M. Zhou, Y. Shyy, and H. Thomas, "Checkerboard and minimum member size control in topology optimization," *Structural and Multidisciplinary Optimization*, vol. 21, no. 2, pp. 152–158, 2001.

[84] O. Sigmund, "Morphology-based black and white filters for topology optimization," *Structural and Multidisciplinary Optimization*, vol. 33, no. 4-5, pp. 401–424, 2007.

[85] O. Sigmund, "On the design of compliant mechanisms using topology optimization*," *Journal of Structural Mechanics*, vol. 25, no. 4, pp. 493–524, 1997.

[86] T. E. Bruns and D. A. Tortorelli, "Topology optimization of non-linear elastic structures and compliant mechanisms," *Computer Methods in Applied Mechanics and Engineering*, vol. 190, no. 26, pp. 3443–3459, 2001.

[87] B. Bourdin, "Filters in topology optimization," *International Journal for Numerical Methods in Engineering*, vol. 50, no. 9, pp. 2143–2158, 2001.

[88] M. Y. Wang and S. Wang, "Bilateral filtering for structural topology optimization," *International Journal for Numerical Methods in Engineering*, vol. 63, no. 13, pp. 1911–1938, 2005.

[89] J. K. Guest, J. Prévost, and T. Belytschko, "Achieving minimum length scale in topology optimization using nodal design variables and projection functions," *International Journal for Numerical Methods in Engineering*, vol. 61, no. 2, pp. 238–254, 2004.

[90] T. S. Kim, J. E. Kim, J. H. Jeong, and Y. Y. Kim, "Filtering technique to control member size in topology design optimization," *KSME International Journal*, vol. 18, no. 2, pp. 253–261, 2004.

[91] S. Xu, Y. Cai, and G. Cheng, "Volume preserving nonlinear density filter based on heaviside functions," *Structural and Multidisciplinary Optimization*, vol. 41, no. 4, pp. 495–505, 2010.

[92] A. Kawamoto, T. Matsumori, S. Yamasaki, T. Nomura, T. Kondoh, and S. Nishiwaki, "Heaviside projection based topology optimization by a pde-filtered scalar function," *Structural and Multidisciplinary Optimization*, vol. 44, no. 1, pp. 19–24, 2011.

[93] B. S. Lazarov and O. Sigmund, "Filters in topology optimization based on helmholtz-type differential equations," *International Journal for Numerical Methods in Engineering*, vol. 86, no. 6, pp. 765–781, 2011.

[94] R. Haber, C. Jog, and M. P. Bendsøe, "A new approach to variable-topology shape design using a constraint on perimeter," *Structural Optimization*, vol. 11, no. 1-2, pp. 1–12, 1996.

[95] J. Petersson and O. Sigmund, "Slope constrained topology optimization," *International Journal for Numerical Methods in Engineering*, vol. 41, no. 8, pp. 1417–1434, 1998.

[96] M. Stolpe and K. Svanberg, "An alternative interpolation scheme for minimum compliance topology optimization," *Structural and Multidisciplinary Optimization*, vol. 22, no. 2, pp. 116–124, 2001.

[97] T. Buhl, C. B. Pedersen, and O. Sigmund, "Stiffness design of geometrically nonlinear structures using topology optimization," *Structural and Multidisciplinary Optimization*, vol. 19, no. 2, pp. 93–104, 2000.

[98] O. Sigmund and S. Torquato, "Design of materials with extreme thermal expansion using a three-phase topology optimization method," *Journal of the Mechanics and Physics of Solids*, vol. 45, no. 6, pp. 1037–1067, 1997.

[99] A. Gersborg-Hansen, M. P. Bendsøe, and O. Sigmund, "Topology optimization of heat conduction problems using the finite volume method," *Structural and Multidisciplinary Optimization*, vol. 31, no. 4, pp. 251–259, 2006.

[100] N. Wiker, A. Klarbring, and T. Borrvall, "Topology optimization of regions of darcy and stokes flow," *International Journal for Numerical Methods in Engineering*, vol. 69, no. 7, pp. 1374–1404, 2007.

[101] T. Borrvall and J. Petersson, "Topology optimization of fluids in stokes flow," *International Journal for Numerical Methods in Fluids*, vol. 41, no. 1, pp. 77–107, 2003.

[102] N. Wiker, *Optimization in continuum flow problems*. PhD thesis, Jönköping University, 2008.

[103] A. R. Díaaz and N. Kikuchi, "Solutions to shape and topology eigenvalue optimization problems using a homogenization method," *International Journal for Numerical Methods in Engineering*, vol. 35, no. 7, pp. 1487–1502, 1992.

[104] S. Nishiwaki, M. I. Frecker, S. Min, and N. Kikuchi, "Topology optimization of compliant mechanisms using the homogenization method," 1998.

[105] Y. El-Kahlout and G. Kiziltas, "Inverse synthesis of electromagnetic materials using homogenization based topology optimization," *Progress In Electromagnetics Research*, vol. 115, pp. 343–380, 2011.

[106] P. Borel, A. Harpøth, L. Frandsen, M. Kristensen, P. Shi, J. Jensen, and O. Sigmund, "Topology optimization and fabrication of photonic crystal structures," *Optics Express*, vol. 12, no. 9, pp. 1996–2001, 2004.

[107] J. S. Jensen and O. Sigmund, "Topology optimization of photonic crystal structures: a high-bandwidth low-loss t-junction waveguide," *JOSA B*, vol. 22, no. 6, pp. 1191–1198, 2005.

[108] J. S. Jensen and O. Sigmund, "Systematic design of photonic crystal structures using topology optimization: Low-loss waveguide bends," *Applied Physics Letters*, vol. 84, no. 12, pp. 2022–2024, 2004.

[109] A. R. Diaz and O. Sigmund, "A topology optimization method for design of negative permeability metamaterials," *Structural and Multidisciplinary Optimization*, vol. 41, no. 2, pp. 163–177, 2010.

[110] S. Zhou, W. Li, and Q. Li, "Design of 3-d periodic metamaterials for electromagnetic properties," *Microwave Theory and Techniques, IEEE Transactions on*, vol. 58, no. 4, pp. 910–916, 2010.

[111] O. Sigmund, "Systematic design of metamaterials by topology optimization," in *IUTAM Symposium on Modelling Nanomaterials and Nanosystems*, pp. 151–159, Springer, 2009.

[112] E. Wadbro and M. Berggren, "Topology optimization of an acoustic horn," *Computer Methods in Applied Mechanics and Engineering*, vol. 196, no. 1, pp. 420–436, 2006.

[113] H. Xiuchang, J. Aihua, Z. Zhiyi, and H. Hongxing, "Design and optimization of periodic structure mechanical filter in suppression of foundation resonances," *Journal of Sound and Vibration*, vol. 330, no. 20, pp. 4689–4712, 2011.

[114] X. Zhang and Z. Kang, "Topology optimization of damping layers for minimizing sound radiation of shell structures," *Journal of Sound and Vibration*, 2013.

[115] T. Yamamoto, S. Maruyama, K. Terada, K. Izui, and S. Nishiwaki, "A generalized macroscopic model for sound-absorbing poroelastic media using the homogenization method," *Computer Methods in Applied Mechanics and Engineering*, vol. 200, no. 1, pp. 251–264, 2011.

[116] T. Yamamoto, S. Maruyama, S. Nishiwaki, and M. Yoshimura, "Topology design of multi-material soundproof structures including poroelastic media to minimize sound pressure levels," *Computer Methods in Applied Mechanics and Engineering*, vol. 198, no. 17, pp. 1439–1455, 2009.

[117] J. W. Lee and Y. Y. Kim, "Topology optimization of muffler internal partitions for improving acoustical attenuation performance," *International Journal for Numerical Methods in Engineering*, vol. 80, no. 4, pp. 455–477, 2009.

[118] C. J. Rupp, A. Evgrafov, K. Maute, and M. L. Dunn, "Design of phononic materials/structures for surface wave devices using topology optimization," *Structural and Multidisciplinary Optimization*, vol. 34, no. 2, pp. 111–121, 2007.

[119] Y. Huang, S. Liu, and J. Zhao, "Optimal design of two-dimensional band-gap materials for uni-directional wave propagation," *Structural and Multidisciplinary Optimization*, vol. 48, no. 3, pp. 487–499, 2013.

[120] S. L. Vatanabe and E. C. Silva, "Design of phononic band gaps in functionally graded piezocomposite materials by using topology optimization," in *SPIE Smart Structures and Materials+ Nondestructive Evaluation and Health Monitoring*, pp. 797811–797811, International Society for Optics and Photonics, 2011.

[121] O. R. Bilal and M. I. Hussein, "Ultrawide phononic band gap for combined in-plane and out-of-plane waves," *Physical Review E*, vol. 84, no. 6, p. 065701, 2011.

[122] C. Rupp, M. Frenzel, A. Evgrafov, K. Maute, and M. L. Dunn, "Design of nanostructured phononic materials," ASME, 2005.

[123] S. Halkjær, O. Sigmund, and J. S. Jensen, "Inverse design of phononic crystals by topology optimization," *Zeitschrift Für Kristallographie*, vol. 220, no. 9-10, pp. 895–905, 2005.

[124] M. Hussein, K. Hamza, G. Hulbert, and K. Saitou, "Optimal synthesis of 2d phononic crystals for broadband frequency isolation," *Waves in Random and Complex Media*, vol. 17, no. 4, pp. 491–510, 2007.

[125] O. R. Bilal and M. I. Hussein, "Optimization of phononic crystals for the simultaneous attenuation of out-of-plane and in-plane waves," ASME, 2011.

[126] S. Osher and J. A. Sethian, "Fronts propagating with curvature-dependent speed: algorithms based on hamilton-jacobi formulations," *Journal of Computational Physics*, vol. 79, no. 1, pp. 12–49, 1988.

[127] J. A. Sethian and A. Wiegmann, "Structural boundary design via level set and immersed interface methods," *Journal of Computational Physics*, vol. 163, no. 2, pp. 489–528, 2000.

[128] S. J. Osher and F. Santosa, "Level set methods for optimization problems involving geometry and constraints: I. frequencies of a two-density inhomogeneous drum," *Journal of Computational Physics*, vol. 171, no. 1, pp. 272–288, 2001.

[129] M. Y. Wang, X. Wang, and D. Guo, "A level set method for structural topology optimization," *Computer Methods in Applied Mechanics and Engineering*, vol. 192, no. 1, pp. 227–246, 2003.

[130] G. Allaire, F. Jouve, and A.-M. Toader, "Structural optimization using sensitivity analysis and a level-set method," *Journal of Computational Physics*, vol. 194, no. 1, pp. 363–393, 2004.

[131] G. Allaire, F. De Gournay, F. Jouve, and A. Toader, "Structural optimization using topological and shape sensitivity via a level set method," *Control and cybernetics*, vol. 34, no. 1, p. 59, 2005.

[132] S. Wang, K. Lim, B. Khoo, and M. Wang, "An extended level set method for shape and topology optimization," *Journal of Computational Physics*, vol. 221, no. 1, pp. 395–421, 2007.

[133] J. A. Sethian, *Level set methods and fast marching methods: evolving interfaces in computational geometry, fluid mechanics, computer vision, and materials science*, vol. 3. Cambridge university press, 1999.

[134] C. Li, C. Xu, C. Gui, and M. D. Fox, "Level set evolution without re-initialization: a new variational formulation," in *Computer Vision and Pattern Recognition, 2005. CVPR 2005. IEEE Computer Society Conference on*, vol. 1, pp. 430–436, IEEE, 2005.

[135] S. Wang and M. Y. Wang, "Radial basis functions and level set method for structural topology optimization," *International Journal for Numerical Methods in Engineering*, vol. 65, no. 12, pp. 2060–2090, 2006.

[136] P. Wei and M. Y. Wang, "Piecewise constant level set method for structural topology optimization," *International Journal for Numerical Methods in Engineering*, vol. 78, no. 4, pp. 379–402, 2009.

[137] T. Yamada, K. Izui, S. Nishiwaki, and A. Takezawa, "A topology optimization method based on the level set method incorporating a fictitious interface energy," *Computer Methods in Applied Mechanics and Engineering*, vol. 199, no. 45, pp. 2876–2891, 2010.

[138] Z. Luo and L. Tong, "A level set method for shape and topology optimization of large-displacement compliant mechanisms," *International Journal for Numerical Methods in Engineering*, vol. 76, no. 6, pp. 862–892, 2008.

[139] X. Zhang and G. Ouyang, "A level set method for reliability-based topology optimization of compliant mechanisms," *Science in China Series E: Technological Sciences*, vol. 51, no. 4, pp. 443–455, 2008.

[140] B. Zhu, X. Zhang, and N. Wang, "Topology optimization of hinge-free compliant mechanisms with multiple outputs using level set method," *Structural and Multidisciplinary Optimization*, pp. 1–14, 2013.

[141] X. M. Zhang and B. L. Zhu, "Topology optimization of compliant mechanisms using level set method without re-initialization," *Applied Mechanics and Materials*, vol. 130, pp. 3076–3082, 2012.

[142] H. Hashimoto, M.-G. Kim, K. Abe, and S. Cho, "A level set-based shape optimization method for periodic sound barriers composed of elastic scatterers," *Journal of Sound and Vibration*, vol. 332, no. 21, pp. 5283–5301, 2013.

[143] C. Zhuang, Z. Xiong, and H. Ding, "Topology optimization of multi-material for the heat conduction problem based on the level set method," *Engineering Optimization*, vol. 42, no. 9, pp. 811–831, 2010.

[144] T. Yamada, K. Izui, and S. Nishiwaki, "A level set-based topology optimization method for maximizing thermal diffusivity in problems including design-dependent effects," *Journal of Mechanical Design*, vol. 133, p. 031011, 2011.

[145] C. Zhuang, Z. Xiong, and H. Ding, "A level set method for topology optimization of heat conduction problem under multiple load cases," *Computer Methods in Applied Mechanics and Engineering*, vol. 196, no. 4, pp. 1074–1084, 2007.

[146] S. Zhu, C. Liu, and Q. Wu, "Binary level set methods for topology and shape optimization of a two-density inhomogeneous drum," *Computer Methods in Applied Mechanics and Engineering*, vol. 199, no. 45, pp. 2970–2986, 2010.

[147] Q. Xia, T. Shi, and M. Y. Wang, "A level set based shape and topology optimization method for maximizing the simple or repeated first eigenvalue of structure vibration," *Structural and Multidisciplinary Optimization*, vol. 43, no. 4, pp. 473–485, 2011.

[148] Z. Luo, L. Tong, and H. Ma, "Shape and topology optimization for electrothermomechanical microactuators using level set methods," *Journal of Computational Physics*, vol. 228, no. 9, pp. 3173–3181, 2009.

[149] Z. Luo, L. Tong, J. Luo, P. Wei, and M. Y. Wang, "Design of piezoelectric actuators using a multiphase level set method of piecewise constants," *Journal of Computational Physics*, vol. 228, no. 7, pp. 2643–2659, 2009.

[150] S. Zhou and Q. Li, "A variational level set method for the topology optimization of steady-state Navier–Stokes flow," *Journal of Computational Physics*, vol. 227, no. 24, pp. 10178–10195, 2008.

[151] X. B. Duan, Y. C. Ma, and R. Zhang, "Shape-topology optimization for Navier–Stokes problem using variational level set method," *Journal of Computational and Applied Mathematics*, vol. 222, no. 2, pp. 487–499, 2008.

[152] X. B. Duan, Y. C. Ma, and R. Zhang, "Shape-topology optimization of stokes flow via variational level set method," *Applied Mathematics and Computation*, vol. 202, no. 1, pp. 200–209, 2008.

[153] S. Yamasaki, T. Nomura, A. Kawamoto, K. Sato, and S. Nishiwaki, "A level set-based topology optimization method targeting metallic waveguide design problems," *International Journal for Numerical Methods in Engineering*, vol. 87, no. 9, pp. 844–868, 2011.

[154] K. Hirayama, Y. Tsuji, S. Yamasaki, and S. Nishiwaki, "Design optimization of h-plane waveguide component by level set method," *IEICE Transactions on Electronics*, vol. 94, no. 5, pp. 874–881, 2011.

[155] G. Fujii, H. Watanabe, T. Yamada, T. Ueta, and M. Mizuno, "Level set based topology optimization for optical cloaks," *Applied Physics Letters*, vol. 102, no. 25, pp. 251106–251106, 2013.

[156] M. Otomori, T. Yamada, K. Izui, S. Nishiwaki, and N. Kogiso, "Level set-based topology optimization for the design of a ferromagnetic waveguide," *Magnetics, IEEE Transactions on*, vol. 48, no. 11, pp. 3072–3075, 2012.

[157] S. Zhou, W. Li, and Q. Li, "Level-set based topology optimization for electromagnetic dipole antenna design," *Journal of Computational Physics*, vol. 229, no. 19, pp. 6915–6930, 2010.

[158] M. Otomori, T. Yamada, J. Andkjaer, K. Izui, S. Nishiwaki, and N. Kogiso, "Level set-based topology optimization for the design of an electromagnetic cloak with ferrite material," *IEEE Transactions on Magnetics*, vol. 49, no. 5, pp. 2081–2084, 2013.

[159] S. Yamasaki, T. Nomura, K. Sato, N. Michishita, Y. Yamada, and A. Kawamoto, "Level set-based topology optimization targeting dielectric resonator-based composite right-and left-handed transmission lines," *International Journal for Numerical Methods in Engineering*, vol. 89, no. 10, pp. 1272–1295, 2012.

[160] M. Otomori, T. Yamada, K. Izui, S. Nishiwaki, and J. Andkjær, "A topology optimization method based on the level set method for the design of negative permeability dielectric metamaterials," *Computer Methods in Applied Mechanics and Engineering*, vol. 237, pp. 192–211, 2012.

[161] S. Zhou, W. Li, Y. Chen, G. Sun, and Q. Li, "Topology optimization for negative permeability metamaterials using level-set algorithm," *Acta Materialia*, vol. 59, no. 7, pp. 2624–2636, 2011.

[162] S. Zhou, W. Li, G. Sun, and Q. Li, "A level-set procedure for the design of electromagnetic metamaterials," *Optics Express*, vol. 18, no. 7, pp. 6693–6702, 2010.

[163] L. Shu, M. Y. Wang, Z. Fang, and Z. Ma, "Level set based structural topology optimization for coupled acoustic-structural system," in *Proceeding of the 9th World Congress on Structural and Multidisciplinary Optimization, Shizuoka, Japan*, 2011.

[164] V. G. Veselago, "The electrodynamics of substances with simultaneously negative values of ε and μ," *Physics-Uspekhi*, vol. 10, no. 4, pp. 509–514, 1968.

[165] V. Veselago and E. Narimanov, "The left hand of brightness: past, present and future of negative index materials," *Nature Materials*, vol. 5, no. 10, pp. 759–762, 2006.

[166] J. Pendry, A. Holden, W. Stewart, and I. Youngs, "Extremely low frequency plasmons in metallic mesostructures," *Physical Review Letters*, vol. 76, no. 25, p. 4773, 1996.

[167] J. B. Pendry, A. J. Holden, D. Robbins, and W. Stewart, "Magnetism from conductors and enhanced nonlinear phenomena," *Microwave Theory and Techniques, IEEE Transactions on*, vol. 47, no. 11, pp. 2075–2084, 1999.

[168] D. R. Smith, W. J. Padilla, D. Vier, S. C. Nemat-Nasser, and S. Schultz, "Composite medium with simultaneously negative permeability and permittivity," *Physical Review Letters*, vol. 84, no. 18, p. 4184, 2000.

[169] W. Cai, D. A. Genov, and V. M. Shalaev, "Superlens based on metal-dielectric composites," *Physical Review B*, vol. 72, no. 19, p. 193101, 2005.

[170] S. Hrabar, J. Bartolic, and Z. Sipus, "Waveguide miniaturization using uniaxial negative permeability metamaterial," *Antennas and Propagation, IEEE Transactions on*, vol. 53, no. 1, pp. 110–119, 2005.

[171] D. Schurig, J. Mock, B. Justice, S. Cummer, J. Pendry, A. Starr, and D. Smith, "Metamaterial electromagnetic cloak at microwave frequencies," *Science*, vol. 314, no. 5801, pp. 977–980, 2006.

[172] Y. Wang and R. Lakes, "Composites with inclusions of negative bulk modulus: Extreme damping and negative poisson's ratio," *Journal of Composite Materials*, vol. 39, no. 18, pp. 1645–1657, 2005.

[173] G. W. Milton, M. Briane, and J. R. Willis, "On cloaking for elasticity and physical equations with a transformation invariant form," *New Journal of Physics*, vol. 8, no. 10, p. 248, 2006.

[174] M. Hirsekorn, P. Delsanto, N. Batra, and P. Matic, "Modelling and simulation of acoustic wave propagation in locally resonant sonic materials," *Ultrasonics*, vol. 42, no. 1, pp. 231–235, 2004.

[175] B. S. Lazarov and J. S. Jensen, "Low-frequency band gaps in chains with attached non-linear oscillators," *International Journal of Non-Linear Mechanics*, vol. 42, no. 10, pp. 1186–1193, 2007.

[176] H. Huang, C. Sun, and G. Huang, "On the negative effective mass density in acoustic metamaterials," *International Journal of Engineering Science*, vol. 47, no. 4, pp. 610–617, 2009.

[177] J. Sánchez-Pérez, D. Caballero, R. Martinez-Sala, C. Rubio, J. Sánchez-Dehesa, F. Meseguer, J. Llinares, and F. Gálvez, "Sound attenuation by a two-dimensional array of rigid cylinders," *Physical Review Letters*, vol. 80, no. 24, p. 5325, 1998.

[178] P. Sheng, *Introduction to wave scattering, localization, and mesoscopic phenomena*, vol. 88. Springer, 2006.

[179] V. Fokin, M. Ambati, C. Sun, and X. Zhang, "Method for retrieving effective properties of locally resonant acoustic metamaterials," *Physical Review B*, vol. 76, no. 14, p. 144302, 2007.

[180] M. P. Bendsøe, "Optimal shape design as a material distribution problem," *Structural Optimization*, vol. 1, no. 4, pp. 193–202, 1989.

[181] M. B. Dühring, J. S. Jensen, and O. Sigmund, "Acoustic design by topology optimization," *Journal of Sound and Vibration*, vol. 317, no. 3, pp. 557–575, 2008.

[182] O. Sigmund and J. S. Jensen, "Systematic design of phononic band–gap materials and structures by topology optimization," *Philosophical Transactions of the Royal Society of London. Series A: Mathematical, Physical and Engineering Sciences*, vol. 361, no. 1806, pp. 1001–1019, 2003.

[183] M. B. Dühring, O. Sigmund, and T. Feurer, "Design of photonic bandgap fibers by topology optimization," *JOSA B*, vol. 27, no. 1, pp. 51–58, 2010.

[184] F. Murat and L. Tartar, "Optimality conditions and homogenization," *Research Notes in Mathematics*, vol. 127, pp. 1–8, 1985.

[185] J. K. Guest, "Topology optimization with multiple phase projection," *Computer Methods in Applied Mechanics and Engineering*, vol. 199, no. 1, pp. 123–135, 2009.

[186] D. Smith, S. Schultz, P. Markoš, and C. Soukoulis, "Determination of effective permittivity and permeability of metamaterials from reflection and transmission coefficients," *Physical Review B*, vol. 65, no. 19, p. 195104, 2002.

[187] D. Smith, D. Vier, T. Koschny, and C. Soukoulis, "Electromagnetic parameter retrieval from inhomogeneous metamaterials," *Physical Review E*, vol. 71, no. 3, p. 036617, 2005.

[188] C. de Blok and R. van den Brink, "Full characterization of linear acoustic networks based on n-ports and s parameters," *Journal of the Audio Engineering Society*, vol. 40, no. 6, pp. 517–523, 1992.

[189] X. Chen, T. M. Grzegorczyk, B. I. Wu, J. Pacheco Jr, and J. A. Kong, "Robust method to retrieve the constitutive effective parameters of metamaterials," *Physical Review E*, vol. 70, no. 1, p. 016608, 2004.

[190] G. Huang and C. Sun, "Band gaps in a multiresonator acoustic metamaterial," *Transactions of the ASME-L-Journal of Vibration and Acoustics*, vol. 132, no. 3, p. 031003, 2010.

[191] X. Ao and C. Chan, "Far-field image magnification for acoustic waves using anisotropic acoustic metamaterials," *Physical Review E*, vol. 77, no. 2, p. 25601, 2008.

[192] J. Li, L. Fok, X. Yin, G. Bartal, and X. Zhang, "Experimental demonstration of an acoustic magnifying hyperlens," *Nature Materials*, vol. 8, no. 12, pp. 931–934, 2009.

[193] V. García-Chocano, L. Sanchis, A. Díaz-Rubio, J. Martínez-Pastor, F. Cervera, R. Llopis-Pontiveros, and J. Sánchez-Dehesa, "Acoustic cloak for airborne sound by inverse design," *Applied Physics Letters*, vol. 99, no. 7, pp. 074102–074102, 2011.

[194] H. Huang and C. Sun, "Wave attenuation mechanism in an acoustic metamaterial with negative effective mass density," *New Journal of Physics*, vol. 11, no. 1, p. 013003, 2009.

[195] Z. Liu, C. Chan, and P. Sheng, "Analytic model of phononic crystals with local resonances," *Physical Review B*, vol. 71, no. 1, p. 014103, 2005.

[196] Z. Yang, J. Mei, M. Yang, N. Chan, and P. Sheng, "Membrane-type acoustic metamaterial with negative dynamic mass," *Physical Review Letters*, vol. 101, no. 20, p. 204301, 2008.

[197] S. H. Lee, C. M. Park, Y. M. Seo, Z. G. Wang, and C. K. Kim, "Acoustic metamaterial with negative density," *Physics Letters A*, vol. 373, no. 48, pp. 4464–4469, 2009.

[198] G. Rozvany, M. Zhou, and T. Birker, "Generalized shape optimization without homogenization," *Structural Optimization*, vol. 4, no. 3-4, pp. 250–252, 1992.

[199] D. C. Dobson and S. J. Cox, "Maximizing band gaps in two-dimensional photonic crystals," *SIAM Journal on Applied Mathematics*, vol. 59, no. 6, pp. 2108–2120, 1999.

[200] J. Sethian, "Evolution, implementation, and application of level set and fast marching methods for advancing fronts," *Journal of Computational Physics*, vol. 169, no. 2, pp. 503–555, 2001.

[201] S. Osher and R. P. Fedkiw, "Level set methods: an overview and some recent results," *Journal of Computational Physics*, vol. 169, no. 2, pp. 463–502, 2001.

[202] L. Ambrosio and G. Buttazzo, "An optimal design problem with perimeter penalization," *Calculus of Variations and Partial Differential Equations*, vol. 1, no. 1, pp. 55–69, 1993.

[203] N. Dijk, M. Langelaar, and F. Keulen, "Explicit level-set-based topology optimization using an exact heaviside function and consistent sensitivity analysis," *International Journal for Numerical Methods in Engineering*, vol. 91, no. 1, pp. 67–97, 2012.

[204] G. Allaire and F. Jouve, "A level-set method for vibration and multiple loads structural optimization," *Computer Methods in Applied Mechanics and Engineering*, vol. 194, no. 30, pp. 3269–3290, 2005.

[205] H. Shim, V. T. T. Ho, S. Wang, and D. A. Tortorelli, "Topological shape optimization of electromagnetic problems using level set method and radial basis function," *CMES: Computer Modeling in Engineering & Sciences*, vol. 37, no. 2, pp. 175–202, 2008.

[206] A. Iga, S. Nishiwaki, K. Izui, and M. Yoshimura, "Topology optimization for thermal conductors considering design-dependent effects, including heat conduction and convection," *International Journal of Heat and Mass Transfer*, vol. 52, no. 11, pp. 2721–2732, 2009.

[207] V. J. Challis and J. K. Guest, "Level set topology optimization of fluids in stokes flow," *International Journal for Numerical Methods in Engineering*, vol. 79, no. 10, pp. 1284–1308, 2009.

[208] C. Y. Kao, S. Osher, and E. Yablonovitch, "Maximizing band gaps in two-dimensional photonic crystals by using level set methods," *Applied Physics B*, vol. 81, no. 2-3, pp. 235–244, 2005.

[209] W. Frei, D. Tortorelli, and H. Johnson, "Geometry projection method for optimizing photonic nanostructures," *Optics Letters*, vol. 32, no. 1, pp. 77–79, 2007.

[210] T. Yamada, S. Yamasaki, S. Nishiwaki, K. Izui, and M. Yoshimura, "Design of compliant thermal actuators using structural optimization based on the level set method," *Journal of Computing and Information Science in Engineering*, vol. 11, no. 1, 2011.

[211] L. Lu, T. Yamamoto, M. Otomori, T. Yamada, K. Izui, and S. Nishiwaki, "Topology optimization of an acoustic metamaterial with negative bulk modulus using local resonance," *Finite Elements in Analysis and Design*, vol. 72, pp. 1–12, 2013.

[212] M. Kadic, T. Buckmann, N. Stenger, M. Thiel, and M. Wegener, "On the practicability of pentamode mechanical metamaterials," *Applied Physics Letters*, vol. 100, no. 19, pp. 191901–191901, 2012.

Publications

International journal Papers

(1) Lirong Lu, Takashi Yamamoto, Masaki Otomori, Takayuki Yamada, Kazuhiro Izui, Shinji Nishiwaki, Topology optimization of an acoustic metamaterial with negative bulk modulus using local resonance, Finite Elements in Analysis and Design, Vol.72 (2013), pp.1-12.

(2) Lirong Lu, Masaki Otomori, Takayuki Yamada, Takashi Yamamoto, Kazuhiro Izui, Shinji Nishiwaki, Topology optimization of acoustic metamaterials with negative effective mass density using a level set-based method, Journals of the Japan Society of Mechanical Engineers, submitted.

Domestic Journal Papers (in Japanese)

乙守正樹，陸麗蓉，山田崇恭，山本崇史，泉井一浩，西脇眞二,レベルセット法による形状表現を用いた音響メタマテリアルのトポロジー最適化,日本機械学会論文集(C 編), 79巻 802号, pp.2138-2151.

Refereed International Proceedings

(1) Lirong Lu, Takashi Yamamoto, Masaki Otomori, Takayuki Yamada, Kazuhiro Izui, Shinji Nishiwaki, Level set-based topology optimization method for the design of an acoustic metamaterial with negative bulk modulus, Proceedings of 7th

China-Japan-Korea Joint Symposium on Optimization of Structural and Mechanical Systems (CJK-OSM7), June 18-21, 2012, Huangshan, China, J-98.

(2) Masaki Otomori, Lirong Lu, Shinji Nishiwaki, Takayuki Yamada, Kazuhiro Izui, Takashi Yamamoto, Level set-based topology optimization of acoustic metamaterials, Proceedings of 10th World Congress on Structural and Multidisciplinary Optimization (WCSMO-10), May 19-24, 2013, Orland, USA, No. 5142.

Non refereed International Proceedings

Lirong Lu, Takashi Yamamoto, Takayuki Yamada, Masaki Otomori, Kazuhiro Izui, Shinji Nishiwaki, Optimal design of acoustic metamaterials by topology optimization, JSME-CMD International Computational Mechanics Symposium 2012 (JSME-CMD ICMS2012), October 9-11, 2012, Kobe, Japan, MS11-2-3(66).

Non refereed Domestic Proceedings (in Japanese)

乙守正樹，陸麗蓉，山田崇恭，山本崇史，泉井一浩，西脇眞二,トポロジー最適化を用いた音響メタマテリアルの構造最適設計法,第13回「運動と振動の制御」シンポジウム(D&D2013), 2013年8月26-29日,福岡, No.305.